NOS-Related Natural Antisense Transcripts: Sequence Analysis and Characterization of Expression

Natalia Lorena Bettini

Thesis submitted for the degree of

Doctor of Philosophy

at the University of Sussex

March 2011

UNIVERSITY OF SUSSEX

Natalia Lorena Bettini

Thesis submitted for the degree of Doctor of Philosophy

NOS-RELATED NATURAL ANTISENSE TRANSCRIPTS: SEQUENCE ANALYSIS AND CHARACTERIZATION OF EXPRESSION

SUMMARY

Endogenous nitric oxide (NO) produced by the enzyme NO synthase (NOS) has an important role in a variety of physiological processes. However, NO becomes noxious to cells if produced in excess. Therefore, the production of NO is tightly regulated. A particularly exciting and novel aspect of the regulation of NO signalling is the possibility that the expression of NOS genes is controlled by unconventional mechanisms that depend on the presence of natural antisense transcripts (NATs).

In this thesis I investigate the important properties of two distinct NOS-related NATs: *Lym-antiNOS2* and *Mm-antiNOS1*. I show that *Lym-antiNOS2* RNA is widely expressed in the CNS of the pond snail *Lymnaea stagnalis.* Furthermore, I demonstrate that the expression of *Lym-antiNOS2* is differentially regulated by training leading to long-term memory formation. Moreover, my results indicate that *Lym-antiNOS2* RNA is subjected to peripheral trafficking in neurons. As for *Mm-antiNOS1*, I find that its expression is restricted to embryonic brain tissue and is almost undetectable in the adult brain of *Mus musculus.*

Declaration

The work in this thesis in entirely my own, except where the work of others is acknowledged or referenced. This thesis has not been submitted before in whole or in part to this or any other University as a part of a degree.

Natalia Lorena Bettini

Acknowledgements

I would first like to thank BBSRC for their generous support, as well as my supervisor, Sergei Korneev, and my co-supervisor Michael O'Shea, who were always available and with whom we spent countless sessions of discussion and thinking aloud.

I would like to thank all people involved in this thesis, in particular Michael Schofield for his unconditional help and disposition, and Ildiko Kemenes for her help with the behavioural experiments.

Finally I am especially grateful to my husband Ignacio for his unconditional love and patience, who makes my life full of happiness, and to my sons, Nicolás and Federico, who gave up priceless moments with mum along the way, and for all the smiles that fill my life every day. This thesis is for them.

Contents

Chapter 1 : Introduction 1
1.1. Discovery of Endogenous Nitric Oxide (NO) as a Signalling Molecule 1
1.2. Discovery of NO Signalling in the Brain 4
1.2.1. Discovery of NO Synthases 4
1.2.2. Expression of NOS Enzymes in the Brain 10
1.2.3. Canonical Mechanisms of the Regulation of NO 10
1.3. The NO-cGMP Signalling Pathway 16
1.4. Unconventional Mechanisms in Regulation of Gene Expression 20
1.4.1. Regulation by Natural Antisense Transcripts (NATs) 20
1.4.2. Unconventional Mechanisms Involved in the Regulation of NO Production 28
1.5. Role of NO in Memory Formation 31
1.5.1. The Role of the NO-cGMP Pathway in Synaptic Plasticity and Memory 33
1.6. Role of nNOS During Embryonic Development and Neurogenesis 40
1.7. Thesis outline 43
Chapter 2 **:** Materials and Methods 44
2.1. Animal Maintenance 44
2.2. Behavioural Experiments 44
2.3. General Dissection 45
2.4. RNA Isolation and Purification from *Lymnaea stagnalis* Brain Tissue 47
2.5. RNA Extraction from Single Identified Neuron 49
2.6. DNase Treatment 49
2.7. RNA Precipitations 50
2.8. Quantification of Total RNA 50
2.9. First Strand Synthesis of cDNA 51
2.10. Oligonucleotide Primer Design 51
2.11. Reverse Transcription PCR 54
2.12. Agarose Gel Electrophoresis of DNA 55
2.13. Isolation of Cerebral Giant Cells 56

2.14. *In situ* Hybridisation 57
2.15. Quantitative Real-Time PCR 65
2.15.1. Relative Quantification Method 65
2.15.2. cDNA Synthesis and Gene-Specific Primer Design 66
2.15.3. Primer Optimization 67
2.15.4. Assay Performance 68
2.15.5. Amplification 69
Chapter 3 **:** Analysis of the Sequence of *Lym*-antiNOS2 NAT and its Expression in *Lymnaea* CNS 72
3.1. Introduction 72
3.1.1. Lym-antiNOS2 RNA Structure 72
3.1.2. Cellular Localization of *Lym-NOS1* in *Lymnaea stagnalis* CNS 76
3.2. Sequence Analysis of *Lym-antiNOS2* RNA 76
3.3. Analysis of the Expression of *Lym-antiNOS2* NAT in CNS by *In Situ* Hybridisation 81
3.3.1. General Staining 83
3.3.2. The Cerebral Giant Cells Express *Lym-antiNOS2* NAT 85
3.4. *Lym-antiNOS2* RNA is Expressed in the CGCs 93
3.4.1. RT-PCR on Isolated Identified CGC 93
3.5. Discussion 97
Chapter 4 : Quantitative Analysis of *Lym-antiNOS2* NAT Expression in Trained and Naïve Animals 100
4.1. Introduction 100
4.2. Feeding behaviour in *Lymnaea* 101
4.3. Optimization of Quantitative RT-PCR 102
4.4. Long Term Memory Formation Induces Timed Changes in the Expression of *Lym-antiNOS2* NAT 115
4.5. Single Conditioning Trial Induces Changes in the Expression of *Lym-antiNOS2* RNA Differently Depending on the Ganglia 120
4.6. Single Conditioning Trial Changes the Levels of Expression of *Lym-NOS1* mRNA in *Lymnaea* Brain 126
4.7. Discussion 130
Chapter 5 : *Lym-antiNOS2* NAT is Subjected to Peripheral Trafficking 133
5.1. Introduction 133

5.2. *In Situ* Hybridisation Reveals the Presence of *Lym-antiNOS2* in the Cerebrobuccal Connectives 135

5.3. RT-PCR Confirms the Presence of *Lym-antiNOS2* RNA in the CBCs 137

5.4. Analysis of the Sequence of *Lym-antiNOS2* Reveals a *cis*-acting Transport Element within the 3'UTR 141

5.5. Discussion 146

Chapter 6 : Sequence Analysis of *Mm-antiNOS1* RNA and Characterization of the Expression during Brain Development 149

6.1. Introduction 149

6.2. Sequence Analysis of *Mm-antiNOS1* RNA 151

6.3. *Mm-antiNOS1* NAT is Detected in Embryonic and Adult Brain of Mice 162

6.4. Quantitative Analysis of *Mm-antiNOS1* NAT Expression in Embryonic CNS 163

6.5. Discussion 171

Chapter 7 : General Discussion and Future Work 174

7.1. Introduction 174

7.2. The Role of NOS-Related NATs in Memory Formation 174

7.3. The Role of NOS-Related NAT during Embryonic Brain Development 179

7.4. Future Work 180

Bibliography 184

Abbreviations

AC	adenylyl cyclase
BH4	tetrahydrobiopterin
CaM	calmodulin
CBC	cerebrobuccal connective
CGC	cerebral giant cell
cGMP	cyclic guanosine 3′,5′-monophosphate
CPEB	CPE-binding protein
CPG	central pattern generator
CR	conditioned response
CREB	cAMP response element-binding protein
CS	conditioning stimulus
Ct	cycle threshold
dsRNA	double-stranded RNA
EDRF	endothelium-derived relaxing factor
eNOS, NOS3	endothelial NOS
FAD	flavin adenine dinucleotide
FMN	flavin mononucleotide
GAPDH	glyceraldehyde 3-phosphate dehydrogenase
GTP	guanosine 5P-triphosphate
heme	iron protoporphyrin IX
hESC	human embryonic stem cell
Hsp90	heat-shock protein 90
iNOS, NOS2	inducible NOS
LTM	long term memory
miRNA	micro RNA
N	naïve
NAT	natural antisense transcript
nNOS, NOS1	neuronal NOS
NO	nitric oxide
NOS	nitric oxide synthase
P	paired
PIN	protein inhibitor of NOS
PKA	cAMP-dependent protein kinase
PKG	cGMP-dependent protein kinase
RT-PCR	reverse transcription polymerase chain reaction
sGC	soluble guanylate cyclase
siRNA	small interfering RNA
snoRNA	small nucleolar RNA
ssRNA	single-stranded RNA
UP	unpaired
UR	unconditioned response
US	unconditioned stimulus
UTR	untranslated region

Chapter 1: Introduction

1.1. Discovery of Endogenous Nitric Oxide (NO) as a Signalling Molecule

Nitric Oxide (NO) is a short-lived, non-polar diatomic gas that acts as a signalling molecule in the body. Signal transmission by a gas is an entirely new principle for signalling in the human organism. NO is a simple, highly reactive molecule that has a lifetime of only a few seconds at low concentrations in tissue. NO has the ability to diffuse across lipidic membranes.

By 1948 nitroglycerin and sodium nitroprusside had already been reported to be used clinically as a vasodilator (Hallberg et al., 1948; Krasno and Ivy, 1950). After many years of investigation, researchers realised that the vasodilatation was produced by the generation of NO in aqueous solution, and that NO itself could cause vasodilatation. In 1977 researchers found that nitroglycerin and related vasodilators activated cytoplasmic guanylate cyclase and thereby the formation of cyclic guanosine 3′,5′-monophosphate (cGMP) in the vascular smooth muscle (Arnold et al., 1977; Gruetter et al., 1979; Ignarro et al., 1991; Jacq et al., 1977; Katsuki et al., 1977; Murad et al., 1978). NO was then found to have similar biologic effects on isolated strips of bovine coronary artery where it was shown that NO was a potent, transient vascular smooth muscle relaxant (Gruetter et al., 1979). Further studies suggested that chemical reactions between certain nitrovasodilators and free thiols, such as cysteine and

glutathione, facilitated the decomposition of the parent drug accompanied by the generation of NO from intermediate unstable S-nitrosothiols. In the closed chest of anesthetized cats, S-nitrosothiols were found to elicit hemodynamic responses that were indistinguishable from those elicited by nitroglycerin. Based on earlier views expressed by Needleman and co-workers, the proposal was forwarded that tolerance to nitroglycerin develops as a result of the depletion of smooth muscle free thiols, so that S-nitrosothiols and therefore NO cannot be generated (Ignarro et al., 1981). Tolerance to nitroglycerin in patients can be abolished, or partially reversed, by the intravenous infusion of N-acetylcysteine, which serves to restore the intracellular thiol concentration.

The physiologic significance of the finding that NO causes vascular smooth muscle relaxation and inhibition of platelet function remained elusive until recently, when nitric oxide was shown to occur naturally in mammalian vascular endothelial cells and to account for the vasodilator action of endothelium-derived relaxing factor (EDRF). Endothelium-derived relaxing factor was first discovered in 1980 to account for the vascular smooth muscle relaxant action of acetylcholine (Furchgott and Zawadzki, 1980), and was subsequently shown to activate cytoplasmic guanylate cyclase, elevate vascular smooth muscle levels of cGMP, and inhibit platelet aggregation (Ignarro et al., 1987; Ignarro et al., 1991).

This body of work led to Robert F Furchgott, Louis J Ignarro and Ferid Murad being awarded the Nobel Prize in Physiology or Medicine for their discoveries concerning “nitric oxide as a signalling molecule in the

cardiovascular system" (Nobelprize.org, 1998). It also made NO grow in importance, so much that in 1992 it was proclaimed by researchers "Molecule of the Year" (Koshland, 1992).

NO is a simple, diatomic molecule. NO is a gas at room temperature and pressure. It is also soluble in water and has the capability of fast diffusion through the lipidic membrane. NO has one unpaired electron and thus it is formally a free radical species. The radical nature of NO confers it the ability to react with other species. Its half-life is only around 7 seconds (Fukoto J.M., 2000).

NO is potentially toxic and yet has the ideal conformation to be both a transient intra- and extra-cellular signalling molecule. NO has evolved into a transducer signal for fundamental physiological processes such as long term memory (LTM) formation, cardiovascular function, immune response and neurogenesis. The discovery of NO as a vasodilator introduced the concept that living systems are able to produce and utilize gaseous molecules as a type of paracrine and autocrine signalling molecule.

NO-related regulatory systems may be as old as cellular organization itself. N_2 is an essential element for life and it is suggested that NO was a crucial intermediate in its utilization. Most of the organisms are not able to use N_2 directly because of the high activation energy required to dissociate nitrogen triple bonds (N≡N); in order to be used, it must be in either reduced or oxidized form (Moroz and Kohn, 2007).

Low levels of NO production are important in signalling cascades, however constantly increased levels of NO could result in tissue damage. Moreover, different types of cancers, diabetes, degenerative diseases (multiple sclerosis, arthritis and ulcerative chronic colitis) have been associated with chronic elevated expression of NO.

1.2. Discovery of NO Signalling in the Brain

1.2.1. Discovery of NO Synthases

In 1989 the enzymatic formation of NO was identified in dialyzed bovine brain cytosol (Schmidt et al., 1989), making bovine brain the second vertebrate tissue –after murine macrophages– where enzymatic formation of nitrogen oxides from L-arginine had been demonstrated. The findings indicate that L-arginine is a substrate for NO-forming enzymes. These NO-forming enzymes discovered in mammalian tissues were named *NO synthases* (NOS). These enzymes were remarkably rapidly characterized, purified and cloned: first described in 1989, purified in 1990 and cloned in 1991 (Bredt and Snyder, 1990; Stuehr et al., 1991).

NOS was shown from the first studies to require Ca^{2+}/calmodulin (Ca^{2+}/CaM) to elicit the conversion of L-arginine to L-citrulline and produce NO. Immediately thereafter, Snyder and colleagues determined that neuronal NOS (nNOS) contains both flavin adenine dinucleotide (FAD) and flavin mononucleotide (FMN) in 1:1 stoichiometry, and reported that the amino acid sequence of its 641-residue C-terminal was highly homologous to NADPH–

cytochrome P-450 reductase (Bredt and Snyder, 1990; Stuehr et al., 1991). They also reported the flavoprotein nature of inducible NOS (iNOS), having already demonstrated that iNOS from mouse macrophages requires tetrahydrobiopterin (BH_4) for activity.

Three groups of NOS isoforms that catalyze NO synthesis in mammalian tissues have been identified. Each of the NOS families is encoded by separate genes. A summary of the properties of the three isoforms of NOS is shown in Table 1.1.

Structural and enzymatic parameters	Active homodimers		
	nNOS (NOS I)	eNOS (NOS III)	iNOS (NOS II)
Subunit molecular mass	160 kDa	135 kDa	125–130 kDa
Inducibility	Constitutive	Constitutive	Inducible
Calmodulin binding	$\sim 30 \times 10^{-9}\ M$	$\sim 30 \times 10^{-9}\ M$	Subunit-like ($\gg 30 \times 10^{-9}\ M$)
Cofactors	H_4B, FAD, FMN, heme, Zn	H_4B, FAD, FMN, heme, Zn	H_4B, FAD, FMN, heme, Zn
Substrates	NADPH, L-arginine, oxygen	NADPH, L-arginine, oxygen	NADPH, L-arginine, oxygen
Posttranslational modifications	Specific phosphorylation sites present	Myristoylation, palmitoylation, phosphorylation sites present	Specific phosphorylation site present
Sources of superoxide formation	Heme domain, reductase domain	Mainly heme domain	Mainly reductase domain
Protein–protein interactions	PSD-95, caveolin3, phosphofructokinase M	Caveolin1, HSP 90, CAT-2, bradykinin receptor	—
Major physiological function	Neurotransmission	Vasodilatation	Cytotoxicity
Role in disease	Stroke, muscular dystrophy, ischemia–reperfusion injury	Endothelial dysfunction, hypercholesterolemia, hypertension	Toxic shock, inflammation, autoimmune disease

Table 1.1 Properties of mammalian NOS isoforms (Masters, 2000).

Endothelial NOS (eNOS or NOS3) and neuronal NOS (nNOS or NOS1) are constitutive and Ca^{2+}-dependent. Inducible NOS (iNOS or NOS2) is Ca^{2+}-independent and stress-induced. All of them have been characterized biochemically, and cloned from several mammalian species with numerous splicing variants. Ca^{2+} influxes associated with either ligand-gated or voltage-

activated Ca^{2+} channels up-regulate NOS activity and result in transient activation of NO synthesis, release of NO and action on neighbouring cells and neuronal terminals (Masters, 2000; Moroz and Kohn, 2007).

NOS in animals is a multi-domain protein consisting of two main subunits: N-terminal oxygenase domain (N-terminal part of NOS, with L-arginine, BH_4 and heme binding sites), which belongs to the class of heme-thiolate proteins, and a C-terminal reductase domain (P-450-type enzymes). The interdomain linker between the oxygenase and reductase domains contains a calmodulin-binding sequence (Liu and Gross, 1996). In contrast, all prokaryotic NOSs are truncated and consist of the oxygenase domain alone. The most likely scenario for the origin of eukaryotic NOSs is the fusion of two previously independent genes, one representing the oxygenase domain (as bacterial NOS) and the P-450 reductase (Alderton et al., 2001). This fusion of oxygenase and P-450 reductase domains may have occurred as a response to the rise of oxygen concentration in Proterozoic time, suggesting the possibility that NOS first appeared in basal animal ancestor groups (Moroz and Kohn, 2007).

All NOS isoforms are flavo-hemoproteins that utilize NADPH as a substrate for reducing equivalents. Illustrated in Figure 1.1 are the binding sites for the cofactors, including NADPH, FAD, FMN, and Ca^{2+}/calmodulin. Calmodulin is constitutively bound to the iNOS isoform and no Ca^{2+} is required for binding. The oxygenase domain of NO synthase contains a conserved cysteine residue that acts as an axial ligand for the heme iron (Ignarro, 2000).

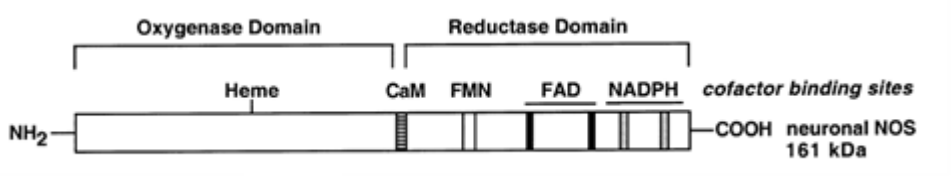

Figure 1.1. Primary sequence map of the three isoforms of human NO synthase (Ignarro, 2000).

In all animal tissues the enzymatic synthesis of NO proceeds according to the following reaction: L-arginine + O_2 → NO + L-citrulline in the presence of NADPH and other co-factors (Figure 1.2). NOS enzymes are known to simultaneously require five bound cofactors, the enzyme with more co-factors known. Animal NOS isozymes are catalytically self-sufficient. They contain relatively tightly-bound cofactors (6R)-5,6,7,8-BH_4, FAD, FMN and iron protoporphyrin IX (heme) and catalyse a reaction of L-arginine, NADPH, and oxygen to the free radical NO, citrulline and NADP (Alderton et al., 2001). The electron flow in the NO synthase reaction is: NADPH → FAD → FMN → heme → O_2 (Knowles and Moncada, 1994).

All the three NOS isoforms require dimerization of two NOS units in their active form. The NOS enzymes are usually referred to as dimeric in their active form, ignoring the required calmodulin (Figure 1.3).

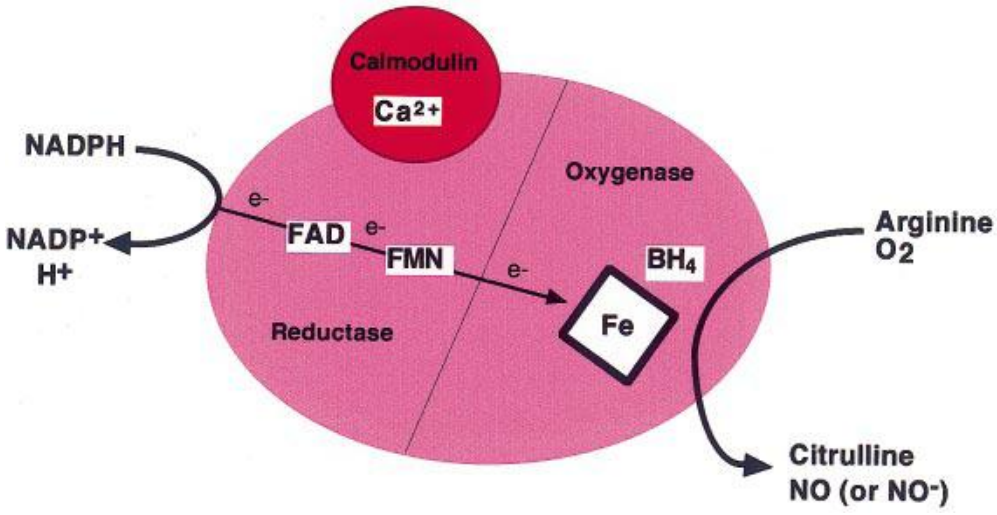

Figure 1.2 Overall reaction catalysed and cofactors of NOS. Electrons (e^-) are donated by NADPH to the reductase domain of the enzyme and proceed via FAD and FMN redox carriers to the oxygenase domain. There they interact with the heme iron and BH_4 at the active site to catalyse the reaction of oxygen with L-arginine, generating citrulline and NO as products. In some circumstances NO^- may be a product instead of NO. Electron flow through the reductase domain requires the presence of bound Ca^{2+}/CaM (Alderton et al., 2001).

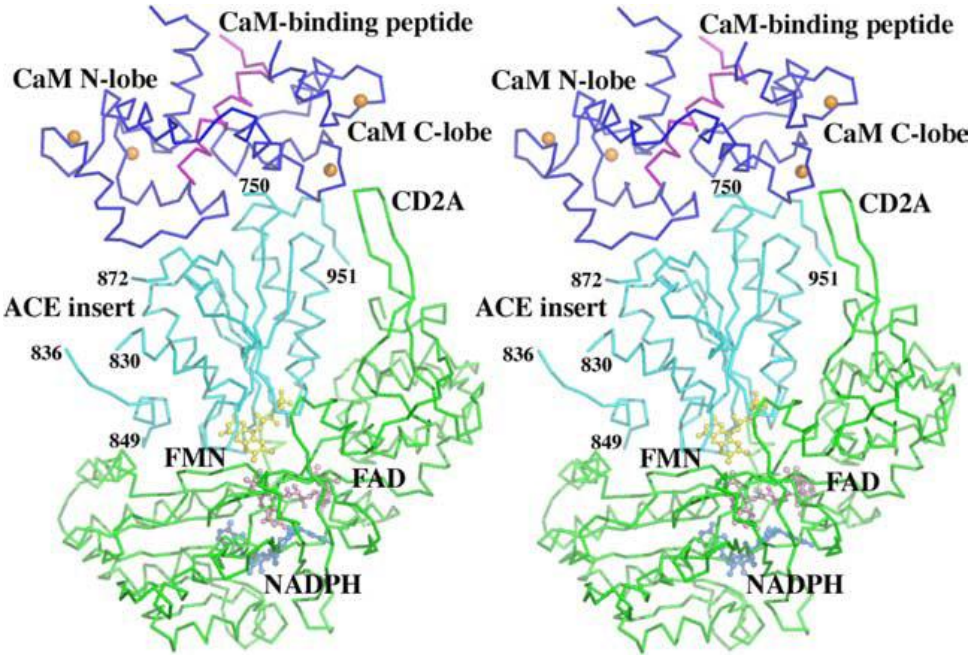

Figure 1.3 A docking model constructed manually showing possible interactions between CaM complexed with a helical peptide from human eNOS and the rat nNOS reductase domain. The autoinhibitory control element (ACE, residues 831–872) of nNOS is partially disordered with two unstructured regions (831–835 and 850–870). The C-terminal helix is hidden behind the FMN binding domain. Cofactors FMN, FAD, and NADPH are shown as ball-and-sticks, while Ca^{2+} ions in CaM are represented as gold spheres (Li and Poulos, 2005).

1.2.2. Expression of NOS Enzymes in the Brain

nNOS activity was first identified in the cerebellum, in a crude supernatant fraction of human cerebellum (Schmidt and Murad, 1991). It is documented that nNOS is the major component of NOS in the hippocampus of mice (Murashima et al., 2005). nNOS is located in the peripheral vagal nerves (Choate et al., 2001), sympathetic nerves (Wang et al., 2006) and in the autonomic control region of the central nervous system (Andrew and Mayer, 1999). nNOS is expressed in neurons, cardiac myocytes and blood vessels.

In *Lymnaea*, *Lym*-nNOS has been localized in the serotonergic cerebral giant cells (CGCs), which modulate synaptic transmission within a neural network that generates feeding behaviour, where the CGCs employ both NO and serotonin in the modulation (Korneev et al., 1998). In zebrafish nNOS was identified to be expressed throughout the adult brain. nNOS may participate in neurotransmission and in mechanisms related to the continuous neurodevelopment and neuronal plasticity. nNOS mRNA was localized within central nuclei of all brain regions and in the proliferation zones, distributed along the ventricular regions from the telencephalon through the entire hypothalamus, optic tectum and rhombencephalon (Holmqvist et al., 2000).

1.2.3. Canonical Mechanisms of the Regulation of NO

Each member of the NOS family is known to regulate different functions. nNOS-derived NO performs a variety of physiological and patho-physiological roles. NO has been shown to be involved in the regulation of long term

potentiation (Schuman and Madison, 1991), in neurodevelopment (Kalb and Agostini, 1993) and in several neurodegenerative disorders such as stroke (Love, 1999), Parkinson's disease, Alzheimer's disease, and amyotrophic lateral sclerosis (Calabrese et al., 2007). Excessive production of NO may exert neurotoxicity, particularly in the presence of oxidative stress, since NO may react with superoxide to form peroxynitrite (Szabo et al., 2007). Because of NO's toxicity and its contribution to the pathogenesis of neurodegenerative disorders, nNOS is under tight regulation through different mechanisms. nNOS is regulated by alternative splicing, protein-protein interaction, covalent modifications and via CaM/Ca^{2+} binding domain.

Active nNOS is dimeric with an extensive interface between the two oxygenase domains creating high-affinity binding sites for BH_4 and L-arginine. The nNOS monomer has two cysteine residues which can form a disulphide bridge or ligate a zinc ion between the monomers, covalently linking the two oxygenase domains. Moreover, there is an N-terminal hook domain which can also stabilize the dimer. Additionally, interactions across the dimer between the reductase domains and between the reductase and oxygenase domains also exist. BH_4 as well as heme and L-arginine all make nNOS a stable dimer. The nNOS inhibitor 7-nitroindazole reduces the affinity of BH_4 and L-arginine. Dimerization increases nNOS activity by creating binding sites for L-arginine and BH4, thus facilitating electron flow. Interestingly, the electrons appears to flow from one monomer to another, which may be a major reason why the nNOS monomer is inactive (Zhou and Zhu, 2009).

CaM was the first protein shown to interact with NOS, and is necessary for the enzymatic activity of all three NOS isoforms. The Ca^{2+} dependence of NO synthesis distinguishes the NOS isoforms, with nNOS and eNOS having a much higher Ca^{2+} requirement than iNOS. CaM binding increases the rate of electron transfer from NADPH to the reductase domain flavins and artificial electron acceptors such as ferricyanide and cytochrome C. It also triggers electron transfer from the reductase domain to the heme centre. nNOS and eNOS differ in their primary structure from iNOS in the former having 40-50 amino acid inserts in the middle of the FMN-binding subdomain, which has been described as an autoinhibitory loop. Analysis of mutants of eNOS and nNOS with this loop deleted has shown that the insert acts by destabilizing CaM binding at low Ca^{2+} and by inhibiting electron transfer from FMN to the heme in the absence of Ca^{2+}/CaM (Abu-Soud et al., 1994; Alderton et al., 2001; Daff et al., 1999; Gachhui et al., 1998; Gachhui et al., 1996).

Phosphorylation of the nNOS and eNOS isoforms has an effect on NOS activity. Fluid shear stress elicits phosphorylation of eNOS and an increase in calcium-independent NOS activity. Mutational studies were carried where Ser^{1179} in eNOS was replaced by alanine. Immunoprecipitation and western blotting of eNOS and protein kinase Akt (co-immunoprecipitation) show that Ser^{1179} of eNOS is phosphorylated by protein kinase Akt, which results in an increase in electron flux through the reductase domain and an increase in NO production. In contrast, the phosphorylation of nNOS at Ser^{847} by CaM-dependent kinases leads to a decrease in NOS activity (Alderton et al., 2001;

Corson et al., 1996; Hayashi et al., 1999; Komeima et al., 2000; Nakane et al., 1991).

The N-terminal extension of nNOS contains a binding site for the 89-amino-acid protein inhibitor of NOS (PIN). Spectroscopy has been used to map the PIN-binding region of rat nNOS to Met^{228}-His^{244} and to determine that PIN binds nNOS with a 1:2 PIN:nNOS stoichiometry. Initial reports suggested that only nNOS associated with PIN and that PIN was inhibitory by destabilization of the nNOS. However, recent reports claim that PIN neither inhibits nNOS nor promotes monomerization, or that PIN has no effect on nNOS dimerization but does inhibit both NOS and NADPH oxidase activity of nNOS, eNOS and iNOS in a time-dependent manner. The identification of PIN as a light chain of myosin and dynein has led to the suggestion of an alternative role for PIN as an axonal transport protein for nNOS rather than a regulator of nNOS (Hemmens et al., 1998; Jaffrey and Snyder, 1996; Rodriguez-Crespo et al., 1998; Xia et al., 2006).

The molecular chaperone Heat-shock protein 90 (Hsp90) has also been identified as a regulator of eNOS activity, possibly as an allosteric modulator. Activation by vascular endothelial growth factor, histamine or fluid shear stress in human endothelial cells increases the interaction between eNOS and Hsp90 and increases eNOS activity. The activity of purified eNOS was also increased by purified Hsp90, suggesting a direct interaction, the details of which are not yet clear. nNOS was not directly activated by hsp90 *in vitro*, but a role for Hsp90 in incorporation of the heme into nNOS in *in vivo* situations where heme is

limited is suggested (Bender et al., 1999). Increased NO production has been inhibited by caveolin. Caveolin by inhibiting Ca-CaM binding suppresses NO synthesis in skeletal muscle, and consequently this inhibition is reversed by Ca-CaM (Venema et al., 1997; Zhou and Zhu, 2009) .

Post-transcriptional regulation of the nNOS gene occurs in the form of alternative mRNA splicing. Figure 1.4 presents a schematic representation of the predicted peptides of the four nNOS splice variants detected so far (nNOSβ, nNOSγ, nNOSμ and nNOS-2).

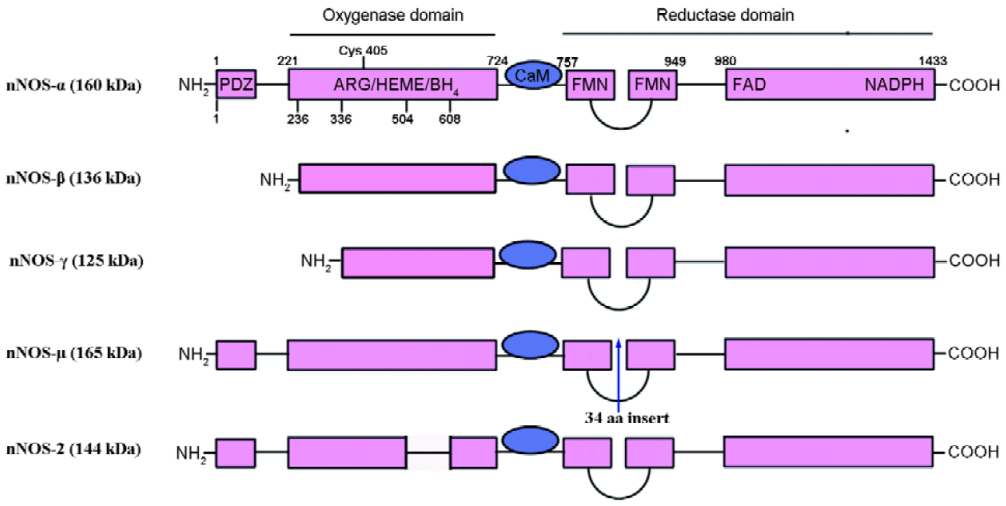

Figure 1.4 Splice variants of rat nNOS. nNOSα: amino acids 1-1433; nNOSβ: amino acids 236-1433 of nNOSα; nNOSγ: amino acids 336-1433 of nNOSα; nNOSμ: amino acids 1-1433 of nNOSα with a 34-amino-acid insert in the FMN-binding domain. nNOS-2 (detected in mouse): amino acids 1-1433 of nNOSα with 504-608 amino acids deleted (Luo and Zhu, 2011).

The human iNOS mRNA is subject to alternative splicing, including deletion of exons 8 and 9 that encode amino acids 242–335 of the oxygenase domain ($iNOS_{8-9}$). The region encoded by exons 8 and 9 is critical for iNOS dimer formation and NO production but not for reductase activity. Heterodimers between full length iNOS and $iNOS_{8-9}$ were not detected after co-expression,

suggesting that $iNOS_{8-9}$ may not exert the suggested dominant negative effect on iNOS activity (Alderton et al., 2001; Eissa et al., 1998). A replication-deficient recombinant adenoviral vector that directs the expression of a truncated form of eNOS was shown to act as a dominant negative inhibitor of wild-type eNOS activity through heterodimerisation with the native protein (Paton et al., 2001).

nNOS is mostly located in the brain, where the synthase is highly enriched in specific neuronal populations (Bredt and Snyder, 1990). Protein interactions involving the nNOS PDZ domain in neurons regulate coupling to upstream calcium stores and specify downstream targets of NO. Most NO synthesis in brain is coupled to calcium influx through the N-methyl-D-aspartate (NMDA) type glutamate receptor, which was first shown to increase cGMP levels via neuron-derived NO (Garthwaite and Boulton, 1995). Physical association of nNOS with the NMDA receptor determines this specificity (Figure 1.5). nNOS does not directly bind to the NMDA receptor. However, both nNOS and NMDAR interact with the postsynaptic density protein 95 (PSD-95). PSD-95 is known to contain three PDZ domains. These PDZ domains mediate the interaction of the PSD-95 with the C-terminal end of the NMDA receptor subunit, and also with the PDZ domain from the nNOS. This leads to the formation of a ternary signalling complex. This complex is essential for the efficient activation of nNOS by calcium and determines downstream signalling specificity. (Bredt, 2003)

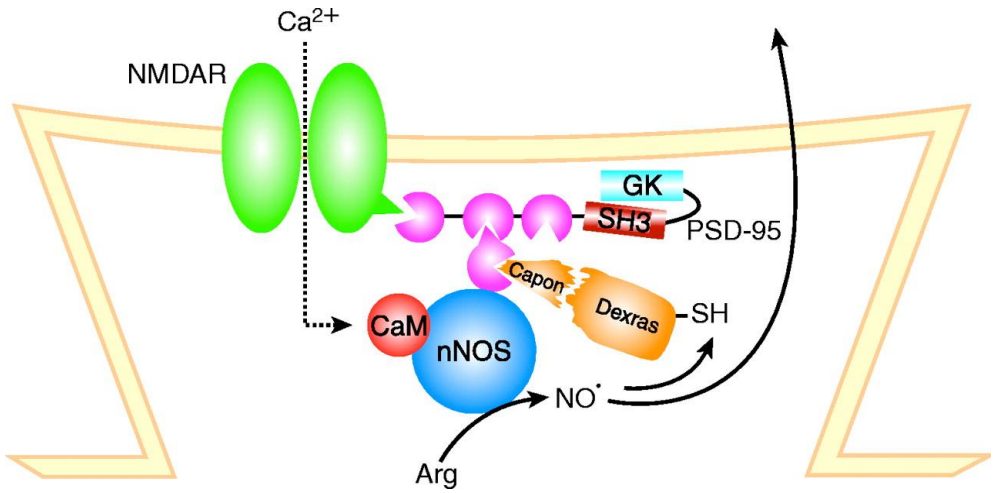

Figure 1.5 Protein interactions regulating NO signalling at neuronal synapses. PDZ domain interactions (pink) function to bring nNOS to the NMDA receptor, allowing specific activation of nNOS in response to glutamate-induced calcium influx. Binding of nNOS to PSD-95 leaves the nNOS PDZ domain peptide binding pocket free to interact with other proteins such as Capon. The NO produced in association with NMDA receptor activity diffuses to presynaptic nerve terminals and nitrosylates Dexras associated with Capon. Abbreviations: Arg, arginine; CaM, calmodulin; GK, guanylate kinase domain. (Bredt, 2003)

1.3. The NO-cGMP Signalling Pathway

Soluble guanylate cyclase (sGC) is the only proven receptor for NO. sGC catalyzes the conversion of guanosine 5P-triphosphate (GTP) to cyclic guanosine 3',5'-monophosphate (cGMP). Because it is one of two enzymes that produce cGMP, and because it is the only definitive receptor for NO, sGC is intimately involved in many signal transduction pathways of many processes.

Soluble guanylate cyclase is a heterodimeric protein composed of α and β subunits; in addition, it is a hemoprotein. NO binds to the sGC heme and this binding event activates the enzyme (Figure 1.6). The activation of sGC and the subsequent rise in cGMP concentration are what allow sGC to transmit a NO signal to the downstream elements of the signalling cascade. Importantly, the free-radical electronic structure of NO makes it an excellent ligand for heme,

allowing it to bind to the sGC heme at a low, non-toxic concentrations (Denninger and Marletta, 1999).

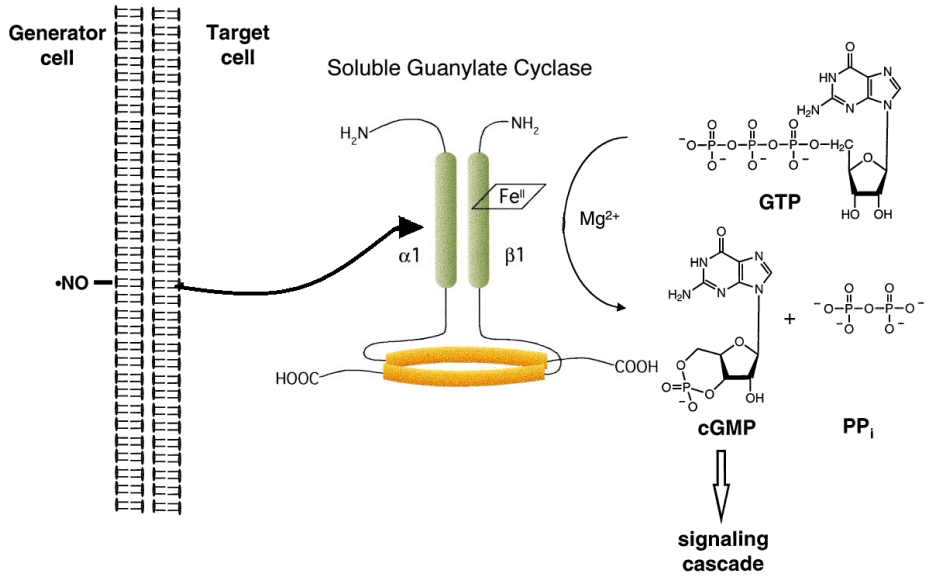

Figure 1.6 The guanylate cyclase reaction and NO signal transduction. Adaptation from (Denninger and Marletta, 1999)

The NO–cGMP signal transduction pathway is employed by NO to carry out many of its biological effects (Figure 1.7). NO as an endogenous activator of soluble guanylate cyclase led to the appreciation of cGMP as a second messenger of immense biological significance and potential. cGMP acts on three main classes of effector proteins: cGMP-dependent protein kinases, cGMP-gated ion channels, and cGMP-regulated phosphodiesterases. These effector proteins mediate protein phosphorylation, cation influx, and cyclic nucleotide metabolism, respectively. The biological actions of cGMP are terminated by its breakdown by phosphodiesterases. cGMP, through its effector proteins, mediates several of the physiological functions of NO including regulation of

smooth muscle tone, inhibition of platelet aggregation, regulation of neurotransmission, and chloride and water secretion in the intestines (Ignarro, 2000).

The cGMP can be degraded by phosphodiesterase or can bind to other proteins including ion channels, protein kinases, and phosphodiesterases as illustrated in Figure 1.7. cGMP can either activate or inhibit specific phosphodiesterase isoforms. Binding of cGMP to protein kinases causes their activation and subsequent phosphorylation of proteins. The phosphorylated proteins can cause or lead to a biological effect and are generally inactivated by dephosphorylation caused by protein phosphatases. Many biological actions of NO are mediated by cGMP via this signal transduction pathway (Ignarro, 2000).

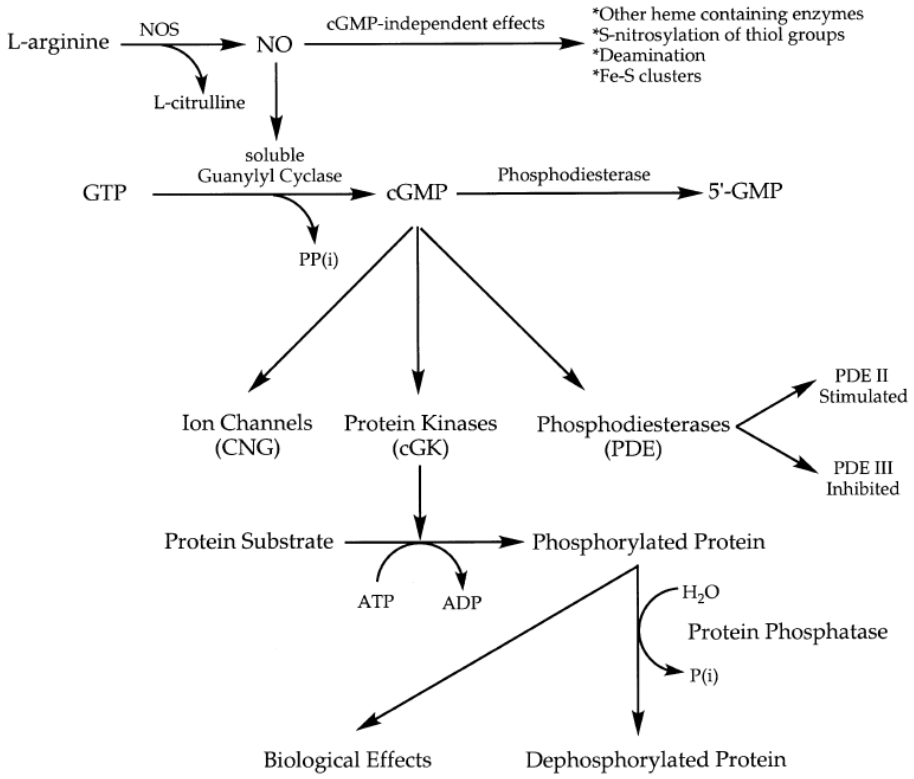

Figure 1.7 Signal transduction pathway for the NO–cGMP system in mammalian cells. NO generated from L-arginine by NOS isoforms activates sGC, thereby increasing production of cGMP (Ignarro, 2000).

1.4. Unconventional Mechanisms in Regulation of Gene Expression

1.4.1. Regulation by Natural Antisense Transcripts (NATs)

Natural antisense transcripts (NATs) are endogenous RNAs that have complementary sequences to transcripts of an already known function. NATs can be divided into two major groups. So-called *cis*-encoded are issued from the same locus as sense transcripts. Transcribed from opposite strands of DNA, *cis*-encoded NAT display perfect complementarity to their sense products. In contrast, *trans*-encoded NATs originate from a different locus and may display only partial complementarity with the sense transcript (Vanhee-Brossollet and Vaquero, 1998).

In 1977 Jacq and co-workers (Jacq et al., 1977) reported for the first time the isolation and sequencing of a 5S-rRNA related gene from *Xenopus laevis* which was truncated at the 5' end (by 16 base pairs) and had 14 base pair mismatches when compared to the productive 5S rRNA gene. As this particular gene could not possibly code for a functional 5S rRNA, Jacq used the term *pseudogene* to describe this truncated 5S rDNA homologue. Since then many different pseudogenes have been reported. Vanin in 1985 redefined the term *pseudogene* (Vanin, 1985) to describe sequences which have been shown to be related to a functional gene, but are defective.

In the past scientists believed that the gene transcription in eukaryotic genomes was simple. We now know a broad spectrum of RNA molecules that

are transcribed, ranging from long protein-coding mRNAs to short noncoding microRNAs (miRNAs), which frequently overlap or are inserted on either strand (Ponting et al., 2009). Today the term *pseudogene* is starting to have a different meaning. Pseudogene formation may act as an evolutionary mechanism that generates *trans*-NATs to the parental gene. For example, this could occur if the parental gene is regulated by a *cis*-NAT that is copied as a *trans*-NAT in the pseudogene (Muro and Andrade-Navarro, 2010).

Trans-NATs are transcribed from a sequence that is not located in the same genomic locus of their target and can then evolve separately, constrained only by keeping a complementary region to the target gene. It is still unclear how relatively large and specific complementary regions can arise to form such antisense transcripts. A possibility that was raised is that given a parental gene regulated by a *cis*-NAT, the duplication of the genomic fragment including the *cis*-NAT may result in a pseudogene holding an active copy of the *cis*-NAT, which is naturally a *trans*-NAT of the parental gene (Figure 1.8). Evolution can then eliminate any of the NATs or tune their expression differently. More generally, the formation of any pseudogene results in complementary regions to the parental gene. If combined with elements of transcriptional control antisense to the pseudogene, these can conceivably lead to the generation of a *trans*-NAT antisense to the pseudogene that is a potential regulator of the parental gene (Muro and Andrade-Navarro, 2010).

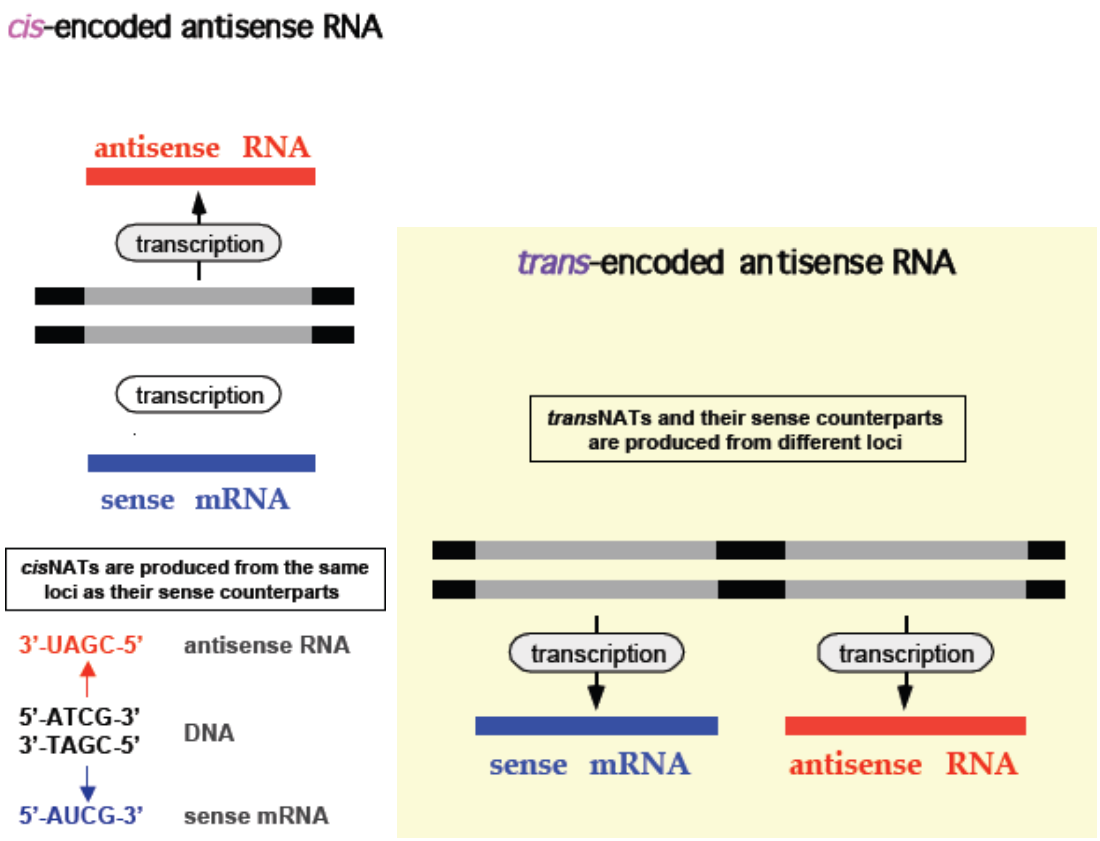

Figure 1.8 Long non-coding RNAs (A) cis-encoded natural antisense transcripts (NATs), (B) trans-encoded NATs

The vast majority of NATs belong to non-coding RNAs that may regulate the activity of sense transcripts to which they bind because of complementarity. NATs that are not located in the gene they regulate (*trans*-NATs) have better chances to evolve than *cis*-NATs (Figure 1.9), since the sense strand of the *cis*-NAT is part of a protein-coding gene. However, the generation of a *trans*-NAT requires the formation of a relatively large region of complementarity to the gene it regulates (Muro and Andrade-Navarro, 2010).

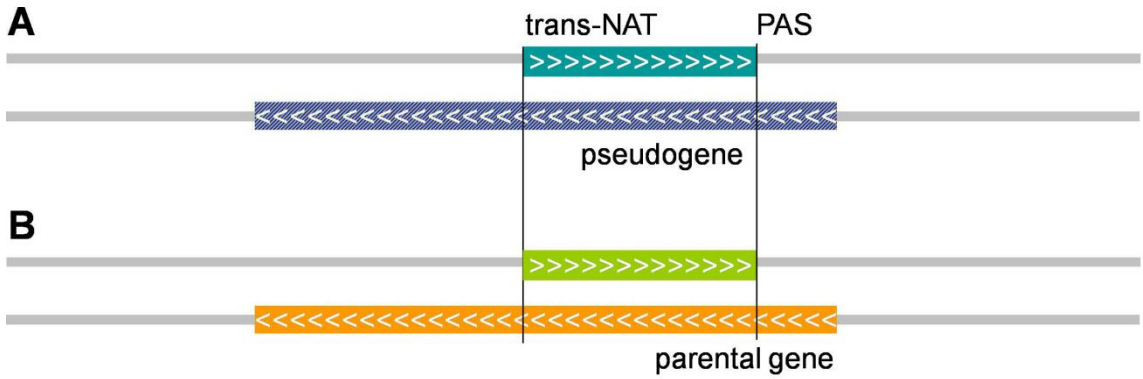

Figure 1.9 Analysis of the patterns of evolution of certain trans-NATs that are fully aligned to the parental gene. (A) Selection of transcripts with PAS and other evidence for transcription (trans-NAT, dark green box) in antisense of pseudogenes (hatched box). (B) Next, the corresponding region in the antisense of the parental gene (light green box) is obtained (Muro and Andrade-Navarro, 2010).

Non-coding RNA transcripts have emerged as an important type of regulatory molecules. It was proposed that NATs that can bind to sense RNA transcripts can modulate the level of RNA. Their generation and mechanism of action are different to those of microRNAs, which are processed into shorter 21nt products and have possibly less specific effects (Muro and Andrade-Navarro, 2010).

Three models have been proposed to explain the regulatory effects that *cis*-NATs have on gene expression. The first model proposes that base pairing between the *cis*-NATs and their complementary sense partner results in cleavage and finally degradation of the mRNA (Borsani et al., 2005). This model asserts that *cis*-NATs form a double strand RNA through their complementary sequences, which leads to the inhibition of the function of mRNAs, leading to the inhibition of protein synthesis. Many of the *cis*-NATs are head-to-head or tail-to-tail complementary to their sense-related gene (Figure 1.10); for these it is expected that the overlap region is at least 6 to 8bp to form stable double strands of RNA.

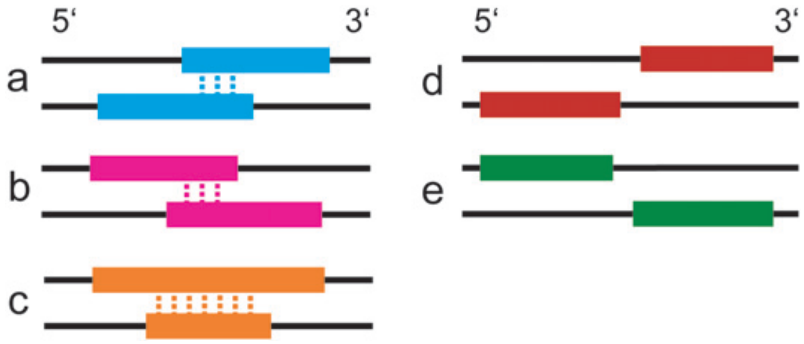

Figure 1.10 Classification of *cis*-NATs and nearby transcripts on the basis of their relative positions in the genome. (a) cis-NATs orientated in a head-to-head manner (5′-end to 5′-end), (b) those in a tail-to-tail manner (3′-end to 3′-end), and (c) those in a full-overlap manner. Full overlap describes the *cis*-NATs where a transcript on a strand of the genome is overlapped by the entire length of the other transcript on the opposite strand of the genome. (d) Nearby transcripts in a head-to-head manner where the 5′-end of a transcript is near the 5′-end of another transcript in the genome. (e) Nearby transcripts in a tail-to-tail manner where the 3′-end of a transcript is near the 3′-end of another transcript in the genome (Osato et al., 2007).

The second model involves epigenetic regulation, where NAT mediates silencing and methylation of the associated gene. Common molecular mechanisms underlie the set up of the epigenetic modifications associated with gene silencing. Of particular interest is the evidence that in some instances

transcriptional silencing is mediated by an RNA component that gives the sequence specificity to precisely target particular DNA regions. Double stranded RNA (dsRNA) molecules are required to direct histone methylation and silencing. In mammals, RNAs have been associated with chromatin silencing in the processes of imprinting (Verona et al., 2003) and X-inactivation, and more recently they have been involved in the methylation and silencing of CpG islands at autosomal and non-imprinted locations (Boumil and Lee, 2001; Tufarelli, 2006; Tufarelli et al., 2003). Another example of epigenetic regulation is the small nucleolar RNA (snoRNA). snoRNAs are a highly evolutionarily conserved class of RNAs that function as ribonucleoprotein complexes to guide the enzymatic modification of target RNAs at sites determined by RNA:RNA antisense interactions. snoRNAs are 70–120 nucleotides in length and guide the methylation of target RNAs (Figure 1.11). These RNAs were initially discovered in the nucleolus and thought to exclusively target ribosomal RNAs, but are now recognized to be a much broader class of RNAs with different functions, targets, and subcellular locations (Matera et al., 2007; Taft et al., 2009)

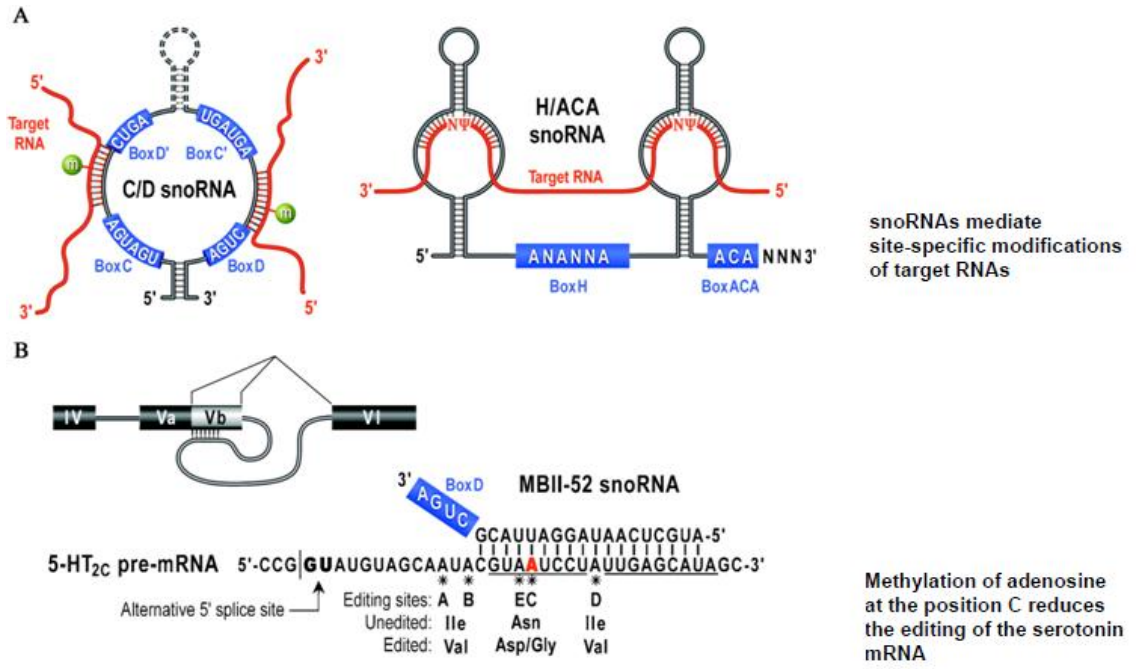

Figure 1.11 Small nucleolar RNAs (snoRNAs) guide site-specific modifications of nucleotides in target RNAs (Cao et al., 2006).

The third model is shows in Figure 1.12, which has gained favour due to recent experimental evidence, is the transcriptional collision model. When cis-NATs are transcribed by RNA polymerases, RNA polymerases bind to the upstream region of a gene encoding a sense mRNA and synthesize the complementary mRNA, moving to the 3'-end of the gene. Similarly, RNA polymerases that are bound to the upstream region of a gene encoding an antisense mRNA move to the 3'-end of the gene. Then, RNA polymerases collide with each other in the overlapping region of the genes, thereby inhibiting the transcription. Transcription is inhibited because RNA polymerases prematurely stop and their incomplete transcripts get degraded (Carmichael, 2003; Osato et al., 2007; Rosok and Sioud, 2005).

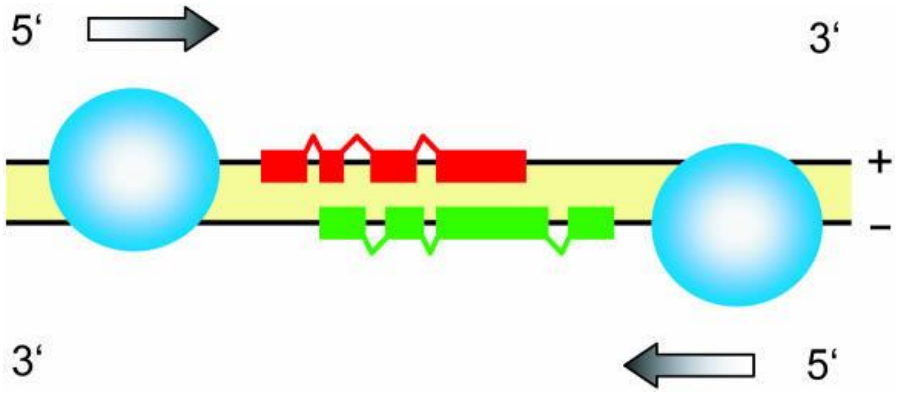

Figure 1.12 Transcriptional collision model When cis-NATs are transcribed by RNA polymerases, RNA polymerases bind to the upstream region of a gene encoding a sense mRNA and synthesize the complementary mRNA, moving to the 3′-end of the gene. Similarly, RNA polymerases that are bound to the upstream region of a gene encoding an antisense mRNA move to the 3′-end of the gene. Then, RNA polymerases collide with each other in the overlapping region of the genes, thereby inhibiting the transcription (Osato et al., 2007).

Studies of *trans*-NAT have mainly focused on small RNAs such as small interfering RNAs (siRNAs) and miRNAs, which function in a trans base-pairing mechanism with their targets and play important regulatory roles such as in mRNA degradation and translational repression (Kim and Nam, 2006). miRNAs are small, highly conserved, noncoding molecules of 18 to 24 nucleotides that regulate gene expression in a wide variety of tissues and cell types (Ambros, 2004). Silencing of the related gene occurs via mRNA degradation or interference in the translation of the mRNA (Chitwood and Timmermans, 2011). It has been found that as much as 20–30% of mammalian transcripts are targets of miRNAs, which bind to complementary mRNAs. This highlights the importance of NATs as regulators across a wide number of genes (Chen et al., 2004; Lehner et al., 2002; Osato et al., 2007).

Regulation of gene expression through RNA interference is less costly and quicker than protein synthesis. This could have given early eukaryotes an advantage during the evolution. For NATs to have a regulatory function, sense-

antisense transcript pairs should at least be co-expressed and inversely expressed. In practice, some individual sense-antisense pairs exhibit more complex and irregular patterns of expression (Ponting et al., 2009).

1.4.2. Unconventional Mechanisms Involved in the Regulation of NO Production

Dr Korneev in 1999 made a particularly important discovery of an unusual non-coding NOS-related polyadenylated RNA of 2,345 nucleotides transcribed from a NOS pseudogene (Korneev et al., 1999). The major part of the transcript exhibits >80% sequence identity to *Lym*-nNOS1 mRNA but cannot be translated into a protein due the presence of multiple stop codons in all the three reading frames. Unexpectedly, the transcript presents a region of approximately 150nt witch shows 80% complementarity to a region close to the middle of the *Lym*-nNOS1 mRNA. For this, the NOS-related RNA was then named *Lym*-antiNOS1, and was shown via stablishing RNA–RNA duplexes form in vivo (Korneev et al., 1999; Korneev et al., 2005).

The neuron-specific co-expression of the NOS1-encoding and *Lym*-antiNOS1 transcripts is strongly supportive of a role for the pseudo-NOS gene in the translational regulation of nNOS expression. However, this could only occur if the NOS1 and *Lym*-antiNOS1 transcripts form stable RNA–RNA duplex molecules. A method commonly used to detect such duplexes involves the treatment of purified cellular RNA with RNase A, an enzyme that specifically

cleaves single-stranded RNA(Korneev et al., 1999). The results of the experiment are shown in Figure 1.13

A

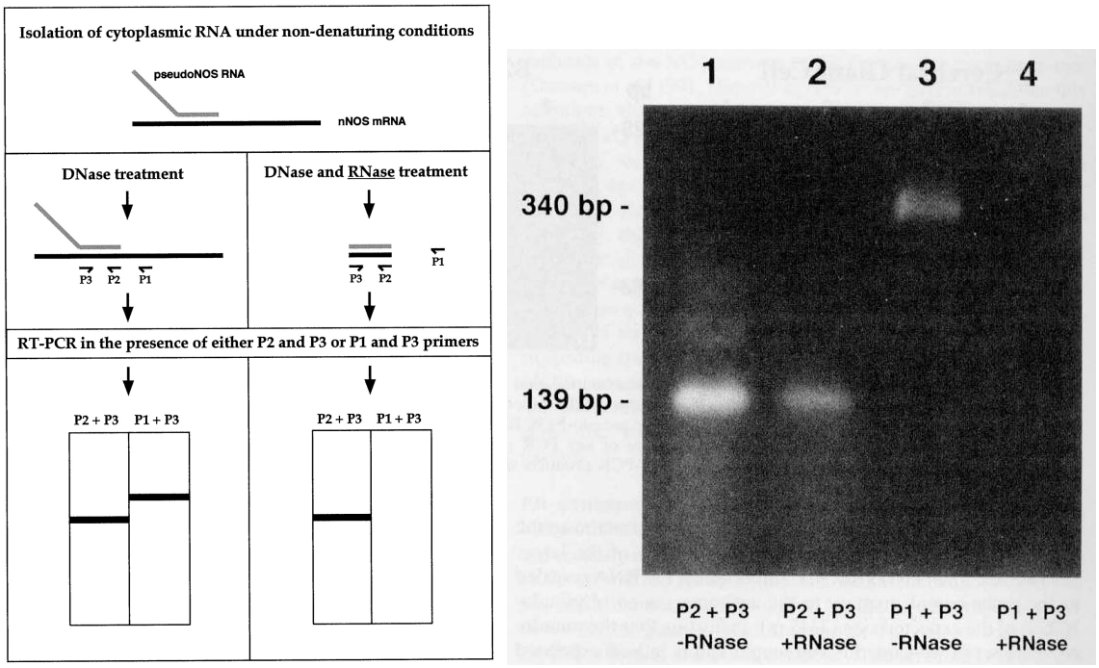

Figure 1.13 A schematic diagram showing the major steps of the ribonuclease protection procedure used to detect RNA–RNA duplexes in vivo. To preserve possible RNA–RNA hybrids, cytoplasmic RNA was purified from the CNS under nondenaturing conditions. To identify our hypothesized RNA–RNA duplex, the RNA has to be treated with RNase A, an enzyme that cleaves single-stranded but not double-stranded RNA molecules.After RNase A treatment, reverse transcription reactions in the presence of either P2 primer (located within the protected area) or P1 primer (located outside the protected area) are performed. After adding the P3 primer, a cDNA generated in the first reaction could be amplified using PCR and then will be revealed as a single band of the expected size by electrophoresis. In contrast, no cDNA could be produced in the second reverse transcription reaction, and subsequently, no PCR product is expected. In the lef t column, the predicted results of the control experiments (no RNase A treatment) are summarized. Two RT-PCR products should be detected in the reverse transcription reaction: one generated by P2 and P3 and the other by P1 and P3.(Korneev et al., 1999)

Furthermore, during the investigation of the function of the NO-signalling pathway in *Lymnaea* another NOS-related transcript was cloned. It has a polyadenylated signal and a polyA tail, characteristic features of messenger RNAs. The novel transcript of about 3,000nt in length was named *Lym*-antiNOS2 NAT (Korneev and O'Shea, 2002).

A PCR was performed on genomic DNA, which revealed that *Lym*-antiNOS2 and *Lym*-antiNOS1 were part of a separate *locus* from the related gene. A detailed sequence comparison between the *anti*-NOS locus and the *nNOS* gene (Korneev and O'Shea, 2002) indicates that an ancestral gene underwent duplication and that subsequently an inversion occurred in one of the copies; the other copy became *nNOS* gene. This comparison has revealed a clear continuous antisense homology between the central region of anti-NOS locus and a corresponding region in the *nNOS* gene. Outside of that region the similarity between the anti-NOS locus and *nNOS* gene reverts to the normal sense homology. Figure 1.14 shows the structural organization of the anti-NOS locus and the nNOS gene. The inverted part of the anti-NOS locus contains the last intron and exon of the *Lym-antiNOS2* gene, an intergenic region, and a part of the first exon of the *Lym-antiNOS1* gene. The corresponding region in the *nNOS* gene is composed of eight exons and eight introns as indicated. Below the upper bar the positions and sequences of inverted repeats which flank the inverted segment are shown.

As a result of the inversion, the exon-intron organization of the locus has been dramatically altered. *Lym-antiNOS2* RNA has acquired some sequences which are not present in the *Lym-nNOS* mRNA. Specifically the last exon in the *Lym-antiNOS2* gene is actually composed of three exons and two introns from the ancestral gene.

The DNA inversion has drastically changed the organization of one duplicate of the ancestral nNOS gene. The sequence analysis suggested a new stop codon,

not present in *Lym*-nNOS mRNA, introduced by the DNA inversion. As a consequence of this an interruption of the original open reading frame is used as a signal for the termination of translation in the *Lym-antiNOS2* RNA (Korneev and O'Shea, 2002).

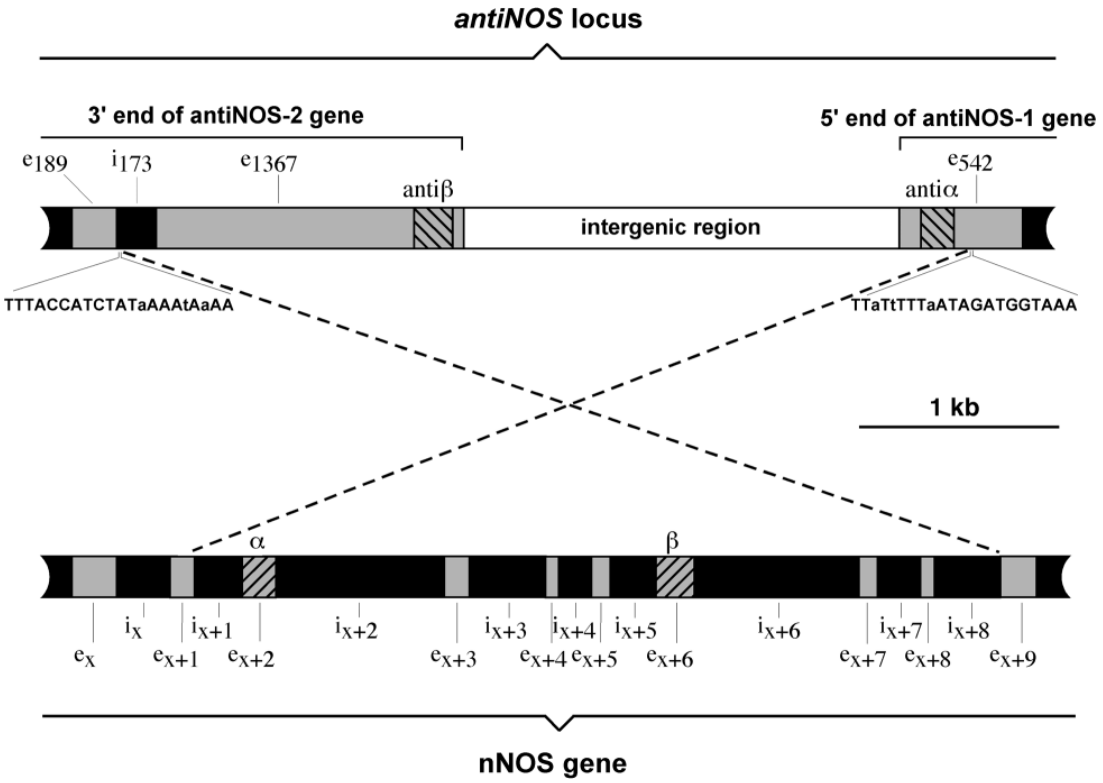

Figure 1.14 Structural organization of the anti-NOS locus and the nNOS gene. The upper bar represents a segment of the anti-NOS locus, and the lower bar shows an internal region of the nNOS gene. Introns are labelled by ''i'' and shown by black boxes. Exons are marked by ''e'' and indicated by gray boxes. Dashed lines indicate the limits of the inverted region in the anti-NOS locus and the corresponding region in the nNOS gene. The hatched boxes labelled antiα and antiβ in the anti-NOS locus and a and b in the nNOS gene correspond to the similarly labelled regions in their associated RNA molecules (Korneev and O'Shea, 2002).

1.5. Role of NO in Memory Formation

Animal behaviour is the result of interactions between organisms with its environment. Those behaviours are combinations of inborn genetically coded instructions and experience-dependent information. The ability to retain

information and modify the behaviour according to previous experience presents great advantages in adapting to new environments. Learning is defined as a process that enables an animal to generate long-lasting internal representations based on the experience. The retention of this internal representation is called memory (Dudai, 1989).

Memory is divided into two categories, *declarative* and *non-declarative*. *Declarative* memory is the ability to recollect events or facts by conscious decision. *Non-declarative* memory is a change in behaviour as an adaptive response to a previous experience; it underlies the ability to perform a learnt task or to recognise objects without conscious thought (Milner et al., 1998). Non-declarative memory, unlike the declarative one, can be studied in animal models under controlled conditions.

Simple forms of non-declarative memory can be divided in two main categories: *associative* and *non-associative*. Non-associative learning requires only one type of stimulus and it is considered the simplest form of learning, and is further classified into *habituation* (the progressive decrease of response to a non-noxious stimulus presented several times in a regular temporal sequence) and *sensitisation* (the strengthening of a response to a stimulus when it is tested after a separate non-neutral as noxious or rewarding).

Associative learning requires the explicit temporal pairing of 2 stimuli in order to associate an Unconditioned Stimulus (US), able to trigger an Unconditioned Response (UR), with a Conditioned Stimulus (CS), generally

neutral. Within the general category of associative learning there are two kinds of conditioning: classical and operant. Classical conditioning, usually referred to as Pavlov's experiment, consists of the pairing of a US with a CS, with a precise time interval between the two types of stimuli. Following conditioning the CS is able to trigger a Conditioned Response (CR) similar to the UR (Kandel, 2000). Operant conditioning is the response to learning by reinforcement of the consequences of a behaviour.

Ever since Ivan Pavlov in 1928 first described classical conditioning, researchers all over the world have been using animals where associative learning can be triggered on a single stimulus (Pavlov, 1927; Pavlov, 1951).

1.5.1. The Role of the NO-cGMP Pathway in Synaptic Plasticity and Memory

Although the first analyses of learning have been made on vertebrates, more recent studies on invertebrates have given us a more complete understanding of the cellular and molecular basis of learning and memory. Invertebrate neural networks are smaller and less complex in invertebrates than those in vertebrates. Moreover, single neurons can be identified through their morphology and electrophysiological features. Studies at the level of a single synapse have allowed to identify the molecules involved in the process of learning and memory. The first results in the identification of changes underlying learning at the level of a single synapse were achieved in the sea slug, *Aplysia californica* (Kandel, 2000).

In *Aplysia*, habituation of the withdrawal reflex correlates with, and is in part due to, depression of transmission at the monosynaptic connection between mechanoreceptive sensory neurons and motor neurons within the abdominal ganglion. Habituation-related short-term depression of the sensorimotor synapse appears to be due exclusively to pre-synaptic changes. However, changes within the sensory neuron, by themselves, do not account for more persistent depression of the sensorimotor synapse. Recent behavioural work suggests that long-term habituation in *Aplysia* critically involves postsynaptic processes, specifically, activation of AMPA- and NMDA-type receptors. In addition, long-term habituation requires activity of protein phosphatases as well as activity of voltage-dependent Ca^{2+} channels (Glanzman, 2009).

Molluscs, in particular *Hermissenda*, *Limax*, *Aplysia* and *Lymnaea,* have been extensively used for the study of associative learning. In *Lymnaea,* the feeding system has been used extensively to investigate reward-based classical conditioning. Feeding in *Lymnaea* is a rhythmic motor behaviour where repeated rasping movements of a toothed tongue or radula scrape at the surface of floating pond-weed or other food substrates leading to the ingestion of food. Sucrose acts a convenient food stimulus in the laboratory and is used as a rewarding stimulus in conditioning experiments. Lymnaea is a generalist in its feeding habits and it is advantageous for it to learn about potentially useful foods using a variety of sensory modalities. In chemical conditioning experiments, snails successfully learn even with only a single trial (Alexander et al., 1984). In this thesis, amyl acetate is the CS and sucrose the rewarding US

and pairing these two chemical stimuli results in a feeding response to the CS when applied in the post-training test elicited more rasping movements. One-trial conditioning only works in snails starved for 4 or 5 days. A single pairing of amylacetate and sucrose in starved snails results in a long-term memory (LTM) trace that lasts for at least 19 days, a remarkable example of associative learning (Benjamin, 2010). In *Lymnaea* it was observed that PKA (protein kinase A enzyme), CREB (cAMP response element-binding protein) and NOS/NO are selectively activated/upregulated by the associative training protocol, so potentially each of these factors could be sufficient for memory consolidation. Also, the prevention of MAPK phosphorylation after training blocks LTM and shows that MAPK is necessary for the consolidation of associative LTM after single-trial reward conditioning. It is likely that these and other signalling molecules make a synergistic contribution to the memory consolidation process, with each molecule and pathway playing an important role in LTM but neither of them alone being sufficient for its consolidation (Kemenes, 2008).

Interestingly, early inhibition of protein synthesis (inhibition of PKA catalytic subunit activity) does not block the expression of memory at 6 hours post-training (Kemenes et al., 2006a), indicating the involvement of a different signalling molecule, possibly CaMKII, in the protein synthesis dependent consolidation of this earlier memory trace (Wan et al., 2010).

In isolated cerebral ganglia, stimulation with the adenylate cyclase activator forskolin resulted in massively increased CREB phosphorylation in neuronal nuclei, indicating a potential link between training-induced PKA activation in

the cerebral ganglia and CREB phosphorylation in conditioned animals (Ribeiro et al., 2003). Additional support for the role of NO as a neurotransmitter was provided by evidence that NO activates the soluble form of sGC in the brain, resulting in the synthesis of a second messenger, cGMP (Ribeiro et al., 2010). Figure 1.15 provides a summary of published data on the known molecular requirements for the early and late phase of the consolidation of long-term memory after single-trial classical conditioning in *Lymnaea*. It is interesting to note that the requirement for PKA and NO outlast the requirement for protein synthesis indicating that these molecules are required for some as yet unidentified transcription and translation independent processes underlying memory consolidation in the 1h to 6hr post-training time window (Benjamin, 2010).

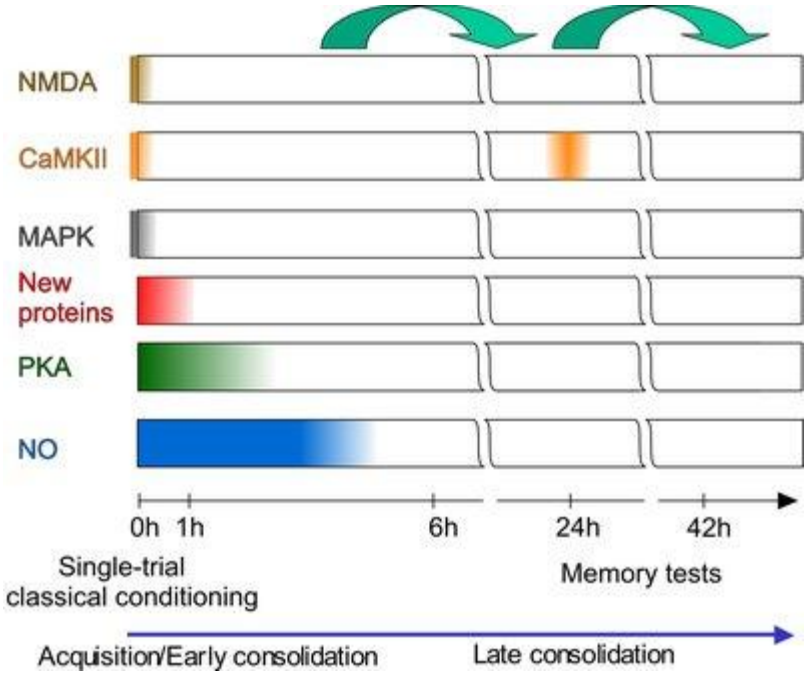

Figure 1.15 Time windows of known molecular requirements for LTM after single-trial food-reward classical conditioning in Lymnaea. The large curved arrows indicate the requirement for the activation or synthesis of molecules in the 0h to 6h (acquisition/early consolidation) and 24hr time window (late consolidation) for memory expressed at 24 hr and 42 hr, respectively (Benjamin, 2010)

A review of molecular mechanisms of memory storage in *Aplysia* (Hawkins et al., 2006) shows a simplified model of long term memory formation (Figure 1.16). This model describes how neurotransmitters release and activate AC (adenylyl cyclase), which in turn leads to the elevation of cAMP levels in the neuron terminals. The cAMP-activated PKA phosphorylates a K^+ channel, causing it to close, and this leads to an action potential and consequently to an increase in Ca^{2+} influx. The increase of Ca^{2+} increases in turn transmitter release. 5-HT causes an elevation of cAMP levels, resulting in the translocation of PKA and MAPK into the nucleus. In the nucleus MAPK will activate transcriptional factor CREB protein, activating several genes, and this leads to long term changes in the neuron underlying long-term memory formation. It has been

shown that learning-induced a decrease in chloride conductance result in depolarization that increases baseline levels of intracellular calcium in the CGC (Kemenes et al., 2006b). But further experiments will need to be performed to establish if this also happens in the CGCs after classical conditioning. This supports synaptic growth and the formation of new synapses for the activation of pre-existing silent synapses, and self-perpetuating mechanisms and the molecular basis of memory persistence (Benjamin et al., 2005).

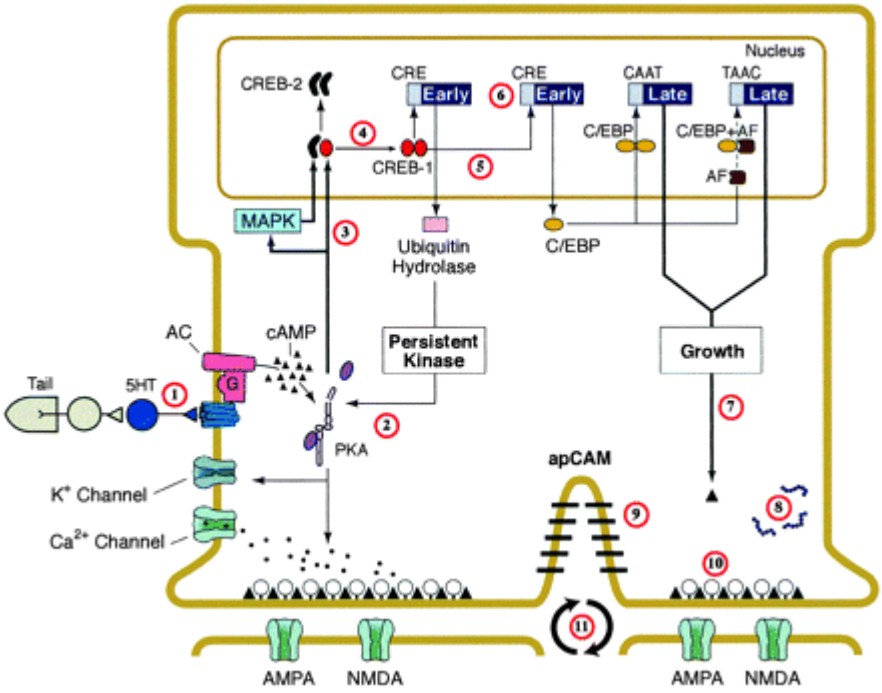

Figure 1.16 Mechanisms of long-term memory formation. Long-term synaptic plasticity contributing to learning involves a sequence of cellular and molecular mechanisms. (1) neurotransmitter release and short-term strengthening of synaptic connections, (2) equilibrium between kinase and phosphatase activities at the synapse, (3) retrograde transport from the synapse to the nucleus, (4) activation of nuclear transcription factors, (5) activity-dependent induction of gene expression, (6) chromatin alteration and epigenetic changes in gene expression, (7) synaptic capture of newly synthesized gene products, (8) local protein synthesis at active synapses, (9) synaptic growth and the formation of new synapses, (10) activation of pre-existing silent synapses, and (11) self-perpetuating mechanisms and the molecular basis of memory persistence. The location of these events, which may act in part to stabilize some of the changes that occur during short- and intermediate term plasticity, moves from the synapse (1–2) to the nucleus (3–6) and then back to the synapse (7–11). (Hawkins et al., 2006).

Many studies have demonstrated that the NO-cGMP-PKG signalling pathway is critical for memory formation. It is thought that the increase of Ca^{2+}-activated calmodulin causes the activation of nNOS, leading to the production of NO (Halvey et al., 2009; Roy and Garthwaite, 2006). In *Lymnaea,* consolidation of the 24-hour memory trace following one-trial chemical conditioning was shown to be dependent on the NO-cGMP-PKG signalling pathway (Korneev et al., 1999). There is a critical period of sensitivity up to 5 hours after conditioning when blocking this pathway by drug injection prevents behavioural LTM formation (Kemenes et al., 2002).

Further evidence for a role of NO in LTM comes from experiments on the CGCs. These neurons express mRNA transcripts from the two related nNOS genes (*Lym*-nNOS1 and *Lym*-nNOS2). Six hours after chemical conditioning, *Lym*-nNOS1 is up-regulated compared with controls. This up-regulation of the NOS coding transcript may be due to an earlier down-regulation of *Lym*-antiNOS1 at 4 hours, which is known to be inhibitory of NOS transcript production. As with many other aspects of NO signalling, in memory formation it can be traced from the beavioural to the network and single neuron level (Kemenes, 2008; Korneev and O'Shea, 2007). NO is known to modulate the strength of serotonergic transmission between the CGCs and motoneurons in the feeding system and this could be involved in conditioning (Kemenes et al., 2011).

1.6. Role of nNOS During Embryonic Development and Neurogenesis

In the mouse, both an excess and a depletion of NO have been shown to arrest embryo development (Tranguch et al., 2003). Similarly, recent studies show that artificially decreased NO levels in the brains of developing tadpoles lead to an increase in size and a proliferation of brain cells, leading to larger than normal brains. Conversely, when NO levels were artificially increased, brain cell proliferation decreased, and the resulting brains were smaller than normal (Peunova et al., 2007).

NO has also been demonstrated to be a physiological inhibitor of neurogenesis in adult subventricular zone and the olfactory bulb. Mice treated with an inhibitor of nNOS exhibit an increase in the number of mitotic cells in the subventricular zone, the rostral migratory stream and the olfactory bulb, but not in the dentate gyrus. However, recently inhibition of nNOS has been shown to be capable of enhancing progenitor cell proliferation in the dentate gyrus in normal and in ischemic brain, and NO administration has been reported to promote neurogenesis (Corsani et al., 2008; Zhou et al., 2007).

NO levels must be tightly regulated for normal embryo development to occur and thus the mRNA of multiple NOS isoforms must be expressed in embryos to support adequate levels of NO production.

Evidence from foetal learning paradigms of classical conditioning, habituation and exposure learning reveal that the foetus can form memories.

Possible functions discussed are: practice, recognition of and attachment to the mother, promotion of breastfeeding, and language acquisition (Hepper, 1996). Researchers from the Netherlands reported that human foetuses were observed to form memories from at least 30 weeks old (Dirix et al., 2009).

Expression of nNOS was first seen in rodent embryos by (Santacana et al., 1998) The expression of nNOS during the development of the rat cerebral cortex from embryonic day E13 (gestation period 21 days) to postnatal day P0 was analyzed by immunocytochemical procedures using a specific antibody against rat brain nNOS. Expression of nNOS was first seen on E14 located in the marginal zone. Neuronal NOS immunoreactivity persisted in this layer throughout the embryonic period and only began to decrease on E20 and disappear with neuronal migration. From E17 onwards, migrating neurons expressing nNOS were observed in the intermediate zone with their leading processes directed towards the cortical plate. At the same time, efferent nNOS-immunoreactive axons originating from cortical plate cells entered the intermediate zone. From E19 onwards, cells expressing nNOS and with the morphological characteristics of migrating cells were observed in and near the subventricular zone (nNOS-positive cells leaving the subventricular zone were not glial cells). Commissural, callosal and fimbrial fibres were seen to express nNOS on E18 and E19. A very interesting result was the decreased of nNOS expression from E20 leading to a very weak signal on E21 and P0. The observations suggest that NO is synthesized during embryonic life in relation to maturational processes such as the organization of cerebral lamination, and is

involved in controlling migrational processes and fibre ingrowth (Santacana et al., 1998).

Further research was conducted on the expression of nNOS during the development of the rat optic vesicles from embryonic day E13 (gestation period 21 days) to postnatal day P0. It was shown that nNOS is first seen at the E14 stage, and it begins to decrease on E20. Therefore NO synthesis was directly linked to embryonic life, in relation to maturational processes in optic vesicles (Nobakht et al., 2007). Other results show that NOS1 (nNOS) is first expressed in mice in extrinsic nerve fibres reaching areas of vascular development at E16, and in the vomeronasal nerve at E15 (Zancanaro et al., 2002).

In human embryos, nNOS-immunoreactive cells appear as early as 18 gestational weeks (GW) in the subcortical plate and then increase predominantly in the subcortical white matter during the fetal period, while weakly immunoreactive neurons were found in the cortical II–IV layers after 26GW. In the basal ganglia, immunoreactive neurons could be detected in the striatum as early as 13GW, and then showed a transient increase with peaks at 23–24GW and 33–36GW in the putamen and caudate nucleus, respectively. In the cerebellum, immunoreactivity was detected in the Purkinje and basket cells after 23GW and 31GW, respectively. The immunoreactivity of internal granule cells was constantly weak. In the brain stem, constant and intense immunoreactive neurons were found in the central gray, pedunculopontine tegmental nucleus, solitary tract nucleus, and lateral reticular nucleus. The immunoreactivity in the neurons of the pontine nucleus and inferior olivary

nucleus was transiently increased, with peaks at 38–40GW and 23–24GW, respectively. This characteristic nNOS development of expression suggests that transient nNOS hyperproduction may contribute to neuron maturation as well as vulnerability in each period and region, and NO may play an important role in the basic development of human brain functions (Ohyu and Takashima, 1998).

1.7. Thesis outline

This thesis addresses the following major questions: What are the physiological functions of the NOS-related antisense RNAs in *Lymnaea*? What are the characteristics and possible functional roles of NOS-related antisense RNAs in mammals?

To answer these questions a multidisciplinary approach was employed. This comprises:

- A detailed sequence analysis of *Lym-antiNOS2* RNA.
- A study of the localization of *Lym-antiNOS2* RNA in *Lymnaea* CNS.
- An investigation into whether memory formation causes changes in the expression of *Lym-antiNOS2* RNA.
- A detailed sequence analysis of a novel NOS-related mouse *cis*-NAT (Mm-*antiNOS1* RNA).
- A study of the expression of *Mm-antiNOS1* RNA during mouse development.

Chapter 2: Materials and Methods

2.1. Animal Maintenance

Laboratory-bred stocks of *Lymnaea stagnalis* were raised in the Sussex University animal house. Snails were kept in holding tanks containing copper-free tap water at 19-21°C on a 12-hour light-dark cycle. Snails were fed lettuce three times a week and vegetable-based fish food twice a week.

2.2. Behavioural Experiments

Before behavioural conditioning experiments, snails of similar weight and age (3-6 months) were selected from home tanks and placed in smaller laboratory tanks containing copper-free tap water (10 snails per tank).

Behavioural experiments were performed to train the animals with a classical conditioning protocol. The experiment used three groups of animals starved for 3 days: paired (P), unpaired (UP) and naïve (N) groups.

The animals of the P group were left in a Petri dish with 90ml of Cu-free water for at least 10 minutes to acclimatise, before adding 5ml of Cu-free water to the dish, using a 10ml syringe. After 15 seconds, 5ml of copper-free water were added; this served to balance the temporal pattern of disturbance between the trained and control groups. The animals were moved to a tank with Cu-free water after 2 minutes. They were kept for 50 minutes in the tank and moved to a Petri dish containing 90ml of Cu-free water, where they were left for at least 10 minutes. 5ml of amyl acetate 21.6mM in Cu-free water were then added to

the dish. 15 seconds later, 5ml of sucrose (S) 0.4 M were added. The animals were moved out from the Petri dish and left in a tank for 10 minutes, 1 hour, 4 hours or 6 hours, in accordance with the protocol described in Section 4.4.

The animals in the UP group were treated in the same way, but the two chemical stimuli were not paired. Snails from this group were placed in dishes containing 90ml of water and allowed to acclimatise for 15 minutes. 5ml of amyl acetate were added, followed 15 minutes later by 5ml of water. After being left in the dish for a further 2 minutes, snails were returned to a laboratory tank for the next part of the control trial for 50 minutes. The snails were placed in new dishes containing 90ml of water and left to acclimatise. The snails were presented with 5ml water followed 2 minutes later by 5ml of sucrose solution. The snails were left in tanks before dissection.

The animals in the naïve (N) group were kept under the same conditions and had the same feeding regimen as those in the P and UP groups, but were not exposed to either trial.

A randomly chosen subset of 18 animals from each group (N, UP, P) was retained and tested for LTM formation at 24 hours after the paired (P) and unpaired (UP) trial (Kemenes et al., 2002).

2.3. General Dissection

Using large forceps the shell was removed to free the foot. Holding the snail from the remaining shell and using large scissors the foot was cut off from the remaining shell which contains the majority of the organs. The foot was placed

into a large Sylgard Petri dish with normal saline and pinned out using two large pins.

A vertical incision through the head was made so that the buccal mass was exposed, and the flaps remained pinned out with smaller pins. After inserting the bent pin through the buccal mass and pushing it forward into the Sylgard, the brain was exposed.

The oesophagus and the two feeding ducts were cut and the penis pinned out for better view. The brain was finally isolated by holding it from the main nerves and cutting off all nerves (maintaining the buccal ganglia intact) as shown in Figure 2.1. In *Lymnaea stagnalis* the shell length ranges from 2 to 6cm, and although the dimensions of central nervous system are small, the cells are highly pigmented and clearly visible (Chase, 2002).

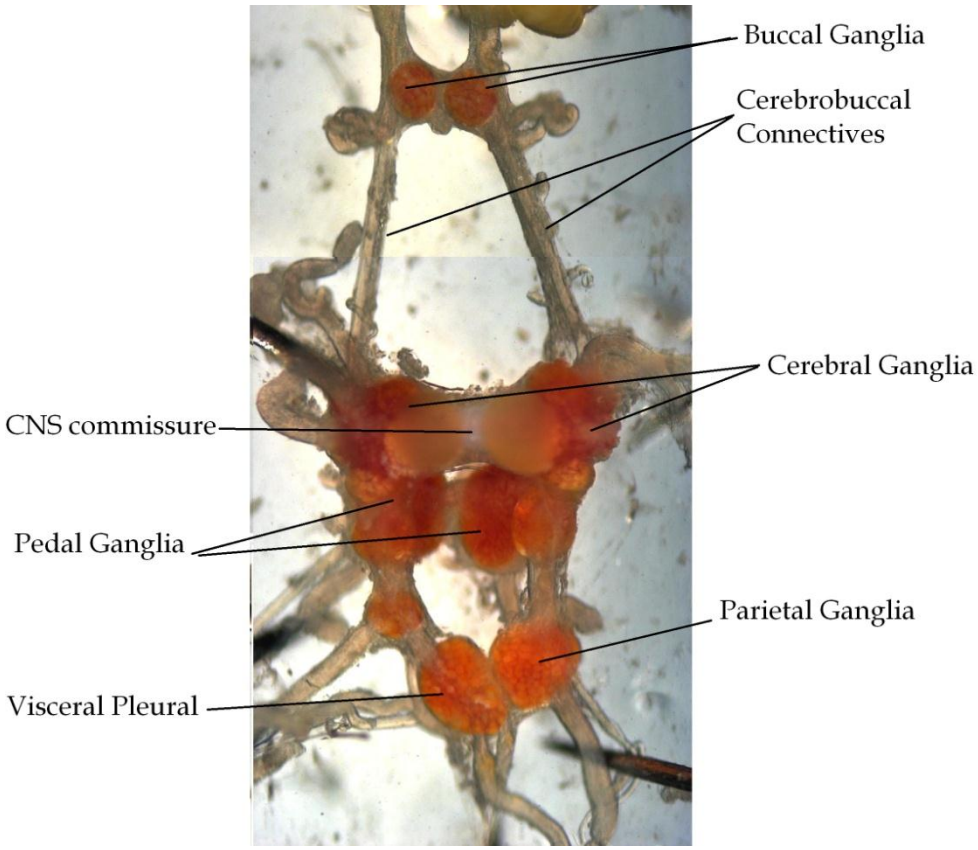

Figure 2.1 *Lymnaea stagnalis* isolated intact brain pinned out in a Sylgard Petri dish.

2.4. RNA Isolation and Purification from *Lymnaea stagnalis* Brain Tissue

After dissection the brains were placed in a sterile Eppendorf tube in ice. Different Absolutely RNA kits (Stratagene**)** were used to extract RNA depending on the amount of material:

- Total RNA from relatively large amounts of material (calibrator cDNA from 5 *Lymnaea stagnalis* brains) was extracted using Absolutely RNA Miniprep Kit reagents and manufacturer's protocol.
- Total RNA for small amounts of material (quantitative PCR) was extracted from a single *Lymnaea stagnalis* brain, and single ganglia of *Lymnaea stagnalis*

brain using Absolutely RNA Microprep Kit reagents and manufacturer's protocol.

For the two cases above, the following protocol was conducted. 100µl lysis buffer–β-ME mixture was added to the brain sample and blended. The sample was disrupted by adding 600µl of homogenisation buffer (containing guanidine thiocyanate and 1% β-mercaptoethanol). 700µl of ethanol 70% was added to provide appropriate binding conditions and the sample was then applied to a silica-gel based column, spun 30 seconds at 11,000g and the flow-through discarded. To avoid genomic DNA contamination a DNA digestion step was performed by adding a 95µl DNase reaction mixture containing 10% of RNase-free rDNase in rDNase reaction buffer to the column. The reaction was incubated at room temperature for 15 minutes.

The column was washed several times with ethanol-based buffers to eliminate the contaminants and the flow-through discarded. The column was transferred into a clean tube and incubated for 2 minutes at room temperature, after which it was eluted by centrifugation for 2 minutes at 11,000g with a volume of 30µl nuclease-free water. The procedure was repeated once more with another volume of RNase-free water. The samples were stored at –80°C until further processing.

2.5. RNA Extraction from Single Identified Neuron

Total cellular RNA from single identified CGC was extracted using the Absolutely RNA Nanoprep Kit (Stratagene) according to the manufacturer's instruction manual. RNA was dissolved in 10µl of RNase-free water.

2.6. DNase Treatment

One widely appreciated property of some gastropod neurons is their large size – they are usually referred to as giant neurons. CGCs in *Lymnaea* belong to this category. The size of the soma can be attributed to the summed metabolic demand of the axonal and dendritic tree associated with synaptic function. To satisfy these metabolic requirements, the nuclei of the giant neurons can contain more than 0.2µg of DNA. This is more than 200,000 times as much DNA as the haploid amount found in sperm (Lasek and Dower, 1971).

To avoid genomic DNA contamination from the multiple copies of DNA existent in the CGC, an extra DNA digestion step was performed using TURBO DNA-free™ Kit (Ambion) reagents and manufacturer's protocol.

1µl 10x TURBO DNase Buffer and 1µl TURBO DNase were added to the RNA extracted (Section 2.5) and mixed gently. The mixture was incubated at 37°C for 45 minutes. After the incubation, 1µl of resuspended DNase Inactivation Reagent was added and mixed well, left for 5 minutes at room temperature and centrifuged at 10,000g for 1.5 minutes, finally transferring the RNA to a fresh tube.

2.7. RNA Precipitations

The total DNA-free RNA (Section 2.6) was precipitated to eliminate any impurity (as DNase Inactivation Reagent) that could inhibit PCR enzymes. Sodium acetate was added to the RNA samples (0.2M final concentration) along with an equal volume of isopropanol, and 1µl of Pellet Paint. The mix was incubated for 1 hour at -20°C followed by 10 minutes centrifuge at 13,000g. The soluble was discarded and 100µl cold 80% ethanol was added to the remaining pellet, followed by centrifugation for 5 minutes at 13,000g. The solution was discarded and the pellet dried for 5 minutes at room temperature. The pure pellet was dissolved in 10µl of nuclease-free water.

2.8. Quantification of Total RNA

The concentration of RNA in a sample was checked by the use of UV spectrophotometry. Both RNA and DNA absorb UV light very efficiently making it possible to detect and quantify either at concentrations as low as 2.5ng/µl. The nitrogenous bases in nucleotides have an absorption maximum at about 260nm. For a given RNA or DNA solution, the ratio [A260/A280] of absorbency readings at 260nm and 280nm provides an estimate of purity of the nucleic acid. Pure preparations of DNA and RNA have ratios of 1.8–2.0.

For quantifying DNA or RNA, readings were taken at wavelengths of 260nm and 280nm. The reading at 260nm allows calculation of the concentration of nucleic acid in the sample. An optical density (OD) of 1 corresponds to a concentration of 50ng/µl of dsDNA, 33ng/µl of ssDNA or 40ng/µl of RNA.

Samples were typically diluted 1µl in 100µl (a dilution factor of 100) and put in a 100µl spectrophotometer cuvette. The RNA concentration will then be calculated as:

$$Molarity = \frac{\text{OD260 x 40ng}}{\text{µl x dilution factor}}$$

where OD260 is the absorbance of oligonucleotide solution at 260nm.

2.9. First Strand Synthesis of cDNA

The iScript cDNA Synthesis Kit (Bio-Rad) was used to synthesize first-strand cDNA from total RNA. 4µl of 5x concentrated Reaction Buffer, 1µl of iScript Reverse Transcriptase and up to 1µg total RNA were added into a PCR Eppendorf tube. Water was added to take the final volume of the reaction to 20µl. The reaction was mixed gently and the sample was incubated for 5 minutes at 25°C and then incubated 30 min at 42°C, followed for 5 minutes at 85°C, and held at 4°C until storage at -20°C. Reactions were carried out in a G-STOM GS1 Thermal Cycler equipped with a heated lid.

2.10. Oligonucleotide Primer Design

Previous results on single isolated CGC RT-PCR RNA expression (Korneev and O'Shea, 2002) show that *Lym-antiNOS2* is not expressed in the CGCs. These results were obtained using the primers complementary to the sequences shown in Figure 2.2 in yellow background (forward) and light-blue background (reverse). The PCR product expected for those primers is an amplicon of 652bp. Since these studies, the availability of more efficient enzymes and kits, and a re-

design of the primers to generate smaller amplicon length product, allows for more efficient reactions.

The oligonucleotide primers used in this study were designed using aligned fragments of *Lym-antiNOS2, Lym*-n*NOS1* and *Lym-NOS2* genes taken from GenBank. The fragments were aligned using the computer program ClustalW2 from the European Bioinformatics Institute and are predicted to amplify a 119bp fragment (Figure 2.2).

Figure 2.2 Lym-antiNOS2 RNA sequence. PCR amplification fragment is shown in red letters. Scorp 1 and 2 positions in the cDNA sequence are shown in orange and green background. Scorp 3 and 4 (used in previous papers) are shown in yellow and light blue. The open reading frame is surrounded by dotted lines; full-line boxes show start and stop codons. The antisense homology sequence between Lym-antiNOS2 RNA and Lym-nNOS mRNA is shown in bold. The sense homology between Lym-antiNOS2 RNA and Lym-nNOS mRNA is indicated in grey background.

2.11. Reverse Transcription PCR

All the reactions were carefully prepared using autoclaved tubes and autoclaved disposable pipette tips in order to avoid contamination of the samples. The reagents used were aliquoted to prevent degradation by repetitive thawing/freezing cycles. Oligonucleotide primers employed in the reaction were synthesized by Eurofins MWG Operon and supplied in lyophilised form. In the laboratory, the primers were resuspended in molecular grade DEPC-treated deionised water to a concentration of 100µM.

The PCRs performed in order to isolate the *antiNOS2* gene in *Lymnaea stagnalis* were carried out in a volume of 25µl consisting of 0.5µl 200µM dNTP, 2.5µl 10x PCR Buffer HotStarTaq (10x concentrated; contains Tris-Cl, KCl, $(NH4)_2SO_4$, 15mM $MgCl_2$; pH 8.7), 5µM of each pair of primers and HotStarTaq DNA Polymerase 0.125µl 0.625 units/reaction (QIAGEN), 4µl cDNA and nuclease-free water. Amplifications were carried out in a G-STOM GS1 Thermal Cycler equipped with a heated lid.

All reactions were initially denatured for 15 minutes at 95°C (HotStarTaq DNA Polymerase is activated by this heating step) then 1 minute at 94°C denaturation, 1 minute at 53-57°C annealing and 1 minute at 72°C elongation. The last three steps were repeated 35 times in total, followed by a final extension step of 1 minute at 72 °C.

RT- negative controls were set up alongside each set of PCR reactions to ensure that there was no contamination. Negative controls consisted of all components of the PCR reaction excluding the reverse transcriptase.

Each reaction was optimised in order to create the right conditions for the amplification of the targeted fragment. This included varying the oligonucleotide primers used and the amount of cDNA, as well as the cycling strategy of annealing and extension temperatures.

2.12. Agarose Gel Electrophoresis of DNA

Agarose gel electrophoresis was performed using a BRL model H5 horizontal system for submerged gel electrophoresis. 0.3g of agarose (Promega) analytical grade was melted in 30ml TBE electrophoresis buffer (45mM Tris-borate, 1mM EDTA) 1% agarose gel by boiling in a microwave oven. The solution was cooled to approximately 60°C and ethidium bromide was added to a final concentration of 0.8µg/ml and mixed thoroughly. The agarose was then poured into the holding tray ensuring that the teeth of the Teflon comb were immersed, and allowed to set for approximate 30 minutes at room temperature prior to removal of the comb and submerging into the electrophoresis buffer in the tank. The samples to be loaded were first mixed with Bromophenol Blue Loading Solution (Promega) to a final concentration of 10% and then loaded into the wells of the gel. A 100bp molecular weight ladder (Invitrogen) was also loaded into the gel in order to size the DNA fragments. A current of 90 volts was then

applied to the gel and stopped when the dye had migrated two thirds of the distance through the gel.

Gels were examined on a GeneFlash UV transilluminator (Syngene) and photographed using a UP-895 video graphic printer (Sony).

2.13. Isolation of Cerebral Giant Cells

All dissection instruments were carefully cleaned with 70% ethanol and wiped with RNaseZAP (Sigma-Aldrich). Snail saline (NaCl 50mM, MKCl 1.6mM, $MgCl_2.6H_2O$ 2mM, $CaCl_2.6H_2O$ 3.5mM, HEPES 10mM) was prepared using autoclaved tubes, autoclaved disposable pipette tips and autoclave distilled water in order to avoid contamination. Snail saline was filtered using a pressure-driven filtration device (syringe-driven filter Millex-GP, 0.22μm).

Animals were dissected under a microscope in a Sylgard-coated Petri dish containing snail saline (Section 2.3). The CNS was exposed by a dorsal body incision and isolated by severing all peripheral nerves. Where the brain was cut away from the buccal mass, a short-length of oesophagus was retained which serves as a useful anchor-point for pinning the preparation. The isolated CNS was placed in a small Sylgard-coated dish containing snail saline. The CNS commissure was cut and the brain pinned down flat to the Sylgard. The brain was incubated for 15 minutes in protease type V111 (1mg/ml in snail saline) and then washed three times in snail saline. The brain was incubated for 30 minutes in propylene glycol (50% in snail saline) at 20^{o}C (room temperature).

While the brain was being incubated, a dissection dish and a suction pipette were filled with high osmolarity saline (30mM glucose in snail saline).

The CGCs were identified by position, colour and size. Once a CGC is identified, the CGCs were bored with glass microelectrodes constructed with a tip diameter of about 10μm, which were fire-melted until round and capped. The glass microelectrode was advanced into the CGC with the state-of-the-art micromanipulators under a stereoscopic microscope, without damaging the soma. The glass microelectrode pipette was connected to a suction system (micrometer syringe 0.2ml, Gilmont) and carefully placed on top of the neuron to slowly suck out the neurons and place them into a microtitre plate.

After placing the neurons on the plate, as much liquid was sucked off the microtitre plate as possible, and the plate was immediately placed in a freezer at –80^{o}C.

2.14. *In situ* Hybridisation

Each brain was pinned out onto Sylgard squares using fine dissection needles (A1) and cut across the cerebral ganglia to flatten the brain out, and fixed immediately following dissection.

The Sylgard squares were immediately placed in 4% paraformaldehyde in 0.2M phosphate buffer (pH 7.2) for 1 hour. After 1 hour the squares were transferred (without wash) into a solution of 30% sucrose in phosphate buffered saline and left overnight at 4°C. This step causes the tissue to swell and prevents it from fracturing out during the freezing process.

The brains were removed from the Sylgard blocks, carefully soaked in a small amount of OCT embedding medium (Raymond Lamb), placed on a metal plate (making sure that the brain is absolutely flat) and surrounded with metal bars to form a square container. The container was filled up with OCT embedding medium. This preparation was lowered gently using a holder onto liquid nitrogen until the brain was frozen completely. The contents of the container were carefully removed from the bars and plate and positioned onto a microtome chuck so that it was level with the chuck, and transferred for storage at -22°C.

After making sure that the crystal blade was cooled down to the correct temperature, the brains were cut into14µm-thick frozen sections.

Sections were mounted on SuperFrost Plus slides (VWR); these slides are suitable for *in situ* hybridisation and have good binding properties with the tissue. The slides were air-dried for at least 30 minutes, and used straight away or stored at -70°C until hybridisation.

GreenStar DIG-hyperlabelled 48-mer oligonucleotide antisense and sense (control) probes were produced by GeneDetect (Auckland, New Zealand). The antisense probe contains three oligonucleotides. The first oligonucleotide was designed to bind at the 5′ end of the sequence (nucleotides 104-183, a short section within the sense homology region showing no homology with the other sequences), closely before the open reading frame for *Lym-antiNOS2*. The other

two oligonucleotides were placed after the open reading frame on the region without homology with the other three sequences (nucleotides 1554 - 2557).

Oligonucleotides mix for *Lym-antiNOS2* RNA probe:

Complementary to nucleotides 101-148:

5′CCATGATTGAACTGCCTGAACACTGCCGATTTCCGTCACGTTAGGCTC3′

Complementary to nucleotides 2044-2091:

5′CGATTGCACACCTCGATCACTCAACATTGTCCAACATTGTGACTTGAT3′

Complementary to nucleotides 2410-2457:

5′ATTTGGGCGTTGTCAAGGGTGTATGATTATCGCGACTGTTGAGTTGGC3′

The localization of these oligonucleotides within the sequence is shown in orange in Figure 2.3.

```
   1 GGGGTGACCA GCTACCTGTA GGGGTGACCA GCTACCTGTA GGGCCATAGA AACAATTTTC
  61 CGGTTTAGGG TGAGTNTTAC TGCTTTCTGA TAATCTTTCA GAGCCTAACG TGACGGAAAT
 121 CGGCAGTGTT CAGGCAGTTC AATCATGGNT TGCCCGTACC GGTCGGCCAA GCTGAAAAAT
 181 GTGCTGAATG ATAAGACTTA TGTGGACACG NTTACACCAG AGATCATTTT CGCCAGTTAC
 241 CTTGCAACAC CCAGCGATGC ATGGGCTCAC TTATGTCCCA ACAGGCAAAT AGGCCCCCTG
 301 GGGTCCCTAG ATCACAGGAG GAACTTTTGG TTCACGCCAC AGGCTTCATT GACCAATATT
 361 TAAACTCATG TGAAATGACA TTCCTGTCCA GGAGCAACAC ACCGGCCCAT TTGAATAGAC
 421 TTAGCGAGAT CCAAGATTAT GTGACAAAGT CCGGTACCTA TGACCTGACA ATGGCTGAAC
 481 TGACATTTGG TGCTAAGCAA GCTTGGAGAT ATGCGTCCAG ATGCACTGGC AGAATGCAGT
 541 GGTCAAAACT TCAGGTTGTT GATGCCAGAT GCATCATGAC ACCCCGAGGG ATGTATACAG
 601 CTTTGTGCGA TCACATCAAA TATGGGACAA ACAAAGAGAA TATTAGGTTT GCCATCACCA
 661 TATTTCCACA ACGAATAGAA GGGCCCCCNG ATTTCCGTGT ATGGAATAGT CAGTTGATAG
 721 GCTACGCTGG CTACAGTATG GATGATGGGA AGATTATTGG GGACCCAGCC AATGTGGAAT
 781 TTACTGATCA ATGTGTAAGG ATGGGTTGGA AACCAAAGTA TGGTATGTTT GACCCATTTC
 841 CACTGGTTCT GTCTGCTGCT GGATTTGATC CTGAAGTTTT CGACCTCCCA CCTGAGCTAG
 901 TGTTAAAGGT CAAGTTGGTG CATCCCGAGA ATCCCTCGTT TTCTGATATT GGTCTAAAAT
 961 GGTACGCCCT ACCAGCTGTA TCTGGAATGC TGTTGGACTG TGGGAGCCTG GAGTTCCCCT
1021 CGTGTCTTTT CAATGGATGG TACATGGGGA CAGAGATTGG TTCCAGGGAT TTGTGCGATT
1081 CTCATAGGTA CAACATGCTG GAGACCATTG CCTTAAAGAT GGGGCTAAAC ACCAGAAATG
1141 CTTCATCCTT GTGGAAAGAT CGTGCACTAT TGGACGCTAA TCCTGCTGTT CTCCACAGTT
1201 TTCAGTCAGC CAATGTTACA ATTGTCAATC ATCACGATGC CAGTGAGTCT TTAATGTTGC
1261 ACTTGGATAC TGAGCAACAT TTAAGAGGTG GCTGCCCAGG TGATTGGGTG TGGGTGGTGC
1321 CACCCATAAG TAGTTCAGCT CTGGACATTT TTCACCAAGA ACTTTTGCTT TATAAGCTCA

1381 AGCCTTCCTT TGAATATCAG GCCTGTAGCT GGGATCTTTC ACTCAAAATG AAGGGCTNTA
1441 CTTTCTTCCC ATGAATTTCG GATAATACTG AAGTAAAAAT TGATTGAGCT ATATGGAAAA
1501 CACATTTTAT TGATGTAAAT AAATATTTGT ATTTCTCAAT TGATATAAGA GACAGATATT
1561 GAATACAAAT TTTAAAAATG ATTTGAGTAA CTTTGCAATT AACAATGTTT TAAGCAATTT
1621 TCCAAATTTT AATGAGGACA CAAAATAAAT ATCCTTACAT TATTTAGACA ATATGCTATC
1681 AGGCAATTTA AGCTAAATAC CATGGCTTAA ATCTTGTTTT TTGCCATTGT CCAATAGCAC
1741 AATCCTAACT TTGTCAAGTG ACCAGCTATG ATCACCCATT TTCGGGGTCC TGTTGCCTCC
1801 TTTATATCAA TATTTTCGAG GCAGNAAGCA TCACATGCAG CCTATGGCNA AAAATTGGAA
1861 ATTTTTTTNA ATAAAGGTAA TAATAGAGNA ATTTTTACAG TTTTGGATAG NTAGTTAAAA
1921 NTTAAATGTA CAAATGNAAG NTTACTTACA AAGTATTGGA CAAGGTAAAN GACATTGTCA
1981 AGTTCATGAA ATTAGCATAA AGTGTGGGTG TTTAATTGTG GGGCTTGTGA GTGAATGTGA
2041 ACTATCAAGT CACAATGTTG GACAATGTTG AGTGATCGAG GTGTGCAATC GATTGACGAG
2101 GATCGAGAGG GATATAGAGA GGATCTGGGT GATAGCTACG TAGAGTCTTG AGTTCACATG
2161 AGTCAGTCTT ACGTTCACTG AGTATTATGT CACTGAGATC CAGGCAACTT GGATCTTGGA
2221 GTTGCAGAGT GAGATAGATG TGTGGTGATA TGTTTTGCTG ATTGGAATAT TGCCCATACA
2281 TTTGGATACA TGTTGCAATT TAACTGAAAC GGATTGCTGT TGTAATACTG CCATAAATAA
2341 ATGACAAATG TACCTTGAAG ATTATTGTTG ATTGAATTAA ACTAGCCTGT TGTGTGGCAA
2401 GTATTTCACG CCAACTCAAC AGTCGCGATA ATCATACACC CTTGACAACG CCCAAATATT
2461 CACTACCAGA ATATTAGACA TATTGAAATT CATTTGAAAA TTATTGAATA TGAAAATTCT
2521 GTAAAGATAT AATATGAAAA CAAGCATGGC ACTTACTCTA TATACTCCCT CAGACCAGGT
2581 CCTAAATCTC TGCTCCTGGC CATATAAAGC ATCGCCTGTG CAATATTCAA CCAACATTTC
2641 TGCTCCCAGT TCTTTGAATG TTTTATCTAT GTACTTTCCA AAGATAGCAA AGTTGGGGTA
2701 AGCATTAGAT CCCAGTGAAA AAACTGCAAA CCTGTATAAA AATTGGATTA AAATAAATTC
2761 TACCATT
```

Figure 2.3 Full cDNA sequence of *Lym-antiNOS2*. *In situ* hybridisation probes are shown in orange background. The open reading frame is surrounded by dotted lines; full-line boxes show start and stop codons. The antisense homology sequence between *Lym-antiNOS2* RNA and *Lym-nNOS* mRNA is shown in bold. The sense homology between *Lym-antiNOS2* RNA and *Lym-nNOS* mRNA is indicated in grey.

In situ hybridisation on frozen sections was performed following the protocol suggested by the probes' manufacturer. The *in situ* hybridisation protocol was performed on three successive days. All the glass was autoclaved and all the solutions were freshly prepared in sterilised and RNA-free conditions and used only once.

The protocol was divided into five stages: a) tissue preparation and post-fixation; b) *in situ* hybridisation; c) post-hybridisation washes; d) detection, and e) colour reaction.

The following two solutions were used throughout this protocol, and were prepared freshly on day 1:

- 1l 0.1M PB: 4.867g NaH_2PO_4, 10.188g Na_2HPO_4, up to 1l nuclease-free H_2O.
- 20ml hybridisation buffer: in a 50ml Falcon tube with screw cap, 4ml 20x SSC, 4g dextran sulphate, 10ml formamide (deionised). The solution was sonicated for about 4 hours and added 0.5ml PolyA (10mg/ml), 0.5ml ssDNA (10mg/ml), 0.5ml tRNA (10mg/ml), 2ml DTT (1M solution), 0.2ml 50x Denhardt's solution. The solution was mixed very well and stored at -20°C.

All the instruments were carefully cleaned with 70% ethanol (in nuclease-free water) and wiped with RNaseZAP (Sigma-Aldrich).

The slides containing the tissue sections were removed from freezer and placed in cold (4°C) 4% PFA in 0.1M PB (freshly made the night before and stored at 4°C) for 15 minutes in a large container.

The slides were washed three times for 5 minutes in 0.1M PB (fresh).

Dehydration of the tissue: slides were incubated with 100% ETOH for 5 minutes in a large container and air-dried. At this point the RNA in the tissue is sufficiently safe from RNases, and GeneDetect oligonucleotide probes are resistant to degradation by RNases so working on ice and utilization of nuclease-free water are not necessary anymore (RO water was used on the following reactions).

The optimal amount of probe to use was determined on a trial-and-error basis, within the recommended concentration range of 100-1000ng probe per ml of hybridisation buffer. Concentrations of 1:100, 1:50 and 1:25mg/ml buffer and a sense control were tested on brains obtained simultaneously, with 1:50mg/ml buffer chosen as the optimal concentration.

Once the optimal probe concentration was determined, different hybridisation temperatures were experimented to minimise background staining: 33°C, 35°C, and 37°C. The optimal staining was obtained at 37°C.

Each *in situ* hybridisation was conducted on a) three brains for the antisense probe; b) two brain slices for hybridisation buffer control (i.e. without probe), and c) one brain for the sense probe control.

The hybridisation buffer was preheated at 37°C. This causes the buffer to lose some of its viscosity and to become more spreadable, allowing for easier pipetting and more homogenous mixes of probe with hybridisation buffer. 100µl of hybridisation buffer were added to each slide, which was then covered

(HybriSlip Hybridization Covers, Sigma-Aldrich) and checked to make sure no air bubbles were trapped between the sections and the cover.

The slides were left overnight for 20 hours at 37°C in a Boekel InSlide Out oven for hybridisation. To keep the humidity of the chamber and the sections from drying out, tissue paper filled with dH_2O was placed in between the lines containing the slides.

Following hybridization, excess probe was removed by SSC washes. For these washes, 0.5 and 1x SSC (Saline-Sodium Citrate) solutions from 20x SSC and DTT (Dithiothreitol) were prepared on the day. Two big glass containers (400ml) were placed on a water bath at 55°C, allowing enough time for the solutions to reach the correct temperature. SSC is a widely used, weak buffer which is used to control stringency of nucleic acid hybrids during *in situ* hybridisation. DTT is used to reduce disulfide bonds in RNases, which are needed by RNases for stability, thereby inhibiting RNase activity and providing RNAs with stability, helping preserve mRNA integrity.

A quick wash of the slices was performed at room temperature using a shaker in 1x SSC (10mM DDT). After this wash the cover slips were carefully removed from the slides using forceps. This was followed by a 1x SSC (10mM DTT) wash for 30 minutes at 55°C, a 0.5x SSC (10mM DTT) wash for 30 minutes at 55°C and a 0.5x SSC (10mM DTT) wash for 10 minutes at room temperature.

The detection procedure was carried out using an anti-DIG antibody conjugated to alkaline phosphatase (Roche). After 3 washes for 5 minutes on

TBS (Trizma buffer solution), the slides were first incubated for 30 minutes at room temperature with 500µl blocking solution, containing 1% sheep serum and 0.1% Triton X-100 in TBS. The blocking reagent was then tipped off, and 500µl of primary antibody solution were added to each slide – anti-DIG antibody conjugated to the enzyme alkaline phosphatase (Roche), diluted 1:250 in blocking reagent. The slides were then left overnight at 4°C.

The colour reaction was conducted in alkaline substrate buffer containing 10mm $MgCl_2$, 0.2m Tris (pH 9.5), 0.4% Triton-X, 50mg /ml 5-bromo-4-chloro-3-indolyl-phosphate (Roche) and 100mg/ml nitro blue tetrazolium chloride (Roche).

The slides were washed three times with PBS and left in PBS while substrate solution was being prepared.

Alkaline phosphatase solution ((200mM Tris base, pH 9.5) + 10mM Magnesium Chloride)) was prepared. 6.6µl BCIP and NBT solutions were added per ml of substrate buffer. 500µl of this solution were allowed for covering each slide; 4µl of 3% Triton X solution per ml were added to make the solution more spreadable.

Slides were placed onto a developing rack. 500µl of substrate solution was added to each slide, using the pipette tip to ensure that slides were fully covered. A lid was placed on the rack, and it was covered with foil as this is a dark-activated reaction. The reaction was left for about 1 hour and kept under watch to look for purple colour development.

When colour had developed, slides were washed off with PBS and mounted in Immu-Mount. Once the mountant had dried, slide edges were sealed with Histo-Clear to prevent them from drying out.

2.15. Quantitative Real-Time PCR

2.15.1. Relative Quantification Method

A relative quantification method was used to analyse changes in gene expression of the target gene in the treatment group compared to a control sample. The amount of target is normalized to an endogenous reference and is related to the calibrator by $2^{-\Delta\Delta Ct}$, where

$$\Delta\Delta Ct = \Delta Ct_{\text{sample}} - \Delta Ct_{\text{calibrator}} \text{ and } \Delta Ct_{\text{sample}} = Ct_{\text{target}} - \Delta Ct_{\text{reference}}$$

The Ct value is calculated using a threshold level of fluorescence set above the background but within the linear phase of amplification. The cycle number at which an amplification plot crosses this threshold fluorescence level is called the Ct or threshold.

To apply this method, the efficiencies of the target and reference genes, established via a standard curve, must be approximately equal (in the 5% range) and close to 100%. A method for assessing if the two amplicons have the same efficiency is to look at how ΔCt varies with the template dilution. To do that, the average Ct for both the target and reference and the ΔCt ($Ct_{target} - Ct_{reference}$) was determined. The data were fit using least-squares

linear regression analysis (n=3). The absolute value of the slope of the plot cDNA dilution versus ΔCt should be lower than 0.1.

2.15.2. cDNA Synthesis and Gene-Specific Primer Design

The cDNA concentrations of all the calibrators (control and experimental) were determined according to the efficiency of each reaction. The primer pairs designed to investigate *Lym-antiNOS2* and *β-tubulin* expression were 20-21 nucleotide long with G-C content between 40-60%, with an annealing temperature close to 54°C (Table 2.1). The length of the amplicons was 119bp and 103bp for *Lym-antiNOS2* and *β-tubulin* respectively.

Primer name		Primer sequence
β-tubulin primers		
Forward	LTUBaRT	5′AAGGGACATTACACAGAGG′3
Reverse	LTUBbRT	5′GTGTCAGTTGGAATCCTTG′3
Lym-antiNOS2 primers		
Forward	Scorp 1RT	5′GTGAACTATCAAGTCACAATG′3
Reverse	Scorp 2RT	5′GAACTCAAGACTCTACGTAG′3

Table 2.1 Oligonucleotide sequences used as primers for the amplification of Anti-NOS2 and *β-tubulin*.

2.15.3. Primer Optimization

Optimal design of the PCR primers is essential for accurate and specific quantification using real-time PCR. The optimisation of annealing temperature and the primer concentration is essential. The theoretical annealing temperature for the set of primers was validated on PCR at four different temperatures (52°C, 53°C, 54°C and 57°C), and a 1% agarose gel was run (Section 2.12) to determine at which temperature the primers are used more efficiently. The amount of template and primers added was the same in all the samples in the optimization exercise.

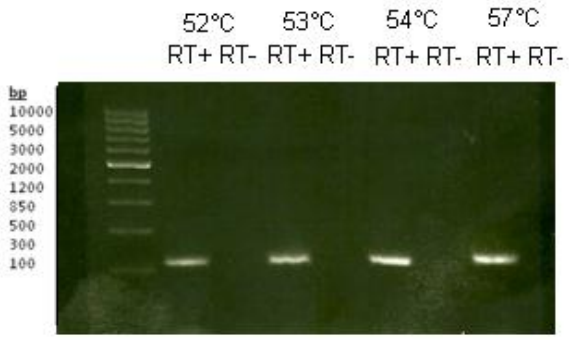

Figure 2.4 Ethidium bromide stained 1% agarose gel displaying PCR amplification products obtained using Lymnaea S cDNA as templates and the primer pair Scorp 1RT and Scorp 2RT. Lanes: 1, molecular size ladder; 2, 4, 6 and 8: RT+ at each annealing temperature; 3, 5, 7, 9: RT- as a negative control at each annealing temperature.

To ensure the efficient and accurate quantification of the target template, real-time PCR assays should be optimized. Assays are first optimized by evaluating primer concentrations. To do that, four concentrations with equimolar amounts of each primer pair were tested: 16nM, 20nM, 40nM and 60nM. The amount of template added was the same in all the samples in the optimization exercise. All the samples were run in duplicates.

The ideal primer pair should yield the lowest average Ct value as well as presenting a dissociation curve that shows a single product.

2.15.4. Assay Performance

Following primer optimization and in order to test the efficiency, precision and sensitivity of the real-time PCR reaction (set up a detaled in Table 2.2 and Table 2.3), a standard curve was performed using a serial dilution of calibrator cDNA. A five-point, two-fold dilution series starting with 1:50-diluted cDNA was generated in triplicates. To obtain the standard curve, the Ct values of the

serial dilution of the calibrator cDNA were plotted against the cDNA dilution value.

2.15.5. Amplification

The real-time PCR experiments were carried out in a total volume of 25µl consisting of 12.5µl of FastStart SYBR Green 2x real-time PCR Master Mix (Roche), 2µl of the cDNA template, 11µl of forward and reverse primers mixture (at different concentrations as detailed in each experiment) and 0.5µl of PCR-grade water. The FastStart SYBR Green 2x real-time PCR Master Mix contained 2x reaction buffer, 0.025U/µl Taq polymerase, 5mM $MgCl_2$, dNTP mix (200µM of each dNTP), ROX (passive reference dye) and SYBR Green.

RNA sample (~100ng/µl)	2.5µl	+	Water	2.5µl

+RT cDNA reaction	
iScrip mix	4 µl
iScrip reverse transcriptase	1 µl
RNA	1 µl
water	14 µl
Total	20 µl

-RT cDNA reaction	
iScrip mix	1 µl
RNA	0.25 µl
water	3.75 µl
Total	5 µl

Table 2.2 Synthesis of first strand cDNA for real-time PCR.

	Sybr Green	+RT cDNA sample	H2O	
	12.5µl	2µl	0.5µl	14µl + 11µl oligos
x6	75µl	12µl	3µl	

	Sybr Green	-RT cDNA sample	H2O	
	12.5µl	1µl	1.5µl	14µl + 11µl oligos
x2	25µl	2µl	3µl	

	Sybr Green	Calibrator cDNA sample	H2O	
	12.5µl	1µl	1.5µl	14µl + 11µl oligos
x4	50µl	4µl	6µl	

Primers mix

β-tubulin	β-tuba		Lym-antiNOS2	Scor1	
(3pM)	β-tubb		(3pM)	Scor2	
	H_2O			H_2O	
	440µl	11µl		440µl	11µl

Table 2.3 Protocol sample for real-time PCR reaction. Each tube was filled with 14µl Sybr Green mix plus 11µl primers mix. Each sample was pipetted by triplicate and duplicates of RT-. Each experiment was performed with a duplicate set of calibrators.

Amplifications were carried out in a Mx3000P real-time PCR system (Stratagene) which includes a built-in thermal cycler equipped with a heated lid, a quartz-tungsten halogen lamp to excite fluorescence, photomultiplier tubes for high-sensitive detection and the Mx3000P real-time quantitative detection software.

All samples were analysed in duplicate. All reactions were initially denatured at 95°C for 15 minutes followed by a three-step protocol of 40 cycles of denaturation at 94°C for 30 seconds, annealing 54°C 1 minute and extension at 72°C for 30 seconds. In order to test the specificity of the primers the products were slowly melted, starting with 1 minute at 95°C followed by 30 seconds at 60°C and 30 seconds at 95°C, and the products analysed in the melting or dissociation curve (plotting fluorescence versus temperature). The temperature at which a DNA molecule melts depends on its length and sequence; therefore if the PCR product consists of molecules of the same sequence a single peak will be detected.

A negative control was set up alongside each set of PCR reactions consisting of all components of the PCR reaction including the template RT- DNA sample, and a calibrator in each of the PCR runs.

Chapter 3: Analysis of the Sequence of *Lym*-antiNOS2 NAT and its Expression in *Lymnaea* CNS

3.1. Introduction

Many studies have been made on understanding the molecular mechanisms underlying neuronal and behavioural plasticity. These studies have implicated several signalling pathways in consolidation of neuronal changes. In molluscs, *Lym-NOS1* (nNOS) activity has been implicated in associative conditioning learning.

In this thesis it was hypothesised that *Lym-antiNOS2* plays a role in the regulation of NOS, and a correlation is expected in the patterns of expression of *Lym-antiNOS2* NAT and *Lym-NOS1* mRNA. In this chapter the characteristics of *Lym-antiNOS2* sequence are analysed, and it is shown that *Lymnaea* CNS expresses the NOS-related *Lym-antiNOS2* transcript.

3.1.1. Lym-antiNOS2 RNA Structure

Lym-antiNOS2 RNA was fully sequenced by Dr Sergei Korneev in 2002 and is available at GenBank (access number for *Lym*-antiNOS2 cDNA is AF373019, AF373020 for the inverted anti-NOS locus) (Korneev and O'Shea, 2002).

Lym-antiNOS2 RNA is a polyadenylated transcript of about 3,000nt in length and contains a polyA tail; both of these features aid messenger RNA stability. It

contains an open reading frame (positions 261-1454nt) encoding a truncated NOS-homologous protein of 397 amino acids (Figure 3.2). The protein-encoding function of *Lym-antiNOS2* RNA was confirmed by in vitro translation experiments where a single band of 45kDa was detected (Korneev and O'Shea, 2002). *Lym-antiNOS2* protein shares about 70% identity with the oxygenase domain of nNOS, which includes the region required for the formation of the functional homodimer. It does not possess the reductase domain (which includes calmodulin-binding sites and cofactor and cosubstrate binding sites), which is essential for enzymatic activity of NOS.

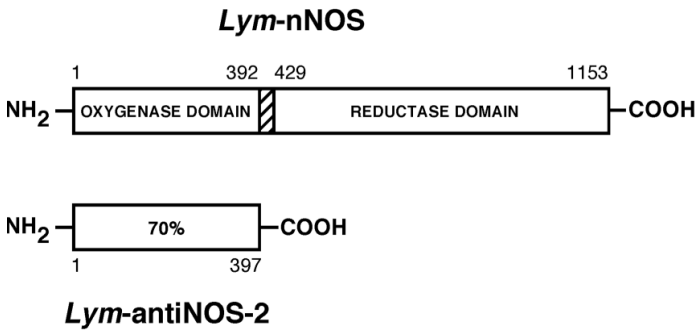

Figure 3.1 Schematic representation of Lymnaea nNOS and Lym-antiNOS2 proteins. The upper bar represents the nNOS protein, which is composed of two major functional domains (oxygenase domain and reductase domain), connected by the calmodulin-binding site (hatched). Importantly, it was shown that the oxygenase domain contains regions essential for NOS dimerization. Note that the antiNOS-2 protein (lower bar) contains the oxygenase domain only. Oxygenase domains in the nNOS and antiNOS-2 proteins share 70% identity (Korneev and O'Shea, 2002).

The two nNOS-related transcripts found in *Lymnaea* (*Lym*-antiNOS-1 and *Lym-antiNOS2*) are homologous to *Lym-NOS1* mRNA and they do not show sequence similarity to each other. In Figure 3.2 it is possible to appreciate that the regions of similarity with nNOS are localized in different parts of the *Lym-NOS1* mRNA and do not overlap. The NOS-related RNA molecules also

contain regions of significant antisense homology to *Lym-NOS1* mRNA (Korneev and O'Shea, 2002).

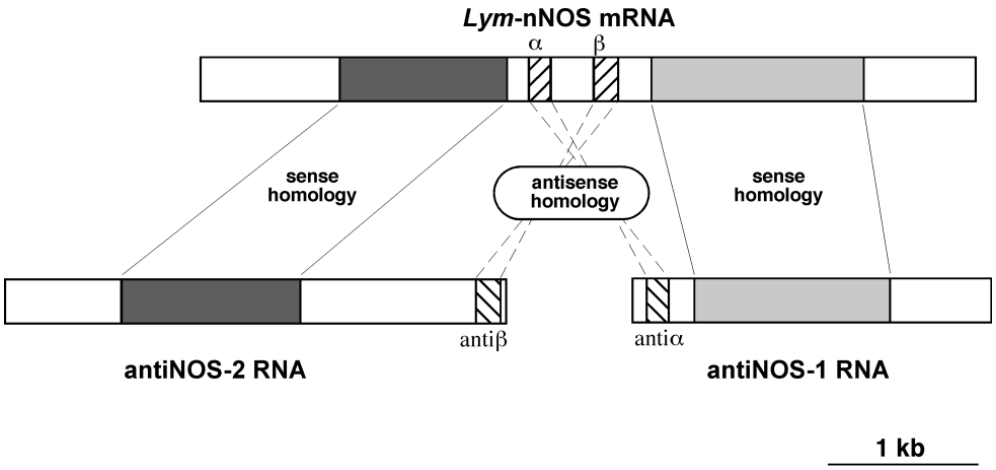

Figure 3.2 Schematic organization of *Lym-NOS1* mRNA and nNOS-related transcripts. Dark gray boxes indicate regions of similarity (76%) shared by *Lym-NOS1* mRNA and *Lym*-antiNOS2 RNA. Light gray boxes show regions of similarity (80%) shared by *Lym-NOS1* mRNA and *Lym-antiNOS1* RNA. Antisense regions in the anti-NOS transcripts (antiα and antiβ) and their complementary counterparts in the *Lym-NOS1* mRNA (α and β) are hatched. The antisense similarity of antiα to α and of antiβ to β is approximately 80% (Korneev and O'Shea 2002).

The full sequence of *Lym-antiNOS2* RNA in Figure 3.3 shows in a grey background the position of the sense homology between *Lym-antiNOS2* RNA and *Lym-NOS1* mRNA. The full-line boxes show the (ATG) start site for translation and the presence of a new termination (TAG) signal indicating the end of the translation. The dotted line box delimits the open reading frame encoding a truncated NOS-homologous protein.

```
   1 GGGGTGACCA GCTACCTGTA GGGGTGACCA GCTACCTGTA GGGCCATAGA AACAATTTTC
  61 CGGTTTAGGG TGAGTNTTAC TGCTTTCTGA TAATCTTTCA GAGCCTAACG TGACGGAAAT
 121 CGGCAGTGTT CAGGCAGTTC AATCATGGNT TGCCCGTACC GGTCGGCCAA GCTGAAAAAT
 181 GTGCTGAATG ATAAGACTTA TGTGGACACG NTTACACCAG AGATCATTTT CGCCAGTTAC
 241 CTTGCAACAC CCAGCGATGC ATGGGCTCAC TTATGTCCCA ACAGGCAAAT AGGCCCCCTG
 301 GGGTCCCTAG ATCACAGGAG GAACTTTTGG TTCACGCCAC AGGCTTCATT GACCAATATT
 361 TAAACTCATG TGAAATGACA TTCCTGTCCA GGAGCAACAC ACCGGCCCAT TTGAATAGAC
 421 TTAGCGAGAT CCAAGATTAT GTGACAAAGT CCGGTACCTA TGACCTGACA ATGGCTGAAC
 481 TGACATTTGG TGCTAAGCAA GCTTGGAGAT ATGCGTCCAG ATGCACTGGC AGAATGCAGT
 541 GGTCAAAACT TCAGGTTGTT GATGCCAGAT GCATCATGAC ACCCCGAGGG ATGTATACAG
 601 CTTTGTGCGA TCACATCAAA TATGGGACAA ACAAAGAGAA TATTAGGTTT GCCATCACCA
 661 TATTTCCACA ACGAATAGAA GGGCCCCCNG ATTTCCGTGT ATGGAATAGT CAGTTGATAG
 721 GCTACGCTGG CTACAGTATG GATGATGGGA AGATTATTGG GGACCCAGCC AATGTGGAAT
 781 TTACTGATCA ATGTGTAAGG ATGGGTTGGA AACCAAAGTA TGGTATGTTT GACCCATTTC
 841 CACTGGTTCT GTCTGCTGCT GGATTTGATC CTGAAGTTTT CGACCTCCCA CCTGAGCTAG
 901 TGTTAAAGGT CAAGTTGGTG CATCCCGAGA ATCCCTCGTT TTCTGATATT GGTCTAAAAT
 961 GGTACGCCCT ACCAGCTGTA TCTGGAATGC TGTTGGACTG TGGGAGCCTG GAGTTCCCCT
1021 CGTGTCTTTT CAATGGATGG TACATGGGGA CAGAGATTGG TTCCAGGGAT TTGTGCGATT
1081 CTCATAGGTA CAACATGCTG GAGACCATTG CCTTAAAGAT GGGGCTAAAC ACCAGAAATG
1141 CTTCATCCTT GTGGAAAGAT CGTGCACTAT TGGACGCTAA TCCTGCTGTT CTCCACAGTT
1201 TTCAGTCAGC CAATGTTACA ATTGTCAATC ATCACGATGC CAGTGAGTCT TTAATGTTGC
1261 ACTTGGATAC TGAGCAACAT TTAAGAGGTG GCTGCCCAGG TGATTGGGTG TGGGTGGTGC
1321 CACCCATAAG TAGTTCAGCT CTGGACATTT TTCACCAAGA ACTTTTGCTT TATAAGCTCA
1381 AGCCTTCCTT TGAATATCAG GCCTGTAGCT GGGATCTTTC ACTCAAAATG AAGGGCTNTA
1441 CTTTCTTCCC ATGAATTTCG GATAATACTG AAGTAAAAAT TGATTGAGCT ATATGGAAAA
1501 CACATTTTAT TGATGTAAAT AAATATTTGT ATTTCTCAAT TGATATAAGA GACAGATATT
1561 GAATACAAAT TTTAAAAATG ATTTGAGTAA CTTTGCAATT AACAATGTTT TAAGCAATTT
1621 TCCAAATTTT AATGAGGACA CAAAATAAAT ATCCTTACAT TATTTAGACA ATATGCTATC
1681 AGGCAATTTA AGCTAAATAC CATGGCTTAA ATCTTGTTTT TTGCCATTGT CCAATAGCAC
1741 AATCCTAACT TTGTCAAGTG ACCAGCTATG ATCACCCATT TTCGGGGTCC TGTTGCCTCC
1801 TTTATATCAA TATTTTCGAG GCAGNAAGCA TCACATGCAG CCTATGGCNA AAAATTGGAA
1861 ATTTTTTTNA ATAAAGGTAA TAATAGAGNA ATTTTTACAG TTTTGGATAG NTAGTTAAAA
1921 NTTAAATGTA CAAATGNAAG NTTACTTACA AAGTATTGGA CAAGGTAAAN GACATTGTCA
1981 AGTTCATGAA ATTAGCATAA AGTGTGGGTG TTTAATTGTG GGGCTTGTGA GTGAATGTGA
2041 ACTATCAAGT CACAATGTTG GACAATGTTG AGTGATCGAG GTGTGCAATC GATTGACGAG
2101 GATCGAGAGG GATATAGAGA GGATCTGGGT GATAGCTACG TAGAGTCTTG AGTTCACATG
2161 AGTCAGTCTT ACGTTCACTG AGTATTATGT CACTGAGATC CAGGCAACTT GGATCTTGGA
2221 GTTGCAGAGT GAGATAGATG TGTGGTGATA TGTTTTGCTG ATTGGAATAT TGCCCATACA
2281 TTTGGATACA TGTTGCAATT TAACTGAAAC GGATTGCTGT TGTAATACTG CCATAAATAA
2341 ATGACAAATG TACCTTGAAG ATTATTGTTG ATTGAATTAA ACTAGCCTGT TGTGTGGCAA
2401 GTATTTCACG CCAACTCAAC AGTCGCGATA ATCATACACC CTTGACAACG CCCAAATATT
2461 CACTACCAGA ATATTAGACA TATTGAAATT CATTTGAAAA TTATTGAATA TGAAAATTCT
2521 GTAAAGATAT AATATGAAAA CAAGCATGGC ACTTACTCTA TATACTCCCT CAGACCAGGT
2581 CCTAAATCTC TGCTCCTGGC CATATAAAGC ATCGCCTGTG CAATATTCAA CCAACATTTC
2641 TGCTCCCAGT TCTTTGAATG TTTTATCTAT GTACTTTCCA AAGATAGCAA AGTTGGGGTA
2701 AGCATTAGAT CCCAGTGAAA AAACTGCAAA CCTGTATAAA AATTGGATTA AAATAAATTC
2761 TACCATT
```

Figure 3.3 Molecular cloning of *Lym-antiNOS2* transcript. Sequence of a full-length cDNA clone isolated from a Lymnaea CNS cDNA library. The antisense region from 2551 to 2735 bp is indicated in bold type. The core region of high homology (.80%) to the nNOS-encoding transcript is shaded. Polyadenylation signal is underlined. Stop and start codons are full-line boxes. The open reading frame is surrounded by dotted lines.

3.1.2. Cellular Localization of *Lym-NOS1* in *Lymnaea stagnalis* CNS

The cellular expression of *Lym-NOS1* mRNA in *Lymnaea* CNS was analysed by *in situ* hybridisation (Korneev et al., 1999) and it has been localized on the modulatory CGCs that are known to have key roles in facilitation and plasticity in feeding (Figure 3.4).

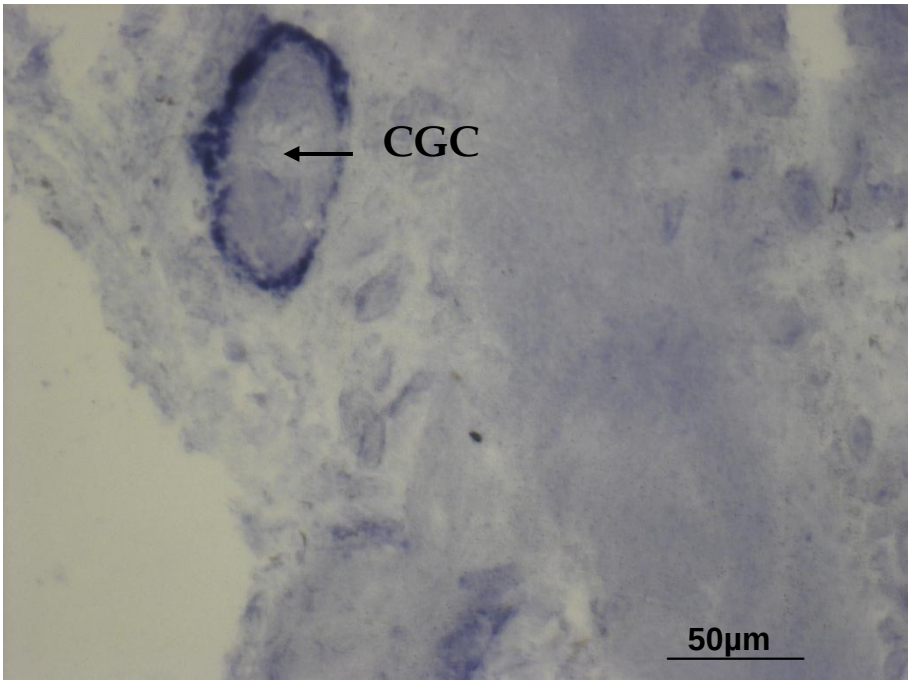

Figure 3.4 *In situ* hybridisation with the probe specifically recognizing *Lym-NOS1* RNA. Cerebral ganglion is shown with CGC staining. Previous laboratory work by Michael Schofield for (Korneev and O'Shea, 2007).

3.2. Sequence Analysis of *Lym-antiNOS2* RNA

Sequence alignment between *Lym-antiNOS2 RNA* and *Lym-NOS* mRNA reveals a 74% antisense homology between 179 nucleotides at the 3′ end of *Lym-antiNOS2* RNA (Figure 3.5). The antisense homology is right at the 3′ end of the sequence of *Lym-antiNOS2* RNA out of the open reading frame, between the nucleotides 2555 and 2735. This antisense homology could trigger the

degradation of functional *Lym-NOS1* RNA via a negative regulator of *nNOS* expression through the formation of an RNA–RNA duplex.

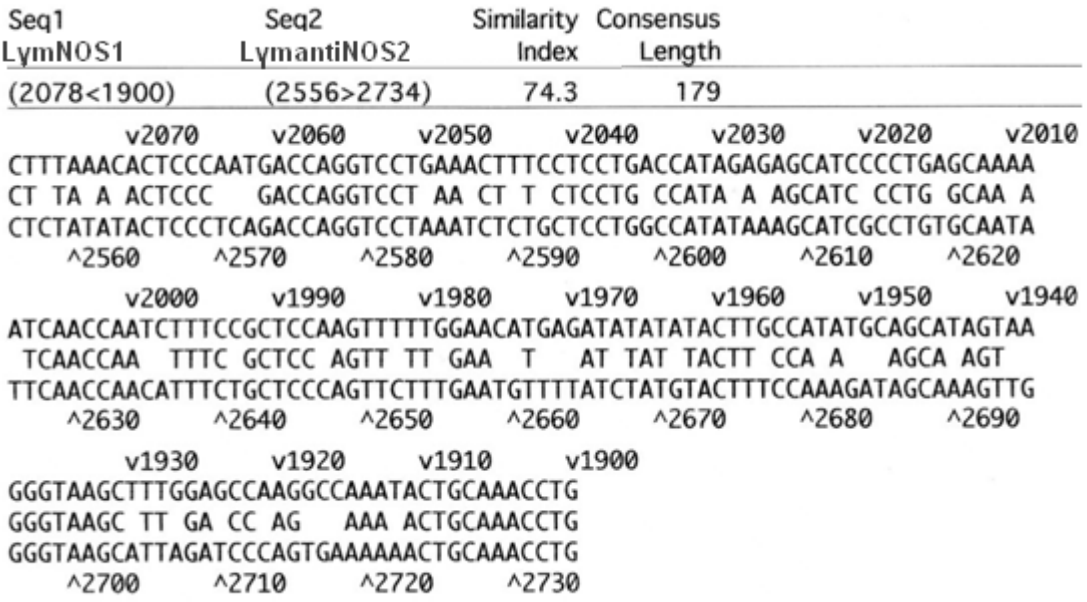

Figure 3.5 Sequence alignment between antisense sequence of *Lym-NOS1* mRNA and *Lym-antiNOS2* RNA. Homology is shown between bases 2078 and 1900 for *Lym-NOS1* (in antisense) on the top line and bases 2556 and 2734 of *Lym-antiNOS2* in the third line. The middle line shows the bases with identity. A 74.3% of identity in the 179bp exists between the sequences.

Lym-antiNOS2 RNA does not show antisense sequence similarities with other nNOS-related transcripts because the regions of similarity are localized in different parts of the *Lym-NOS1* mRNA.

Sense homology between *Lym-NOS1* mRNA and *Lym-antiNOS2* RNA has been found at the 5′ end of the RNA molecule. *Lym*-antiNOS-2 shows high homology with Lym-NOS1 (1389nt - 1472nt and 2557nt - 2734nt) and Lym-NOS2 (2557nt - 2734nt). The sequence alignment is shown in Figure 3.6.

Lym-antiNOS2 sequence shares 70% sense homology within the open reading frame with *Lym-NOS1* RNA. The sense homology starts at the 5′ end right before the open reading frame for *Lym-antiNOS2* at 230nt to 1390nt (Figure 3.6). This suggests that if *Lym-antiNOS2* actually translates to a protein, it could function as a natural dominant negative regulator of *Lym-NOS1* expression through binding to the normal nNOS monomer, forming a non-functional heterodimer (Figure 3.7).

Lym-antiNOS2 NAT does not show sense sequence similarities with other nNOS-related transcripts because the regions of inversion are localized in different parts of the *Lym-NOS1* mRNA (Figure 3.2). Nevertheless, at the 5′ end of the molecule *Lym-antiNOS2* shows high homology with *Lym-NOS1* (274nt - 1394nt).

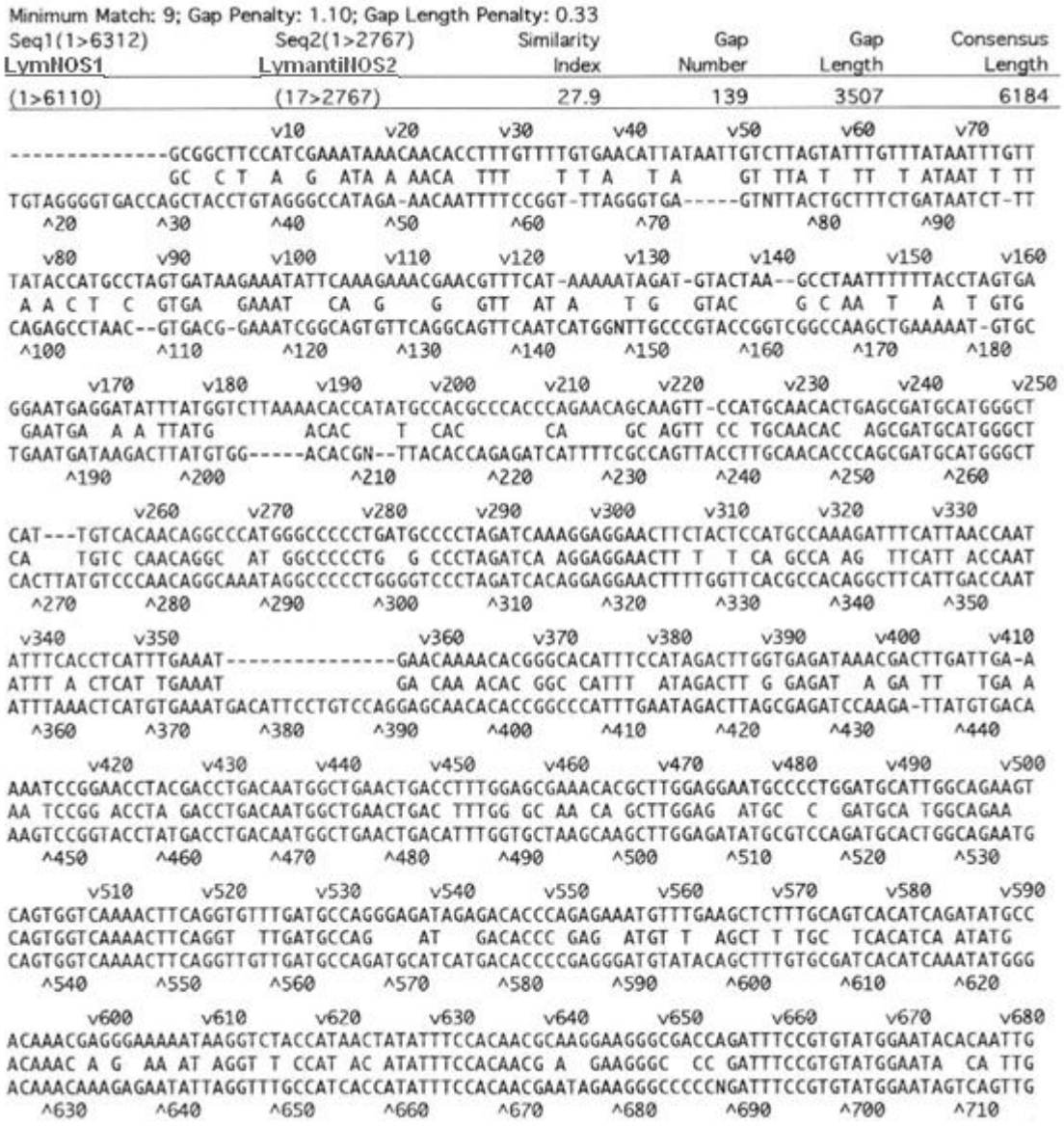

Figure 3.6 Sequence alignment of *Lym-antiNOS2* RNA and *Lym-NOS1* RNA. Homology is shown between bases 220 to 1360 for *Lym-NOS1* on the top line and bases 230 to 1370 of *Lym-antiNOS2* in the third line. The middle line shows those bases with identity. An 80% identity exists between sequences.

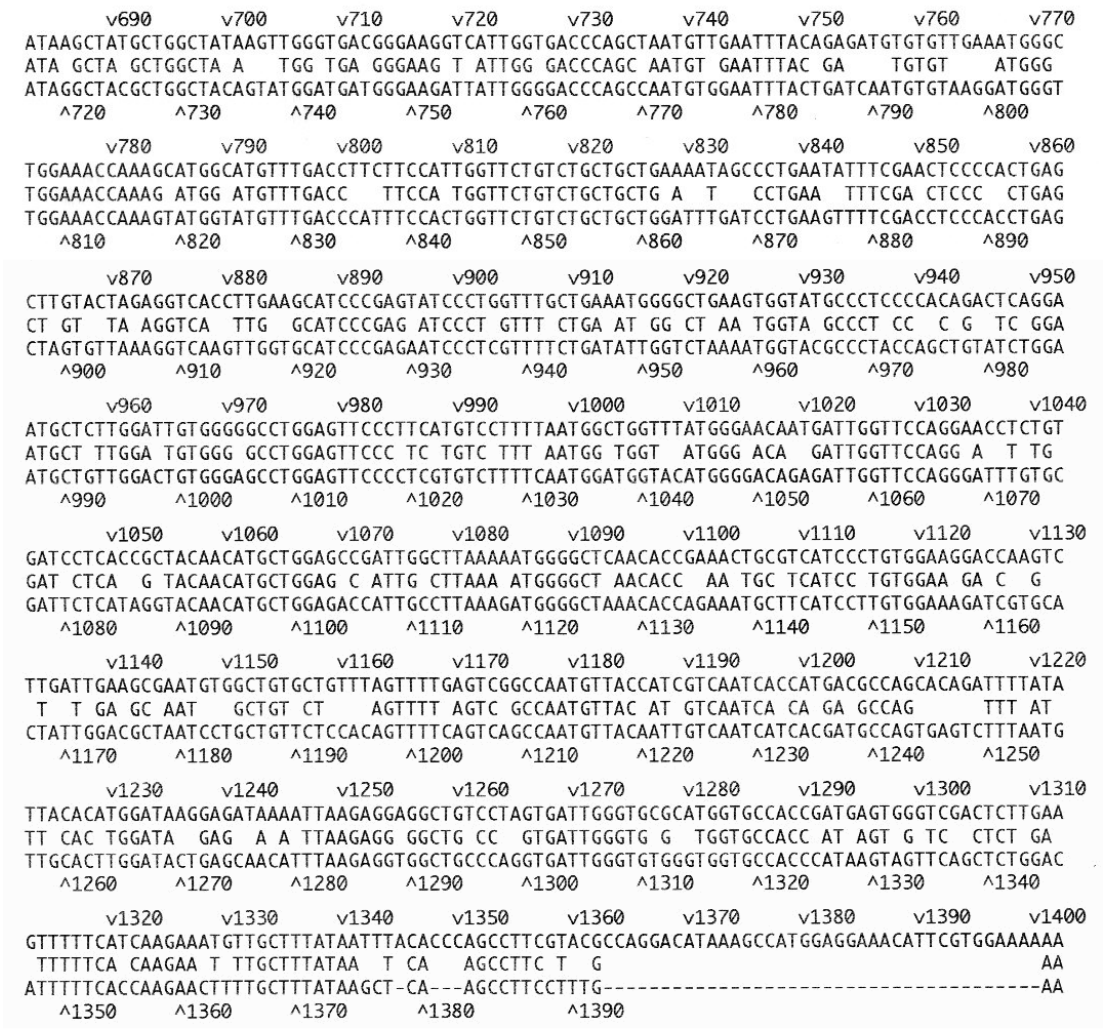

Figure 3.6 (cont.)

Lym-antiNOS2 RNA does not possess similarities with nNOS or NOS-related transcripts on the position between the 5′ end to the nucleotide 270, and at the middle of the sequence at 1500nt to 2500nt. These regions of non-homology are the ideal areas to find specific primers for the reverse transcription polymerase chain reaction, that will permit transcript levels of *Lym-antiNOS2* NAT to be detectedand mesusure (Figure 3.7).

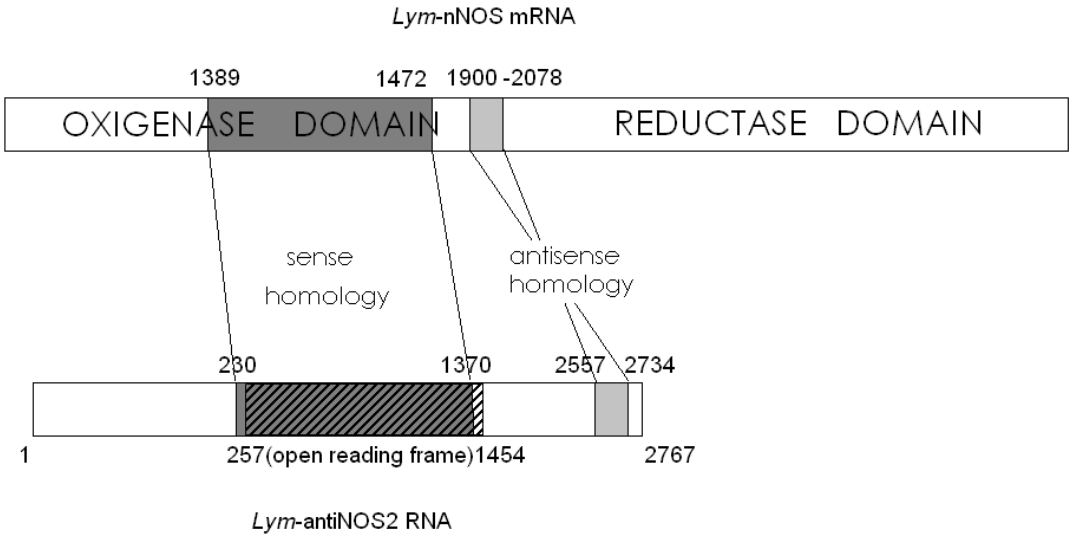

Figure 3.7 Schematic sequence analysis of *Lym,-antiNOS2* RNA. Dark gray boxes indicate regions of similarity (76%) shared by *Lym-NOS1* mRNA and *Lym*-antiNOS2 RNA. Light gray boxes show regions of antisense similarity (80%) shared by *Lym-NOS1* mRNA and *Lym-antiNOS2* RNA. Open reading frame regions in *Lym-antiNOS2* transcripts is hatched.

3.3. Analysis of the Expression of *Lym-antiNOS2* NAT in CNS by *In Situ* Hybridisation

Three *in situ* hybridisation probes (described in Section 2.14) were designed to identify the localization of the expression of *Lym-antiNOS2* RNA in the

central nervous system by *in situ* hybridisation. To increase the sensitivity of the method, the probes were designed to bind specifically to *Lym-antiNOS2* and not to *Lym-NOS-1* or *Lym-NOS-2*. The probes are situated in the two regions of specificity of *Lym-antiNOS2* (Figure 2.3).

All the animals used in this experiment were naïve animals selected randomly from their home tanks. All snails were of similar weight and age (approximately three months old). *In situ* hybridisation on frozen sections was performed following the protocol in Section 2.14. The detection procedure was carried out using an anti-DIG antibody conjugated to alkaline phosphatase.

To assess the specificity of the staining obtained with the antisense probes, an experiment was performed where the sense probe was incubated together with the brain sections. The sense probe has a sequence that is complementary to that of the antisense probes. The absence of staining following the incubation would indicate that the staining obtained from the experiment on antisense probes is highly specific. An additional experiment was performed using only hybridisation buffer (without probes) to establish that none of the staining is a product of the procedure itself (Figure 3.9B, Figure 3.10B, and Figure 3.11).

As compared to the mammalian brain with 10^{11} neurons and *Drosophila melanogaster* ganglia comprising 200,000 neurons, *Lymnaea stagnalis* has a relatively simple central nervous system (CNS) consisting of a total of 20,000 neurons, many of them individually identifiable, organized in a ring of interconnected ganglia (Figure 2.1). Most neurons of the *Lymnaea stagnalis* CNS

are large in size (up to ~100 µm in diameter), thus allowing electrophysiological dissection of neuronal networks that has yielded profound insights in the working mechanisms of neuronal networks controlling relatively simple behaviours such as feeding, respiration, locomotion and reproduction (Feng et al., 2009). A diagram of the snail CNS is shown in Section 2.3 (Figure 2.1), where it is possible to visualise the arrangement of the different ganglia. The pleural ganglia and pedal ganglia lie next to each other on the ventral side of the gut, and the cerebral ganglia are communicated via long connective nerves CBC to the buccal ganglia.

3.3.1. General Staining

Pedal ganglia The pedal ganglia controls locomotion and conjoint muscle movements involving the shell (Benjamin et al., 2005). The pedal ganglia contain many motoneurons involved in locomotion, which are part of the feeding circuit and hence likely to have direct connections with the central ganglia.

Figure 3.8 shows the results of our staining experiments in pedal ganglia. Fewer neurons stain in this area of the brain in comparison with buccal ganglia or cerebral ganglia. The high quantity of neurons of similar size that compose the pedal ganglia makes it difficult to clearly identify particular neurons.

Buccal ganglia The consummatory phase of feeding (cycle of feeding behaviour: protraction, retraction and swallowing) is driven by motor commands generated within the buccal ganglia (CPG), which consists mostly of

interneurons that connect via cerebrobuccal connectives (CBCs) (Figure 3.9A and Figure 3.8), motoneurons and modulatory neurons such as CGCs.

Figure 3.9A depicts the results of the staining experiments on the buccal ganglia. It is possible to see a very widespread staining in the buccal ganglia, with all the neurons presenting staining although not as strongly as in the CGCs (Section 3.3.2). The buccal ganglia are involved in the production and modulation of feeding behaviour and thus these neurons might be involved in plasticity of the feeding behaviour.

In the buccal ganglia all cells appear stained in each ganglion, even though the right ganglion always showed higher staining. This could be an artifact of the technique, but it was consistent along the different preparations. To our knowledge, no previous reports of differentiation between left and right ganglia exist in the literature; moreover, both ganglia are electrically equivalent.

Visceral, pleural and parietal ganglia The visceral ganglia are the rear and upper parts of the circumesophageal ring, a large, single ganglion whose function is to process information from the internal organs and organ systems. The pleural ganglia have a nerve path to the gullet retractor muscle and the main retractor muscle. The parietal ganglia are the starting point of the mantle nerves.

No staining was found in the pleural ganglia, parietal ganglia and visceral ganglia. None of these ganglia are involved in feeding or learning; hence their lack of staining agrees with our hypothesis that *Lym-antiNOS2* expression is

linked to learning processes, and is not expressed arbitrarily in the whole nerve system.

3.3.2. The Cerebral Giant Cells Express *Lym-antiNOS2* NAT

In *Lymnaea*, the CGCs are a pair of very well-known serotonergic neurons that have two distinct roles in the feeding network. Firstly, they act as gating neurons, facilitating the response to food. Secondly, following single-trial appetitive conditioning, persistent depolarization of the CGCs facilitates the feeding response to the CS leading to LTM formation (Kemenes et al., 2006a). Importantly, the associative conditioning of the feeding response is dependent on the NO–cGMP signalling pathway in the early stage of memory formation – disruption of this pathway during the first 6 hours following conditioning prevents LTM formation (Kemenes et al., 2002).

Figure 3.10 shows the results of our staining experiments on cerebral ganglia. Lym-*antiNOS2* NAT *in situ* hybridisation in *Lymnaea* neurons indicates that the expression of *Lym-antiNOS2* NAT is restricted to some areas but can be found in numerous neurons located in central ganglia (Figure 3.10A, C). In particular, we find that *Lym-antiNOS2* RNA is present in the CGCs with extensive staining. This is an important result since it is already known that in central ganglia *Lym-NOS1* mRNA is expressed in CGCs (Korneev et al., 2005) indicating that *Lym-NOS1* and *Lym-antiNOS2* are co-expressed in the CGCs.

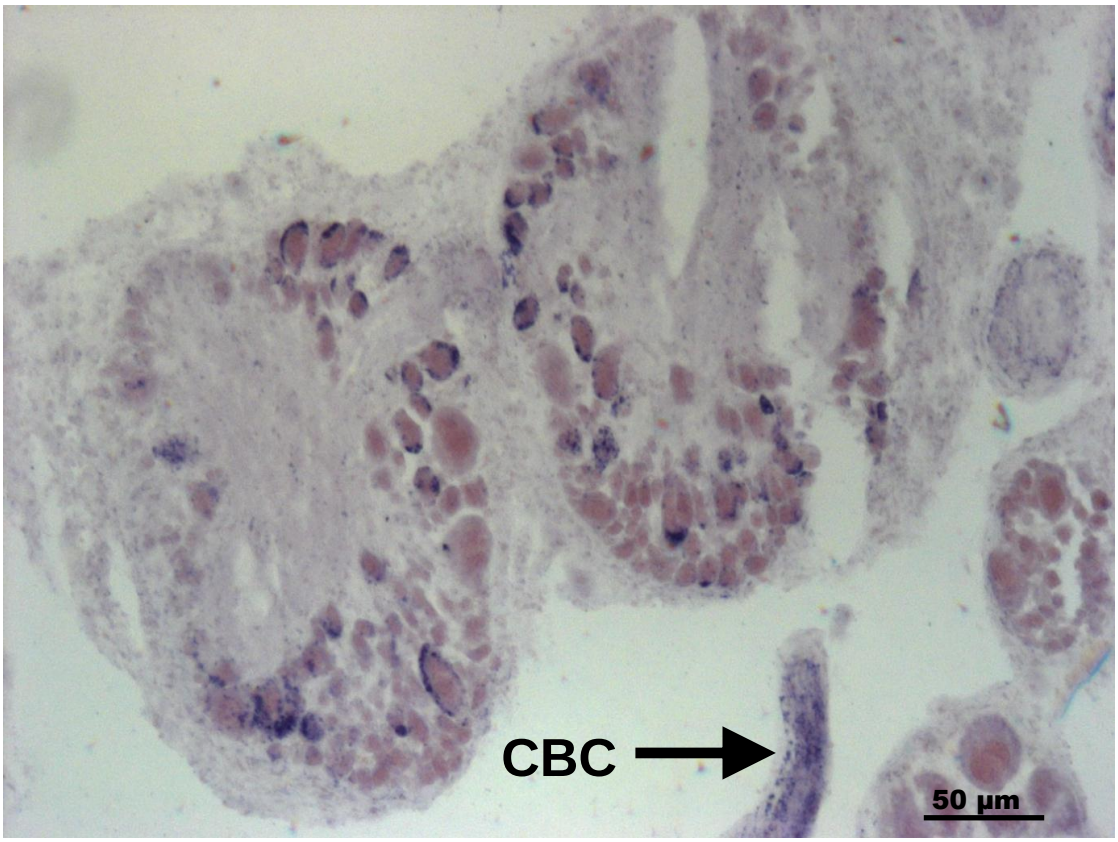

Figure 3.8 The pedal ganglia contain *Lym-antiNOS2* NAT. In situ hybridisation experiments on adjacent sections through the pedal ganglia showing the staining with *Lym-antiNOS2* antisense probe, but not with the sense control probe (not shown). *Lym-antiNOS2* antisense probe shows staining in the CBC.

A

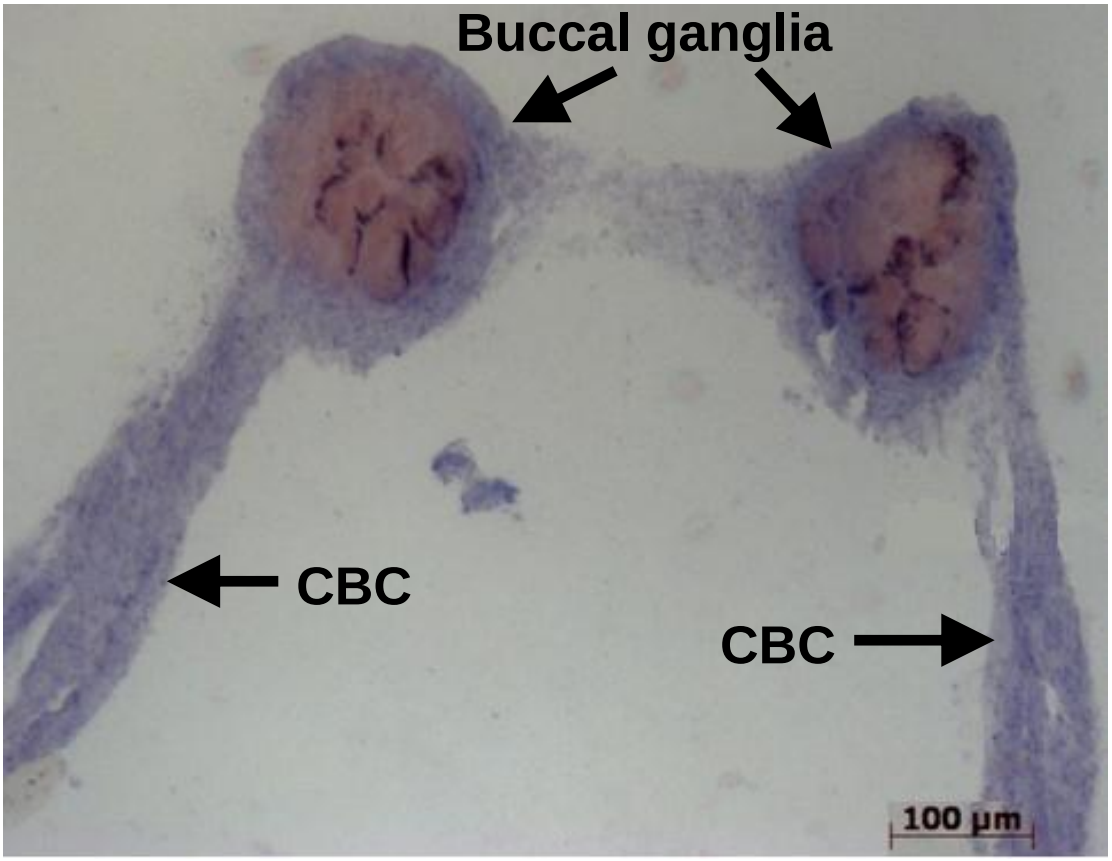

Figure 3.9 The buccal ganglia contain *Lym-antiNOS2* NAT. (A) *In situ* hybridisation experiments on adjacent sections through the buccal ganglia showing the staining with the *Lym-antiNOS2* antisense probe. (B) No staining with the sense control probe.

B

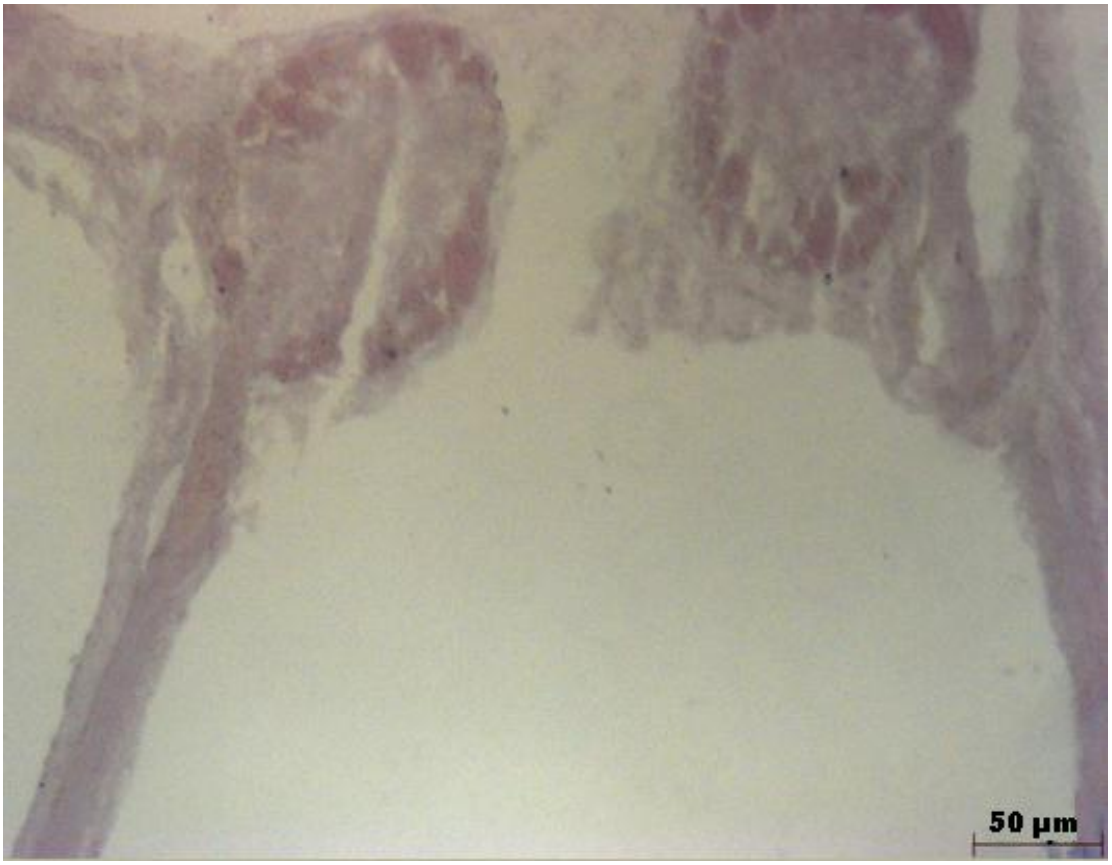

Figure 3.9 (cont.)

A

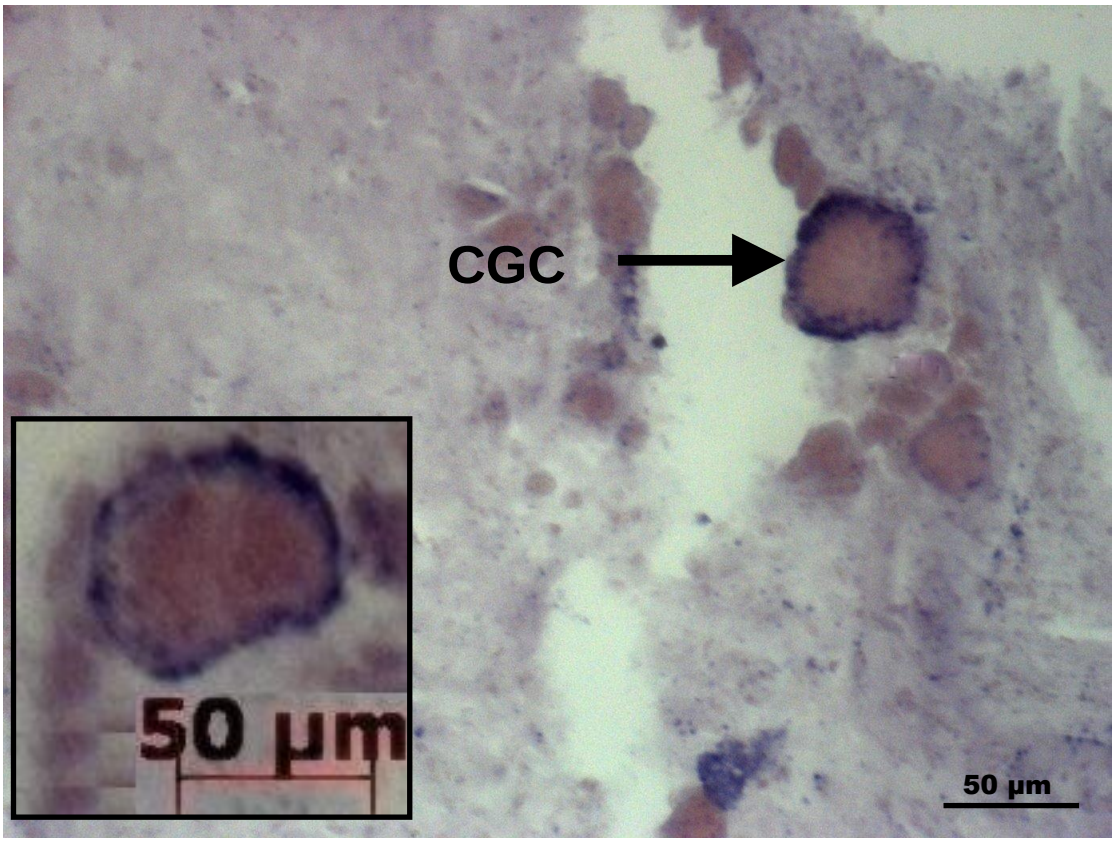

Figure 3.10 The CGC contains *Lym-antiNOS2* NAT. (A) In situ hybridisation experiments on adjacent sections through the cerebral ganglia showing the CGC stained with the Lym-antiNOS2 antisense probe.

B

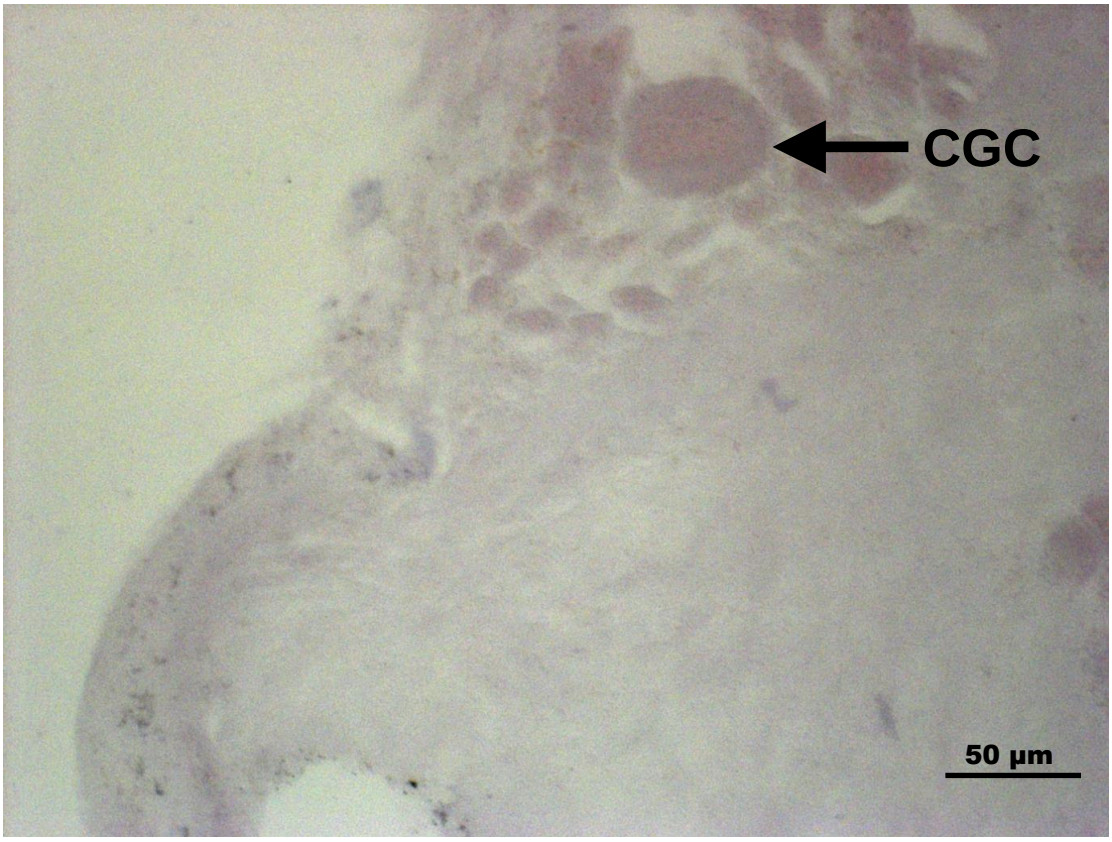

Figure 3.10 (B) In situ hybridisation experiments on adjacent sections through the cerebral ganglia showing no staining with the sense control probe.

C

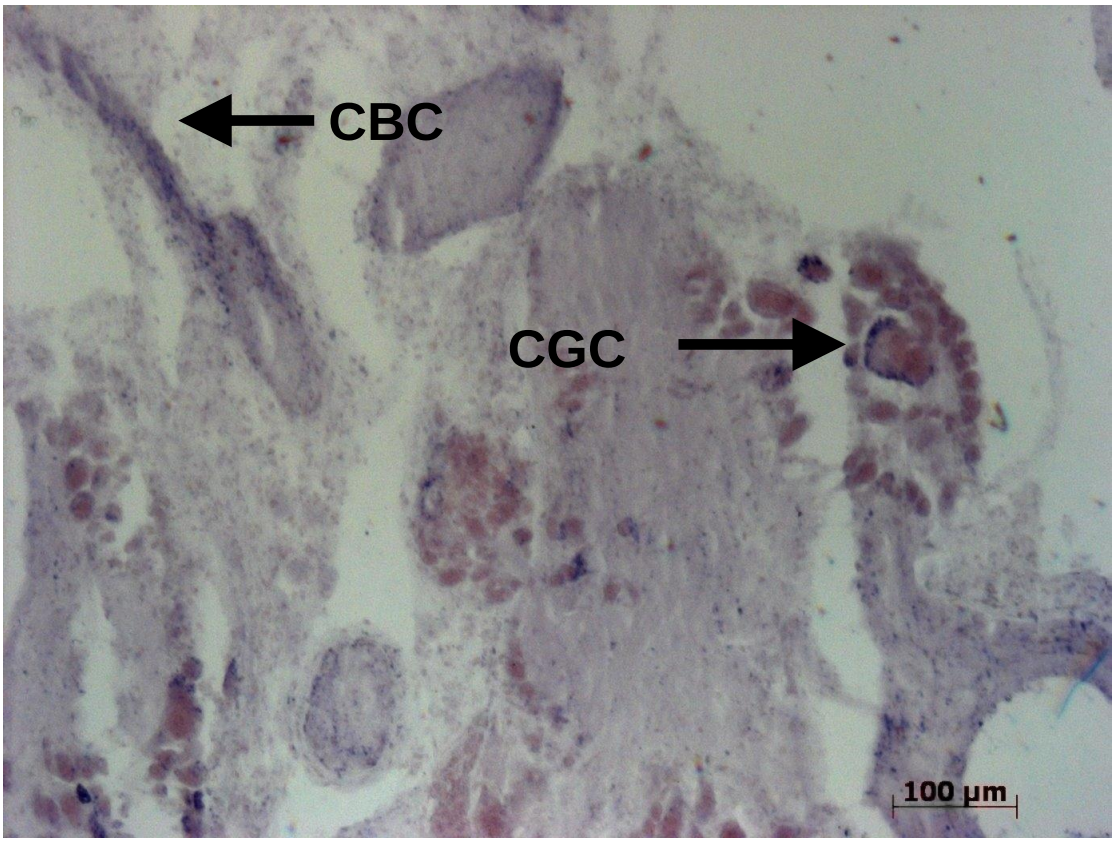

Figure 3.10 (C) In situ hybridisation experiments on adjacent sections through the cerebral ganglia showing the CGC stained with the Lym-antiNOS2 antisense probe.

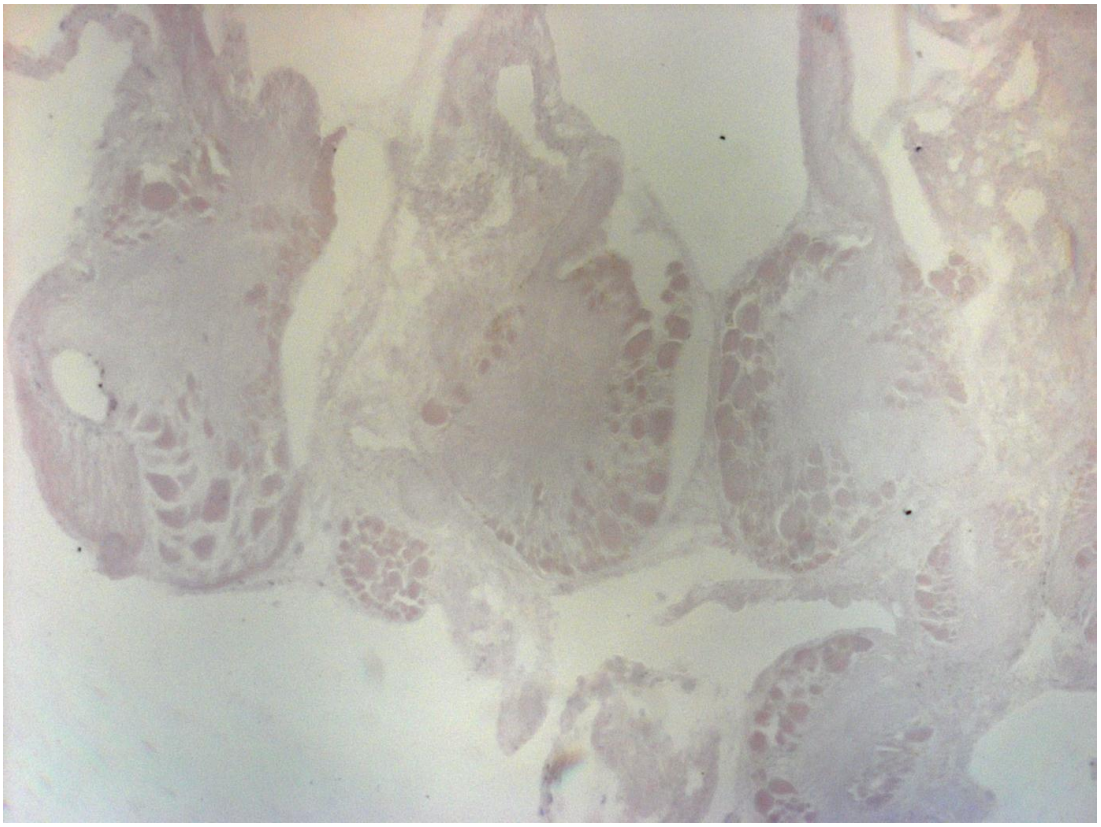

Figure 3.11 *In situ* hybridisation experiments on adjacent sections through the *Lymnaea* CNS with *Lym-antiNOS2* sense control probe, showing no staining.

3.4. *Lym-antiNOS2* RNA is Expressed in the CGCs

In view of the potential significance of our findings on *Lym-antiNOS2* expression on the CGC, we validated the results of *in situ* hybridisation by using the more sensitive RT-PCR technique (reverse transcription polymerase chain reaction).

3.4.1. RT-PCR on Isolated Identified CGC

One widely appreciated property of some gastropod neurons is their large size. The CGCs are frequently classified as giant neurons. The significance of why giant neurons occur is not clear, but giant neurons have 200,000 times the haploid amount of DNA, which represents 16 doublings of the diploid DNA content (Chase, 2002). The cell bodies of CGC are identified easily by size given that they are the largest ones on the ventral side of the anterior part of the cerebral ganglion (100-200µm in diameter). The CGCs are highly pigmented and clearly visible.

A *Lymnaea* brain was isolated from the body (Section 2.3) and the brain was carefully pinned out and the brain commissure was cut to be able to visualise the CGCs. The cell bodies of CGCs were identified by their position and size. CGCs were individually dissected from the CNS of *Lymnaea* as described in Section 2.13.

When RNA extraction is conducted from whole brain or ganglion, the large amount of extra copies of DNA coming from the giant neurons is very small in comparison to the total amount of RNA extracted, and hence no signs of DNA

contamination can be found. But when RNA extraction is performed on a single (giant) cell, these extra copies of DNA could lead to contamination concealing the RNA pool.

Because of the small amount of RNA material, a first attempt at RT-PCR was carried on a pool of ten CGCs, rather than on individual CGCs. To overcome the problem of DNA contamination, total RNA was extracted from the pooled neurons by means of the Absolutely RNA Nanoprep Kit (Section 2.5). The total RNA was treated with extra DNase treatment (Section 2.6). The RNA was copied into cDNA using iScript reverse transcriptase (Section 2.9) and the cDNA produced was subjected to PCRs using the following primers (Section 2.11):

Forward (Scorp1RT): 5′-GTGAACTATCAAGTCACAARG-3′

Reverse (Scorp2RT): 5′-GAACTCAAGACTCTACGTAG-3′

If the CGCs express *Lym-antiNOS2 RNA*, a product of 119bp is the expected output following the amplification of cDNA by RT-PCR. A diagram of the *Lym-antiNOS2* sequence showing the positions of the primers in the sequence and the amplification product using Scorp1RT and Scorp2RT primer on *Lym-antiNOS2* RNA is presented in Figure 2.2.

The product of the PCR was loaded on an agarose gel to perform an electrophoresis of DNA product. RT- controls were set up alongside each set of PCR reactions to ensure that there was no DNA contamination. Negative controls consisted of a cDNA from all components of the RT-PCR reaction

excluding the reverse transcriptase enzyme. If DNA contamination is present in the sample, a band will be present in the gel consisting of the amplification of genomic DNA instead of cDNA (cDNA is produced from fully transcribed mRNA found in the nucleus and therefore contains only the expressed genes).

Figure 3.12A shows the DNA contamination of the RNA extracted from ten CGCs, justifying an extra DNase treatment step on top of the one specified as part of the Nanoprep kit RNA extraction protocol (Section 2.5).

Following the results of the first RT-PCR attempt, an extra TURBO DNase treatment was conducted after the RNA extraction (Section 2.6). An extra precipitation step was also necessary (Section 2.7) to be able to clean the sample from impurities arising from the TURBO DNase buffer, which inhibit the PCR enzyme. This was a critical step due to the small amount of material present in the tube. The utilization of pellet paint was vital to give better visualization of the sample during the precipitation process.

Working on a single, identified CGC, and after the RNA sample from the CGC was cleaned from DNA contamination, cDNA was synthesised (Section 2.9), followed by PCR amplification with Scorp1RT and Scorp2RT primers (Section 2.11). The PCR product was analyzed by agarose gel electrophoresis (Section 2.12), stained with ethidium bromide and compared to a DNA ladder. A photograph of the gel was taken under ultraviolet lighting conditions showed in Figure 3.12B, where it is possible to visualise a band of the expected size and no contamination in the lane corresponding to RT-. The presence of a

band of the expected size (119bp) in RT+ (lane 2) in Figure 3.12B is an overwhelming proof of the expression of *Lym-antiNOS2* NAT in single CGC and verifies our results from *in situ* hybridisation.

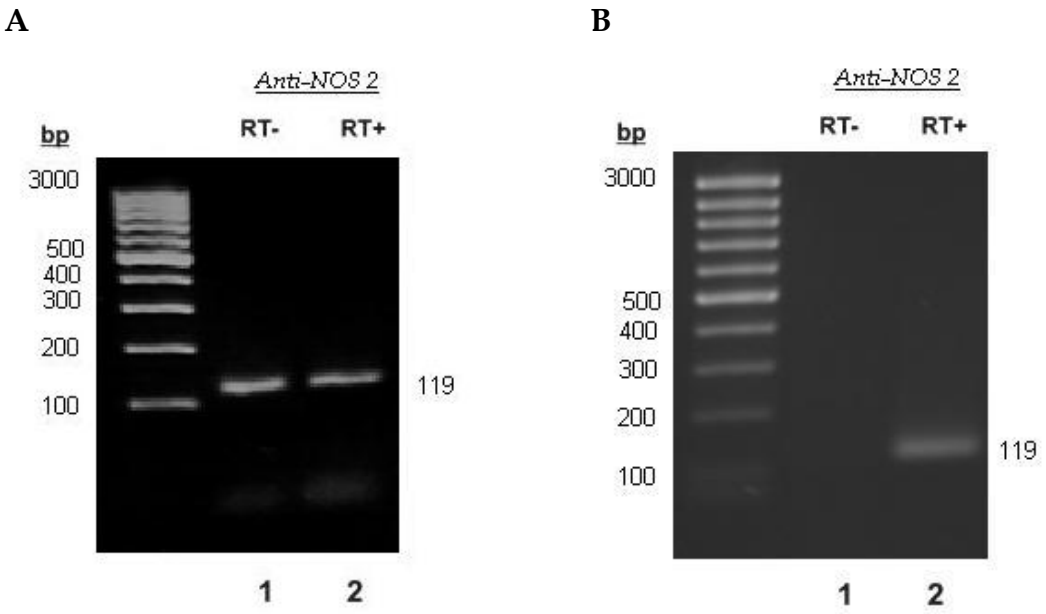

Figure 3.12 RT-PCR experiments on RNA purified from identified CGCs: RT-PCR was performed with primers specific for Lym-antiNOS2 (RT- / lane 1 and RT+/ lane 2). (A) RT-PCR of 10 identified CGCs shows DNA contamination present on the sample (RT- lane 1). (B) The absence of any PCR products in RT- control (lane 1) proves that the RNA samples were free from DNA contamination; lane 2 (RT+) shows a band around the expected size (119bp), proof of the expression of Lym-antiNOS2 in the identified CGC.

3.5. Discussion

Is was already known from previous publications (Korneev et al., 1999) that the NAT transcribed from the *Lym-antiNOS1* gene functions as a negative translational regulator of *Lym-NOS1* expression. The sequence analysis of *Lym-antiNOS2* gene conducted in this chapter shows that it has an open reading frame encoding predicting a protein with 70% identity to the oxygenase domain of NOS. Moreover, it is of considerable interest that the truncated homologue encoded by *Lym-antiNOS2* gene includes the domain required for dimerisation, but not the other regions essential for NO synthesis (Korneev and O'Shea, 2007).

The CGCs are modulatory neurons that have been shown a change in the electrophysiological properties after training. Along with the electrical changes, they show transcription of new RNAs and protein synthesis after training. The neuronal sources of the NO required for LTM formation in *Lymnaea* have not yet been identified. One possibility is that NO is produced by chemosensory neurons involved in mediating the activation of feeding (Elphick et al., 1995). We also know that the CGCs are potentially capable of producing NO under certain specific conditions. Indeed, previous studies showed that although NOS gene expression is usually suppressed in the CGCs (Korneev et al., 1999), reward training leads to its rapid transient activation in these neurons (Korneev and O'Shea, 2005).

It was already reported that *Lym-NOS1* and *anti-NOS* genes are differentially regulated in this neuron as the result of training. Due to the CGCs being interconnected to many neural components of the feeding system, functioning

in a permissive manner to modulate the probability that feeding behaviour will be initiated, it was suggested that the ability of the CGC to signal broadly within the feeding neural network via NO is altered during a critical early stage of memory formation by the training-induced differential regulation of the *Lym-NOS1* and anti-NOS genes (Korneev et al., 2005).

The in situ hybridisation experiments conducted in this chapter show the presence of *Lym-antiNOS2* RNA in the CGCs. Moreover, its expression is not indiscriminate across the whole brain. As the CGCs are known to have an important role in formation of the LTM circuit, this result is of crucial importance. An independent confirmation of the presence of *Lym-antiNOS2* RNA in the CGCs is given by performing single-cell RT-PCR in *Lymnaea* CGCs. These experiments are conducted on RNA extracted from individually identified CGCs. The results of this analysis confirm the *in situ* data and unambiguously demonstrate that *Lym-antiNOS2* RNA is indeed co-expressed in the CGCs with *NOS* mRNA. Therefore it can be suggested that under the conditions that follow training, the production of NO in the CGCs may be regulated by *Lym-antiNOS2* present in the same cells.

The *in situ* hybridisation experiments also show that in neurons where *Lym-antiNOS2* RNA is present it is mainly cytoplasmatic, and absent in the nuclei. The location of *Lym-antiNOS2* RNA in the cytoplasm agrees with the bi-functional RNA hypothesis that *Lym-antiNOS2* RNA might play a role in inhibiting the translation of NOS1 RNA, and might also encode a truncated

NOS-related protein that can form a non-functional heterodimer with normal NOS1 protein.

The expression of *Lym-antiNOS2* RNA was detected by *in situ* hybridisation in buccal ganglia, cerebra ganglia, pedal ganglia, cerebrobuccal connectives but not in the rest of the brain. An unexpected result of the *in situ* hybridisation experiments was the presence of *Lym-antiNOS2* RNA in the CBCs, along with the CGCs. CBCs only contain axons, and are the only connection between the cerebral and buccal ganglia that form the feeding CPG. Further experiments on the CBCs are presented in Chapter 5.

In this chapter we show unambiguously that *Lym-antiNOS2* is expressed in *Lymnaea* brain. Previous research introduced the hypothesis that *Lym-antiNOS2* NAT can be considered as a putative bi-functional RNA because it can function as a protein-encoding mRNA that also contains a potential regulatory antisense region localised in the 3' UTR, but no proof that *Lym-antiNOS2* RNA is co-expressed with *Lym-NOS1* mRNA in the CGCs had been found. Findings bring new light to this hypothesis. Together with the results that the NO-cGMP-PKG signalling pathway is critical for memory formation, this suggests that *Lym-antiNOS2* NAT could be involved in the regulation of NO production during LTM formation. This suggestion is explored further in Chapter 4 by studying changes in the expression of *Lym-antiNOS2* NAT after single-conditioning training.

Chapter 4: Quantitative Analysis of *Lym-antiNOS2* NAT Expression in Trained and Naïve Animals

Three major questions will be addressed in this chapter:

- Are there changes in the expression levels of *Lym-antiNOS2* RNA in whole brain after a single conditioning trial?
- What are the differences in the expression of *Lym-antiNOS2* RNA on different ganglia, after a single conditioning trial?
- Are there changes in the expression levels of *Lym-NOS1* mRNA in *Lymnaea* brain after a single conditioning trial?

To enable the quantification of different levels of expression at small concentrations, the use of real-time PCR is indispensable.

4.1. Introduction

It was shown in previous research in *Lymnaea* that one-trial chemical appetitive conditioning acts selectively and differentially within the *NOS* gene family (Korneev et al., 2005). Specifically, single-conditioning trial induced changes in the expression of *Lym-NOS1* and *Lym-antiNOS1*, while *Lym*-NOS2 is stable. Importantly, it has been shown that the cerebral ganglia are the central locus of plasticity where associative LTM formation occurs. It has also been shown that the expression of the *NOS1* RNA in these neurons is transiently up-regulated after conditioning. The cerebral ganglia contain modulatory neurons

that are essential for the gating or initiation of feeding behaviour in response to the CS.

Previous studies have hypothesized that the decrease in the amount of *Lym-antiNOS1* RNA observed at 4 hours after conditioning can lead to an increase in the production of NO that facilitates memory formation, but no studies have been made on the *Lym-antiNOS2* gene.

4.2. Feeding behaviour in *Lymnaea*

The feeding behaviour in Lymnaea stagnalis has been extensively studied and the interneurons which belong to the Central Pattern Generator (CPG) underling this rhythmic behaviour have been identified. The feeding consists of repetitive rasps, carried out with a toothed radula, each rasp includes three phases: protraction, retraction and swallow. During the protraction phase the radula is extruded over the substrate, after the radula is retracted it to the mouth, which is closed during the swallowing phase (Benjamin et al., 2000).

Each of these phases is generated by a different class of interneurons, respectively N1, N2 and N3. These interneurons form the CPG which drive the motoneurons localised in the buccal ganglia (B1-B10). Applications of sucrose on the lips or on the oesophagus trigger a fictive feeding response that can be recorded from the motoneurons and from the interneurons in the buccal ganglia. Interneurons located in the cerebral ganglia, like the cerebral giant cells (CGCs) gating interneurons and of the cerebro-buccal interneurons (CBIs) command –like interneurons play an important role in the modulation of the

feeding behaviour (Kemenes et al., 2006a). These interneurons in the cerebral ganglia are required for a food-driven response and have been shown to be involved in classical appetitive learning (Kemenes et al., 2006a). The sensory inputs reach the slow oscillator (SO), a single modulatory cell placed either in the left or in the right buccal ganglion. A strong current injection in in the SO can initiate fictive feeding, but the main role of this cell is to control the frequency and maintain the regularity of the feeding rhythm (Kemenes et al., 2001)

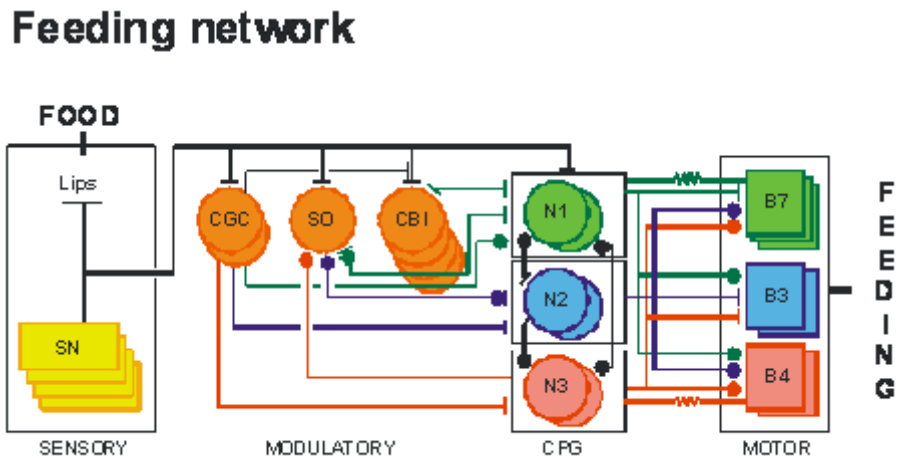

Figure 4.1 Lymnaea feeding network: schematic representation of the identified neurons involve in food-driven feeding behaviour (Benjamin P.R. 2006)

4.3. Optimization of Quantitative RT-PCR

The information for the synthesis of all proteins in an organism is encoded in the DNA in the form of genes. The process of transcription transfers the information of a gene into mRNA, which can be translated into proteins. Therefore, the quantification of mRNA can be used to assess the expression levels of a particular gene. Real-time PCR can quantify alterations in RNA

concentrations that were previously undetectable using earlier techniques such as RT-PCR or RNase protection assays.

The real-time PCR technique enables the quantification of target gene expression by using a fluorescent reporter molecule to monitor the progress of the amplification reaction. In our case, the reported molecule is the dye SYBR Green that binds to double-stranded cDNA emitting a fluorescence signal. The main advantages of this detection method are that it is cost effective and easy to use. One of the limitations on the use of SYBR Green is that it can bind to any double-stranded DNA including primer dimers or unspecific products. Consequently, the primers should be designed and optimized to avoid any non-specific binding.

The levels of expressed genes can be measured by *absolute* quantification (standard curve method) or by *relative* quantification. Absolute quantification uses serially diluted standards of known concentration to generate a standard curve from which the absolute amount of an unknown concentration can be determined. The method employed in this study was a relative quantification method, where gene expression was normalized to a reference gene, and its levels relative to the gene expression of a non-treated sample used for comparison.

In order to control the variability introduced by the real-time PCR technique and assure accurate results, a reference gene that is assumed to have equal levels of expression in each experimental sample should be used. The reference

gene chosen in this study was the β-tubulin gene. This gene encodes for the synthesis of β-tubulin which is a microtubule element of the tubulin family found almost exclusively in neurons. Due to its constant expression in many experimental conditions, the use of β-tubulin as a reference or housekeeping gene is recommended (Martinez-Fernandez et al., 2011).

Relative quantification is used in studies where the experimental objective is to investigate small changes in RNA expression levels. The normalized amount of target is a unitless number that can be used to compare the relative amount of target in different samples. This comparison was designed such that one sample is the calibrator. Naïve whole brain sample was designated as the calibrator.

A comparative Ct (cycle threshold) method was used as described in Section 2.15.1. Before using the ΔΔCt method for quantification, a validation experiment has to be performed to demonstrate that the efficiencies of target (*Lym-antiNOS2*) and reference (β-tubulin) amplification are approximately equal (Figure 4.2).

An amplification plot using a semi-log scale representation (Figure 4.3A, B) was used to determine the fluorescence threshold. Measurements below this threshold were discarded to avoid the noise close to the baseline. An analysis of the dissociation curves (Figure 4.3C, D) shows that the melting temperature of the amplicon is 78.5°C for both PCR products. No contaminating products are present in this reaction. Contaminating DNA or primer dimers would show up

as additional peaks separated from the desired amplicon peak. The no-template control for both genes did not record any amplification.

A

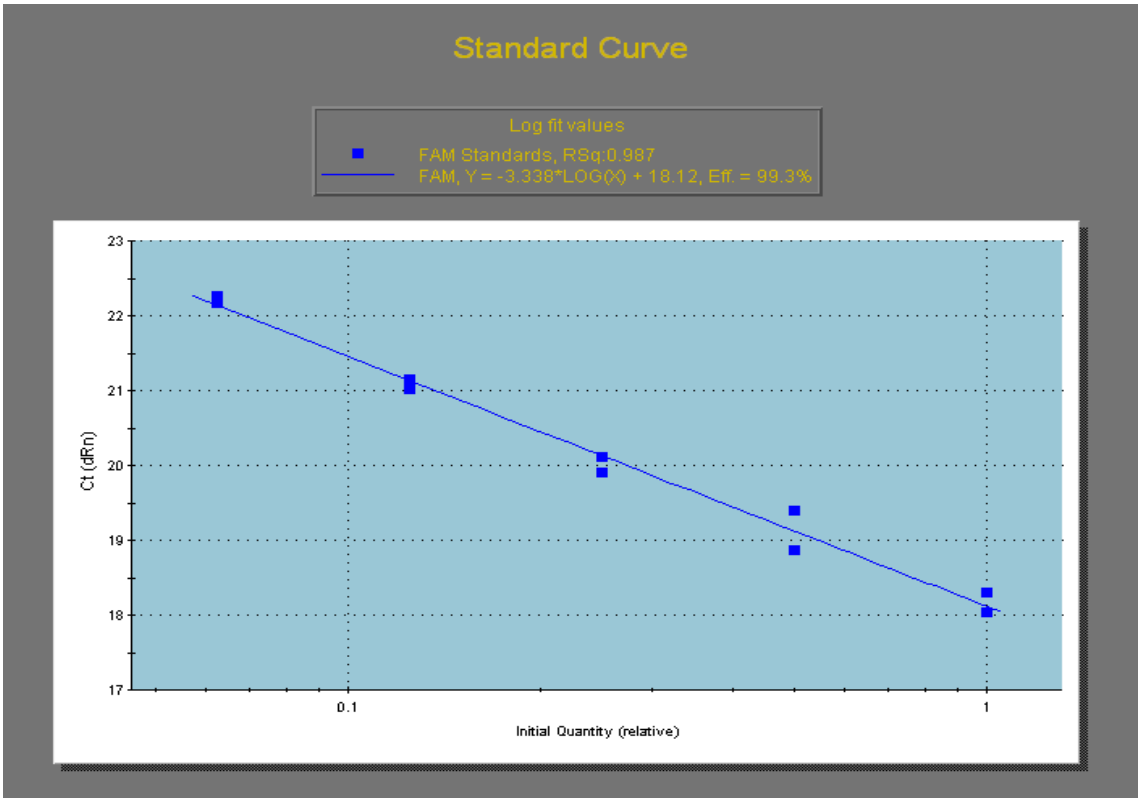

Figure 4.2 Standard curves (a) standard curve generated from *Lym-antiNOS2* amplification data, (b) standard curve generated from *β-tubulin* amplification data, (c) demonstration that the efficiencies of targets are equivalent

B

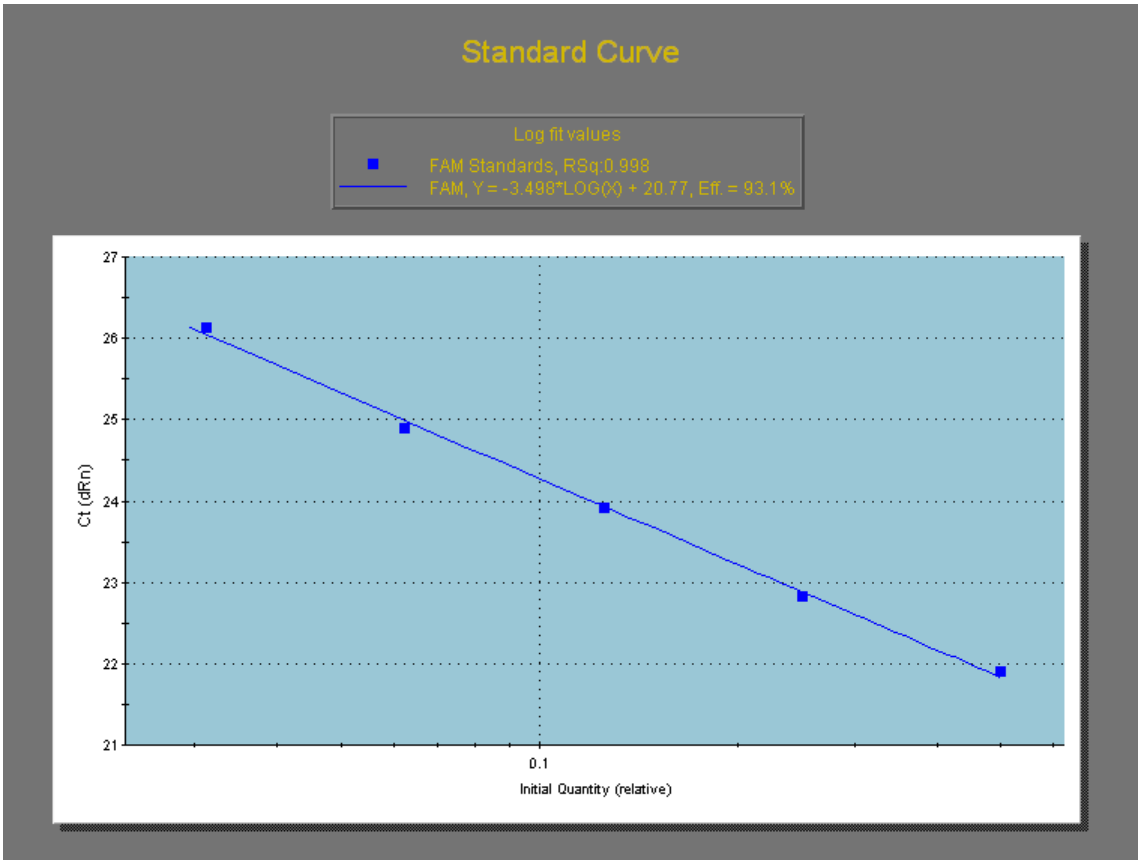

C

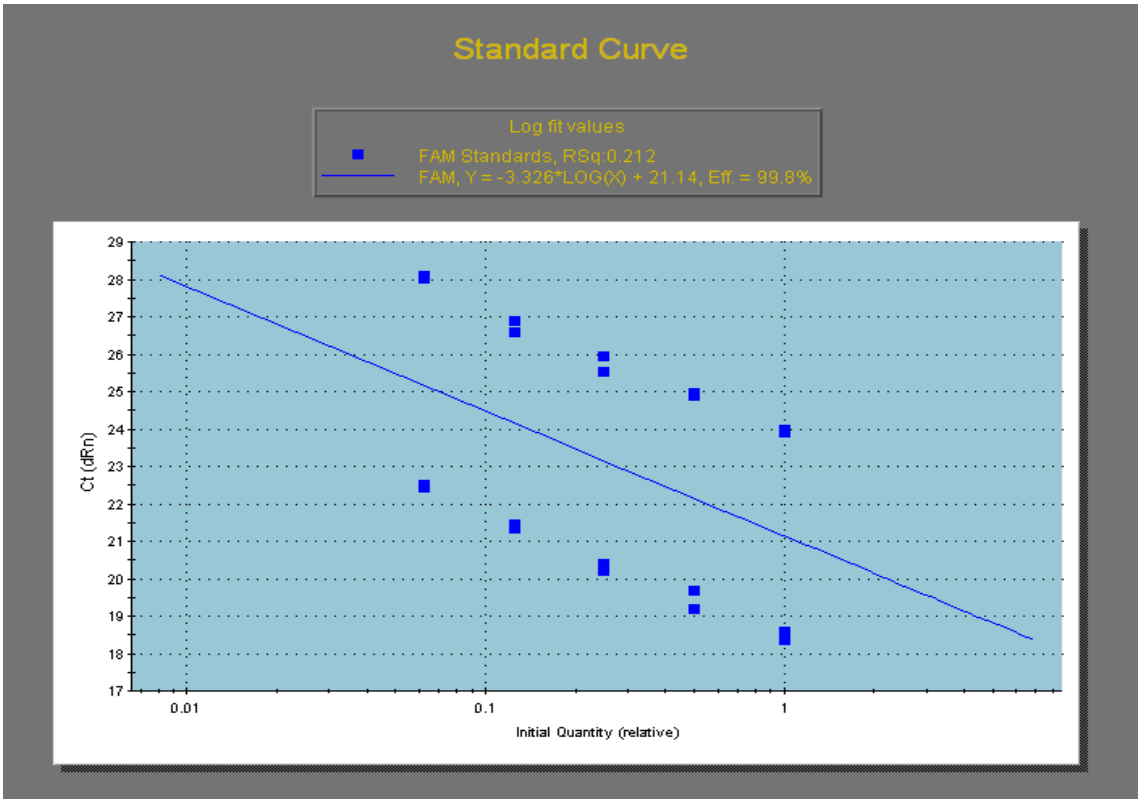

Figure 4.2 Standard curves (a) standard curve generated from Lym-antiNOS2 amplification data, (b) standard curve generated from β-tubulin amplification data, (c) demonstration that the efficiencies of targets are equivalent

A

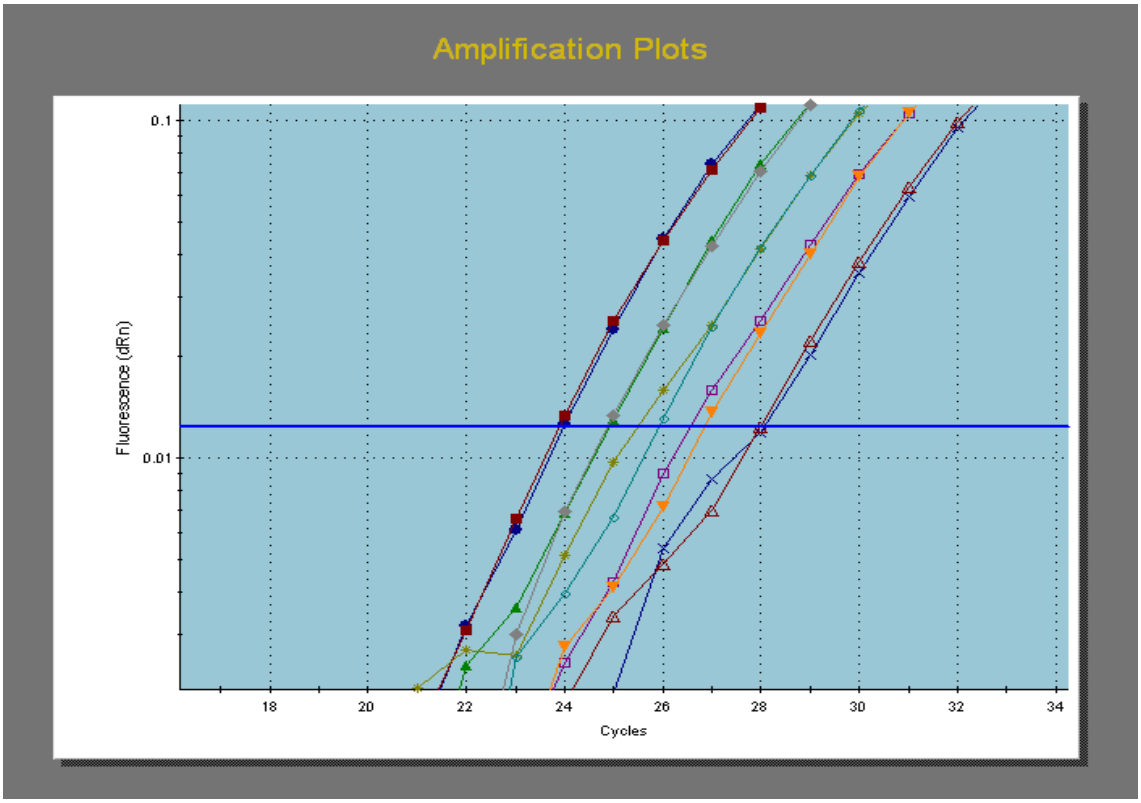

B

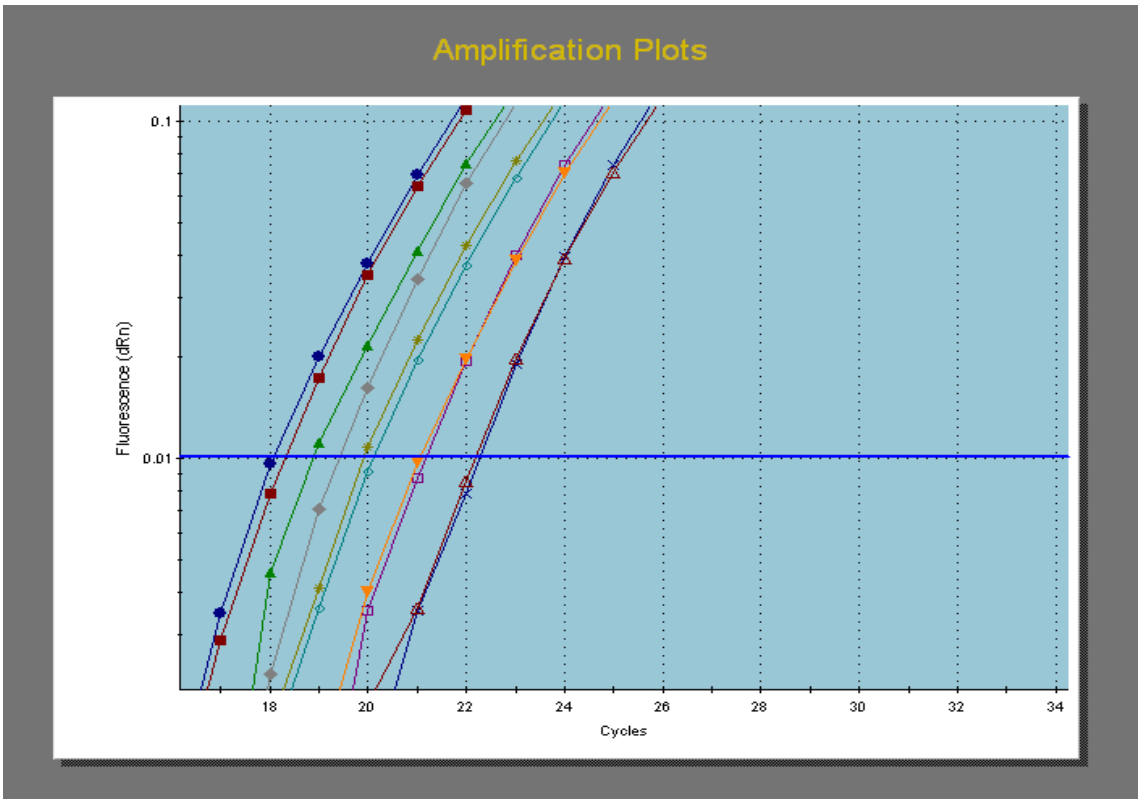

Figure 4.3 Real-time PCR amplification plots of *Lym-antiNOS2* (A) and *β-tubulin* (B).

C

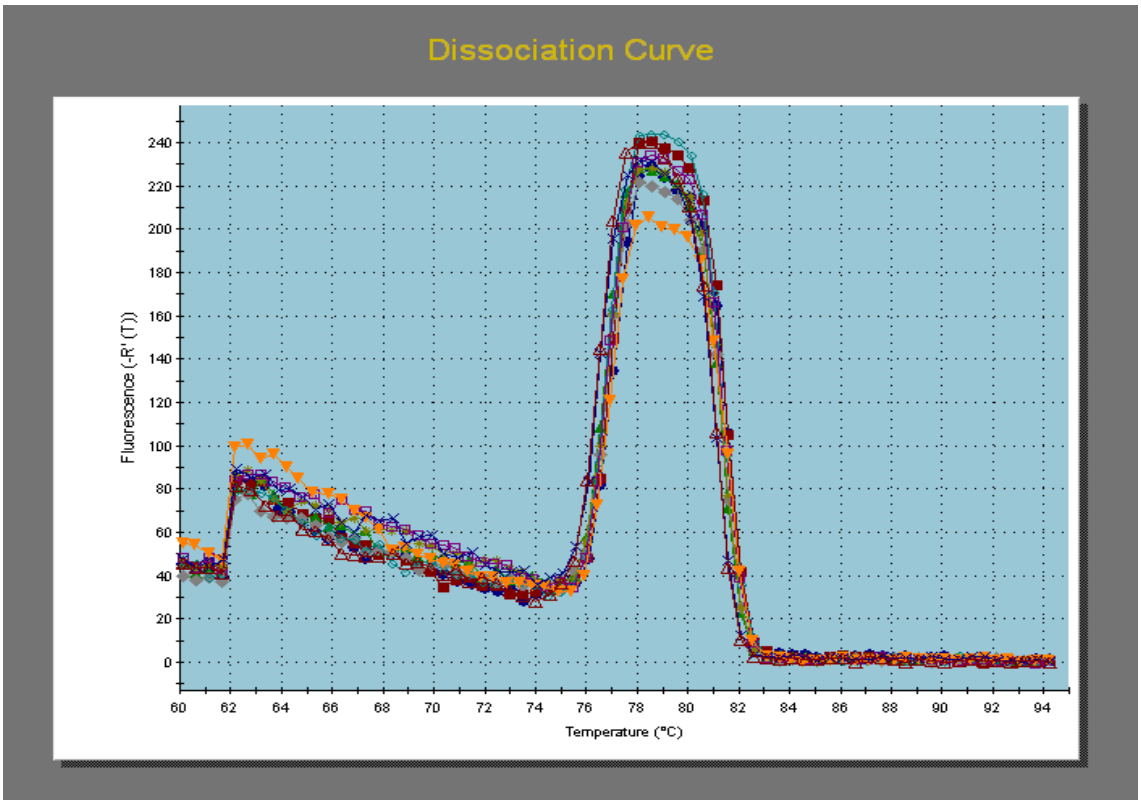

D

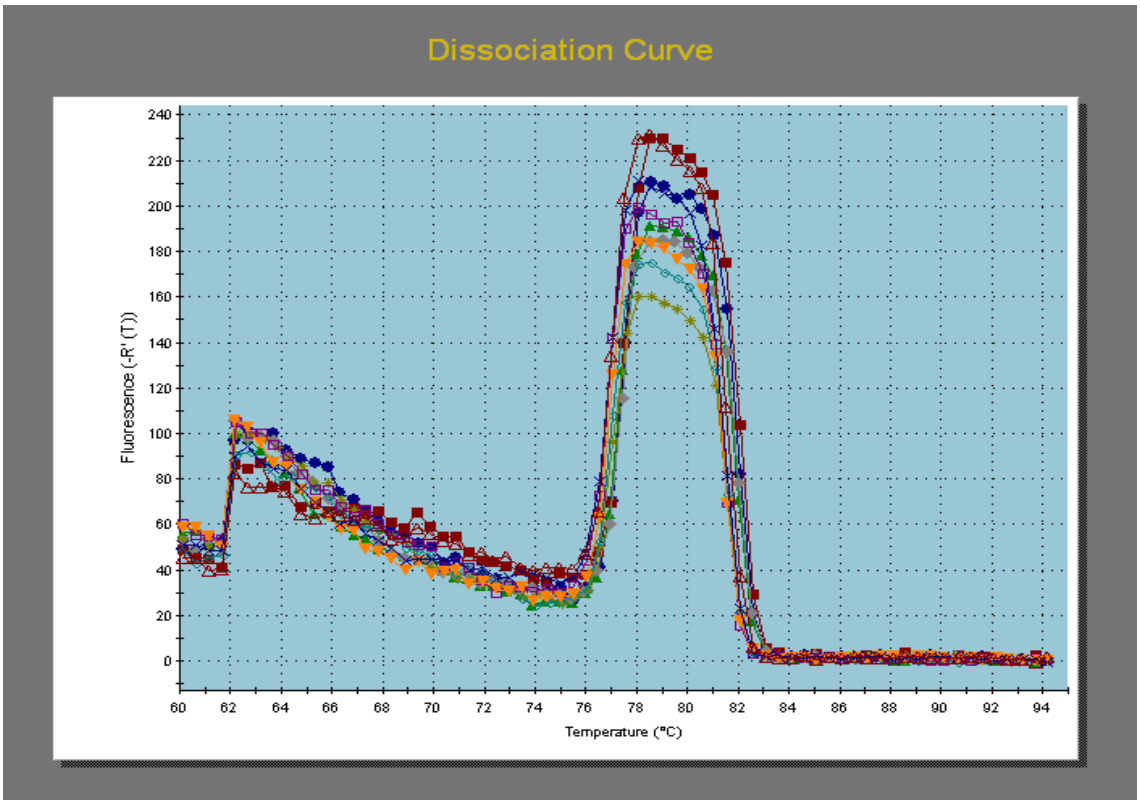

Figure 4.3 (cont.) Dissociation curve of the real-time amplification (C) *Lym-antiNOS2, (D) β-tubulin*

The total RNA extraction from *Lymnaea* CNS was carried out following the protocol described in Section 2.4 and stored at –20°C until further processing. cDNA was synthesised on DNase-treated total RNA following the protocol described in Section 2.9 and stored at –20°C. The gene-specific primers were designed by Dr Sergei Korneev using the *Lym-antiNOS2*, *Lym-NOS1, Lym-NOS2* and *Lym-antiNOS1* sequences described in Section 3.2.

Primer Optimization To ensure the efficient and accurate quantification of the target template, real-time PCR assays should be optimized. Assays are first optimized by primer titration to see the efficiency of the reaction. To do that, four concentrations with equimolar amounts of each primer pair were tested: 100 nM, 200 nM, 400 nM and 600 nM. The amount of template added was the same in all the samples in the optimization exercise. All the samples were run in duplicates. The ideal primer pair concentration should yield the lowest average Ct value as well as presenting a dissociation curve that shows a single product.

Standard Curves for Analysis of Assay Performance Following primer optimization a standard curve was performed using a serial dilution of a calibrator sample in order to test the efficiency, precision and sensitivity of the real-time PCR reaction. In this case, a two-fold dilution series starting with 1:50 diluted cDNA and consisting of four points was generated in duplicate. To obtain the standard curve, the Ct values of the serial dilution of the calibrator sample were plotted (Figure 4.2).

In order to evaluate the overall performance of the real-time PCR reaction, a standard curve was generated for each gene. After amplification, the Ct's for each standard dilution were determined and plotted. The amplification of cDNA serial dilution with Scorp1RT and Scorp2RT primers generated a standard curve with an efficiency of amplification of 99.5% (Figure 4.2A). The slope of the line of best fit determines the efficiency of a reaction using the equation E = 10 (–1/slope) –1. The linearity of the assay, denoted by the R squared (RSq or R2) was 0.985. A value of E close to 1 implies a linear range and that the efficiency of the reaction is consistent at varying template concentrations (sensitivity). It also indicates agreement between replicates.

For the cDNA amplification serial dilution with β-tubulin primers, the amplification was linear with RSq = 0.987 and an amplification efficiency of 99.3% (Figure 4.2B).

After the primer optimization and the assay performance evaluation, the next step was to test the primers at the concentration chosen (600nM for antiNOS-2 and 400nM for β-tubulin) with Lymnaea cDNA from the experimental samples. The amplification of the reference cDNA generated a single product with a melting temperature of 79°C (Figure 4.3C). *Lymnaea* cDNA amplified with primers for the detection of *Lym-antiNOS2* yielded a single product (Figure 4.3D) with a melting temperature of 78°C. The no-template control for both genes did not record any amplification.

Confirmation of the Identity of the Products Formed All the reactions in the real-time PCR amplification generated products that agree with those expected. After cloning, the sequences obtained confirmed the identity of the fragments as *Lym*-antiNOS2 and β-tubulin.

Long Term Memory formation After One-Trial Appetitive Conditioning The one-trial reward conditioning protocol was performed using the method described in Section 2.2. The snails were trained and CNS dissected by Dr Ildiko Kemenes. The snails were separated into six groups: 10 minutes, 1 hour, 4 hours, 6 hours, UP and N. This protocol is illustrated in Figure 4.4.

A total of 270 snails were trained (Table 4.1). After training the snails were separated following the groups on Table 4.1 and separated into tanks according to groups. The CNS's were dissected (Section 2.3) and stored frozen at -80°C. Some of the CNS's were separated into buccal ganglia, cerebral ganglia and remainder of the CNS's, before being frozen and stored at -80°C.

	whole brain	ganglia	Learning test
N	32	16	18
UP	32	16	18
P-6hr	16	8	18
P-4hr	16	8	
P-2hr	16	8	
P-1hr	16	8	
P-10min	16	8	
Total			270

Table 4.1 Experimental groups for the one-trial reward conditioning protocol: separation of animals in naïve (N), unpaired (UP) and (P) paired (dissected after 10 minutes, 1, 2, 4 and 6 hours).

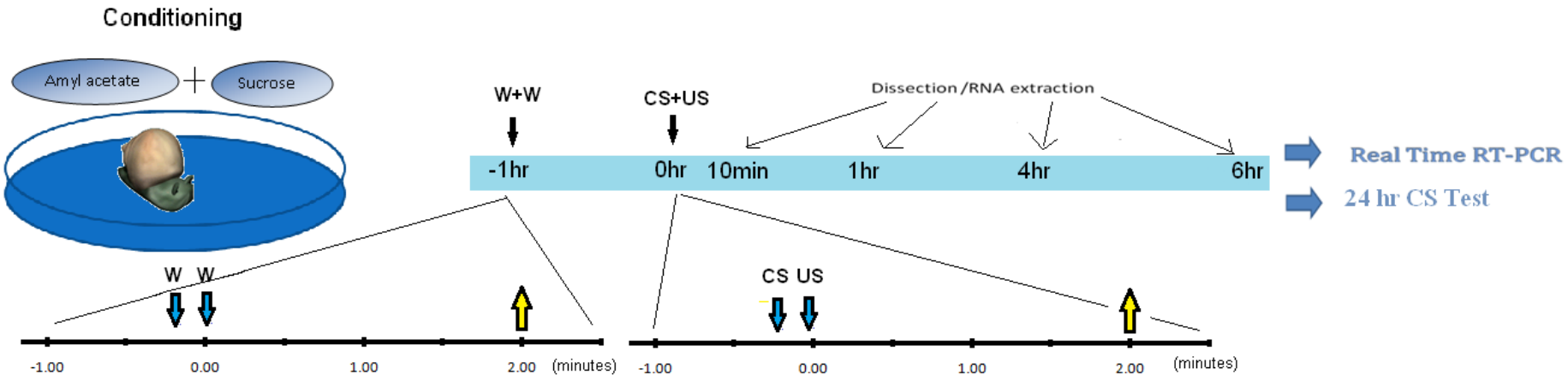

Figure 4.4 One-trial reward conditioning was performed using a method based on a previously published protocol (Alexander et al., 1984) Experimental (conditioned) animals were exposed to a solution of amyl acetate (CS-condition stimulus) and immediately after that to a sucrose solution (US- uncondition stimulus). Unpaired control animals were conditioned to CS an to US, separated by and interval of 1 hour. At different time points (10 min, 1 hour, 4 hours, 6 hours) after the treatment, RNA was extracted and used for real-time PCR analysis. For training protocol refer to Section 2.2

RNA extraction was performed from the frozen CNS (Section 2.4). Part of the RNA was used in a reverse transcriptase reaction (Section 2.9). An equal volume of water was added to the RNA for the synthesis of cDNA and the reaction was set up as shown in Table 2.2.

After the synthesis of cDNA a reaction for the quantification of the gene expression was set up. Nine samples were set up on each run. Each sample was run in triplicate along with a no-template control and a calibrator which is run on duplicate. Table 2.3 shows a sample of the protocol.

18 snails from each group (UP, P and N) were retained and tested for long term memory formation at 24 hours after conditioning (paired and unpaired) trials. The CS alone elicited a conditioned response (CR) as shown by increased rasping frequency. An unpaired control group had the CS and US presented 1 hour apart. Figure 4.5 shows that the snails on the unpaired group had not formed long term memory. A significant increase of the rasping movements in a 2-minute interval was observed as a response to the training protocol in paired animals.

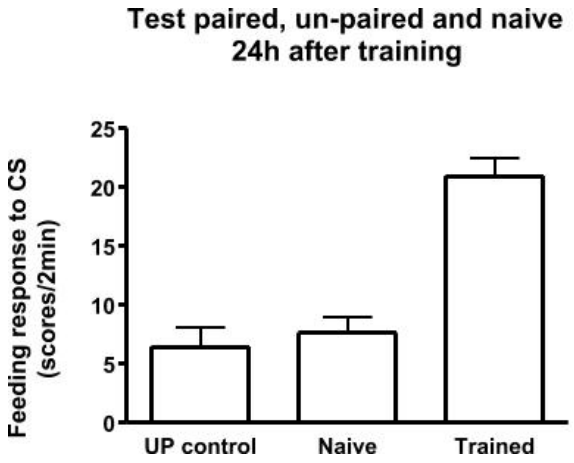

Figure 4.5 Behavioural training. Trained animals exhibited a significantly higher rate of rasping in response to the 24 hours CS test than the animals from the unpaired control group (n=18, $p<0.05$) (Ildiko Kemenes).

4.4. Long Term Memory Formation Induces Timed Changes in the Expression of *Lym-antiNOS2* NAT

LTM formation following reward conditioning of feeding behaviour in Lymnaea requires the NO-cGMP signalling pathway (Kemenes et al., 2002). This requirement is restricted to a window of time lasting about 5 hours following a single pairing of sucrose (US) with amyl acetate (CS). It was found that *Lym-antiNOS1* is significantly down-regulated at 4 hours after conditioning. This is an example of a pseudogene whose expression is regulated by a behavioural stimulus. Interestingly, *Lym-NOS1* RNA also exhibited training-evoked changes of expression, being transiently up-regulated at 6 hours after training, 2 hours after the down-regulation of *Lym-antiNOS1* (Korneev and O'Shea, 2007).

In light of the hypothetical role of *Lym-antiNOS2* in the regulation of NOS expression in the CNS and its possible role in the formation of the

truncated-NOS Lym-antiNOS2 protein, it was important to investigate whether this NO-dependent memory formation is associated with specific changes in the expression of *Lym-antiNOS2* NAT.

The results of the qRT-PCR experiments on the expression of *Lym-antiNOS2* NAT show that the *Lym-antiNOS2* gene was significantly down-regulated at four hours after training (Figure 4.6 and Table 4.3), followed by up-regulation at six hours after training. Within-groups analysis demonstrates that responses to the training on the paired group were statistically significant. T-test performed between paired groups versus unpaired and naïve group shows no difference between groups of the levels of expression of *Lym-antiNOS2* at 10 minutes and 1 hour after training. Results of the statistical analysis are summarised in Table 4.2.

The dynamic sensitivity of *Lym-antiNOS2* expression to a very weak sensory cue (single pairing of US and CS) is remarkable. The analysis of the temporal dynamics of the post-training expression of the *Lym-antiNOS2* NAT in the whole brain by real-time PCR shows that the *Lym-antiNOS2* gene was down-regulated at 4 hours and up-regulated at 6 hours after training. These dynamics for *Lym-antiNOS2* gene are noteworthy, and provide another example of a pseudogene whose expression is regulated by a behavioural stimulus, as with the *Lym-antiNOS1* gene, whose expression is down-regulated at 4 hours after training but shows no changes at 6 hours or 24 hours (Korneev et al., 2005).

Dr Korneev has shown that *Lym-NOS1* was transiently up-regulated at 6 hours and *Lym-antiNOS1* was down-regulated at 4 hours after training (Korneev et al., 2005). It is possible to hypothesise that the decrease in the amount of *Lym-antiNOS1* and *Lym-antiNOS2* NAT at four hours could lead to the increase in the amount of *Lym-NOS1* mRNA molecules available for translation. After its up-regulation at 6 hours, *Lym-antiNOS2* NAT could be acting as a suppressor of NOS through the formation of a non-functional heterodimer, where NOS1 is not required anymore for LTM formation. It is still necessary to prove that translation of *Lym-antiNOS2* RNA into protein does occur in vivo. *Lym-antiNOS2* RNA was confirmed to translate into a protein via *in vitro* translation experiments (Korneev and O'Shea, 2002).

	Paired-Unpaired	Paired-Naïve
10 minutes	p=0.6	p=0.8
1 hour	p=0.5	p=0.2
4 hours	p<0.0005	p<0.03
6 hours	p<0.01	p<0.005

Table 4.2 Statistical analysis of *Lym-antiNOS2* expression in *Lymnaea* CNS after one-trial reward conditioning.

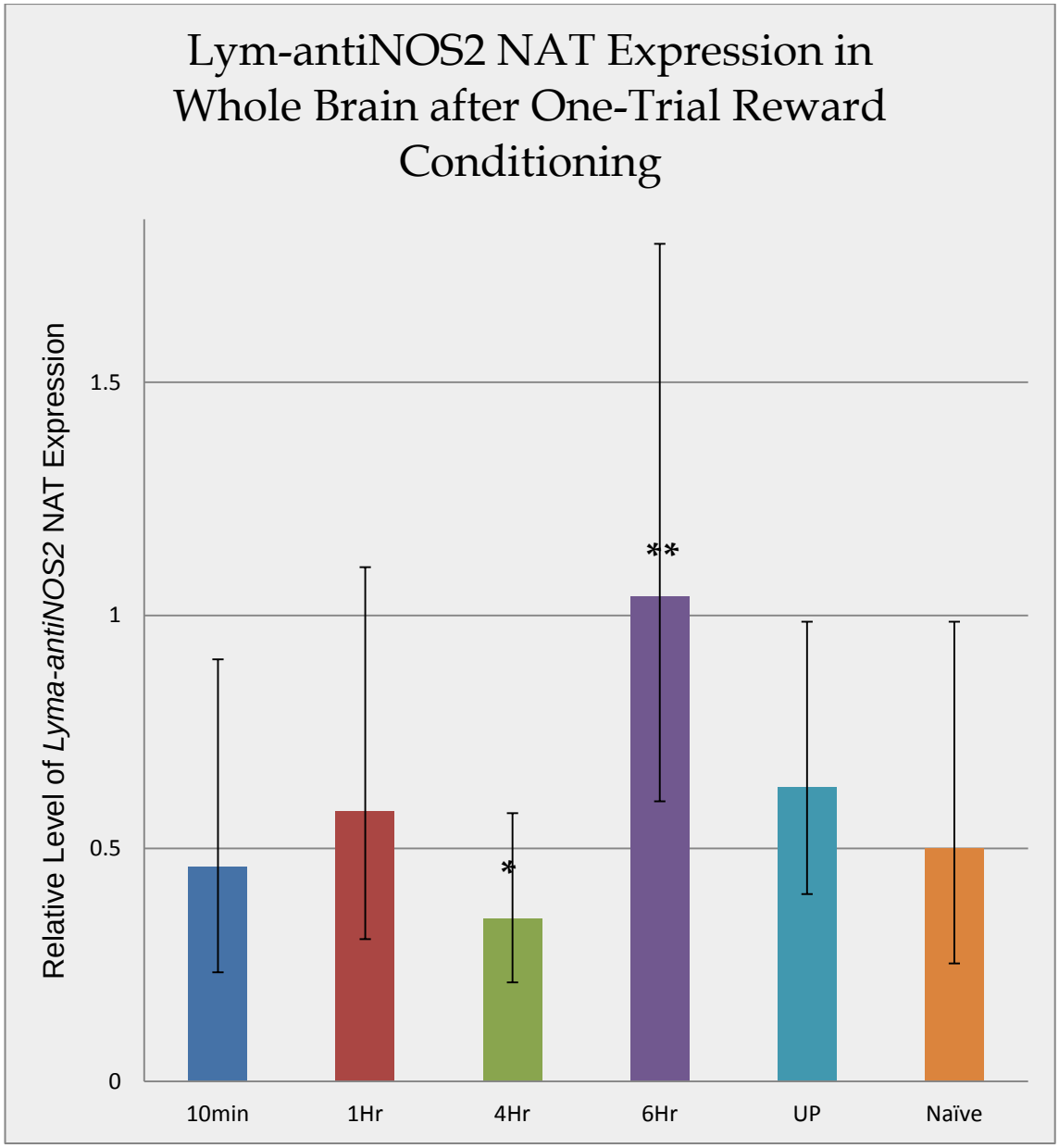

Figure 4.6 Training-induced regulation of *Lym-antiNOS2* NAT in *Lymnaea* CNS. Real-time PCR analysis of the *Lym-antiNOS2* NAT expression in CNS. Levels of *Lym-antiNOS2* in 10min group (blue bar), 1Hr (red bar), 4Hr (green bar), 6Hr (purple bar), unpaired control (UP) (turquoise bar) and naïve group (orange bar) normalised to an endogenous reference (β-tubulin) and relative to a calibrator (CAL) was calculated as $2\text{-}\Delta\Delta C_t = \Delta C_t - \Delta C_{t(cal)}$. ΔC_t and $\Delta C_{t(cal)}$ are the differences in threshold cycles for target (*Lym-antiNOS2*) and reference (β-tubulin) measured in the samples and in the calibrator, respectively. The bars show the mean value of eight samples ± standard deviation of the quotient. Results show a down-regulation of *Lym-antiNOS2* at 4 hours after training and up-regulation at 6 hours after training. The single asterisk at the 4Hr group indicates a statistically significant difference from control $p = 0.0005$. The double asterisk in the 6Hr conditioned group indicates a statistically significant difference from the control $p = 0.01$.

	10min	1Hr	4Hr	6Hr	UP	Naive
antiNOS2 ΔCt	24.79	24.88	24.96	24.42	24.08	24.22
(+/-)	0.58	0.54	0.49	0.60	0.46	0.58
βtub ΔCt	18.12	18.54	17.92	18.95	17.88	17.69
(+/-)	0.79	0.76	0.52	0.51	0.45	0.79
ΔCT antiNOS2- βtub	6.66	6.33	7.04	5.48	6.20	6.54
(+/-)	0.98	0.93	0.71	0.79	0.64	0.98
ΔΔCt	1.13	0.80	1.51	-0.06	0.66	1.00
(+/-)	0.98	0.93	0.71	0.79	0.64	0.98
Relative	0.46	0.58	0.35	1.04	0.63	0.50
-	0.23	0.27	0.14	0.44	0.23	0.25
+	0.45	0.52	0.23	0.76	0.36	0.49

Table 4.3 Relative quantification of *Lym-antiNOS2* NAT using comparative ($\Delta\Delta C_t$) method in its products by Real-Time PCR.

4.5. Single Conditioning Trial Induces Changes in the Expression of *Lym-antiNOS2* RNA Differently Depending on the Ganglia

From the *in situ* hybridisation experiment (Section 3.3) we know that *Lym-antiNOS2* gene is expressed mainly at cerebral ganglia and buccal ganglia, and from the real-time PCR experiment we can see that the levels of expression of *Lym-antiNOS2* gene change over time following reward conditioning of the feeding behaviour. Given that the patterns of spatial expression of *Lym-antiNOS2* gene differ in cerebral and buccal ganglia (widely expressed in buccal ganglia but localized in cerebral ganglia), it is expected that the patterns of expression of *Lym-antiNOS2* gene over time are also different across these two ganglia as revealed by *in situ* hybridisation.

To address this question, intact animals were subjected to one-trial classical conditioning, as described in Section 2.3, dissecting the buccal ganglia and cerebral ganglia from the snails' CNS.

Given the magnitude of the whole training experiment and the number of animals required for it, the dynamics of expression of *Lym-antiNOS2* in post-training buccal ganglia and cerebral ganglia was analysed by real-time PCR only at 1 hour and 6 hours after training. Results show a remarkable difference of the expression levels of *Lym-antiNOS2* over time between buccal and cerebral ganglia after single trial classical conditioning. In the buccal ganglia (Figure 4.7 and Table 4.4), within-groups analysis shows levels of *Lym-antiNOS2* of the

buccal ganglia to the training on the paired group (1 hour and 6 hours) were statistically different to the unpaired group, and point to a negative transient regulation of the expression of *Lym-antiNOS2*. The levels of *Lym-antiNOS2* NAT decrease after training and remain low (no fluctuation) over time after the training at those two time points ($p<0.003$). In cerebral ganglia (Figure 4.8 and Table 4.5), within-group analysis shows a statistically significant difference in the response of the paired group to training between 1 hours and 6 hours ($p<0.03$). The expression of *Lym-antiNOS2* in cerebral ganglia would seem to follow the same temporal pattern as that shown in Figure 4.6 for the whole brain after training.

The results of this experiment and those of the *in situ* hybridisation give strong support to the hypothesis that *Lym-antiNOS2* participates in the regulation of *nNOS* expression in the CNS.

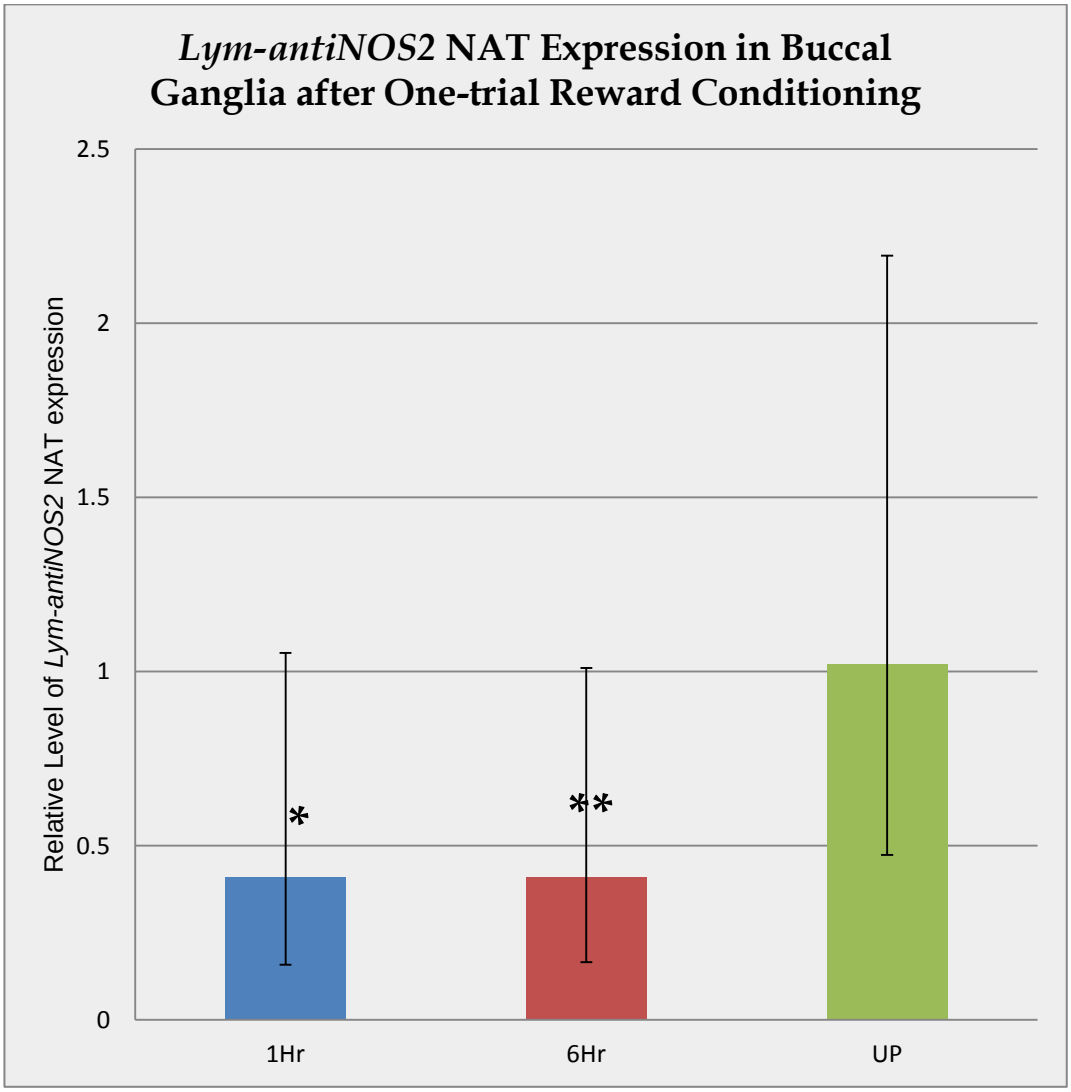

Figure 4.7 Training-induced regulation of *Lym-antiNOS2* NAT in *Lymnaea* buccal ganglia. Real-time PCR analysis of the *Lym-antiNOS2* NAT expression in buccal ganglia. Level of Lym-antiNOS2 in 1Hr (blue bar), 6Hr (red bar), unpaired control (UP) (green bar) normalised to an endogenous reference (β-tubulin) and relative to a calibrator (CAL) was calculated as $2^{-\Delta\Delta C_t}$=ΔC_t- $\Delta C_{t(cal)}$. ΔC_t and $\Delta C_{t(cal)}$ are the differences in threshold cycles for target (*Lym-antiNOS2*) and reference (β-tubulin) measured in the samples and in the calibrator, respectively. The bars show the mean value of eight samples ± standard deviation of the quotient. Note that there is a down-regulation of *Lym-antiNOS2* at 1 hour after training and at 6 hours after training. The single asterisk at 1 hours group (blue bar) indicates a significant difference from control $p<0.003$. The double asterisk in the 6 hours conditioned group (red bar) indicates a significant difference from the control p =0.003.

	1Hr	6Hr	UP
antiNOS2 Ct	31.34	31.17	30.48
(+/-)	0.94	1.14	0.64
Btub Ct	24.50	24.33	24.96
(+/-)	0.98	0.62	0.90
ΔCT antiNOS2-Btub	6.84	6.84	5.52
(+/-)	1.35	1.30	1.10
ΔΔCt	1.28	1.28	-0.03
(+/-)	1.35	1.30	1.10
Relative	0.41	0.41	1.02
-	0.25	0.24	0.55
+	0.64	0.60	1.17

Table 4.4 Relative quantification of *Lym-antiNOS2* NAT using comparative ($\Delta\Delta C_t$) method in its products by real-time PCR.

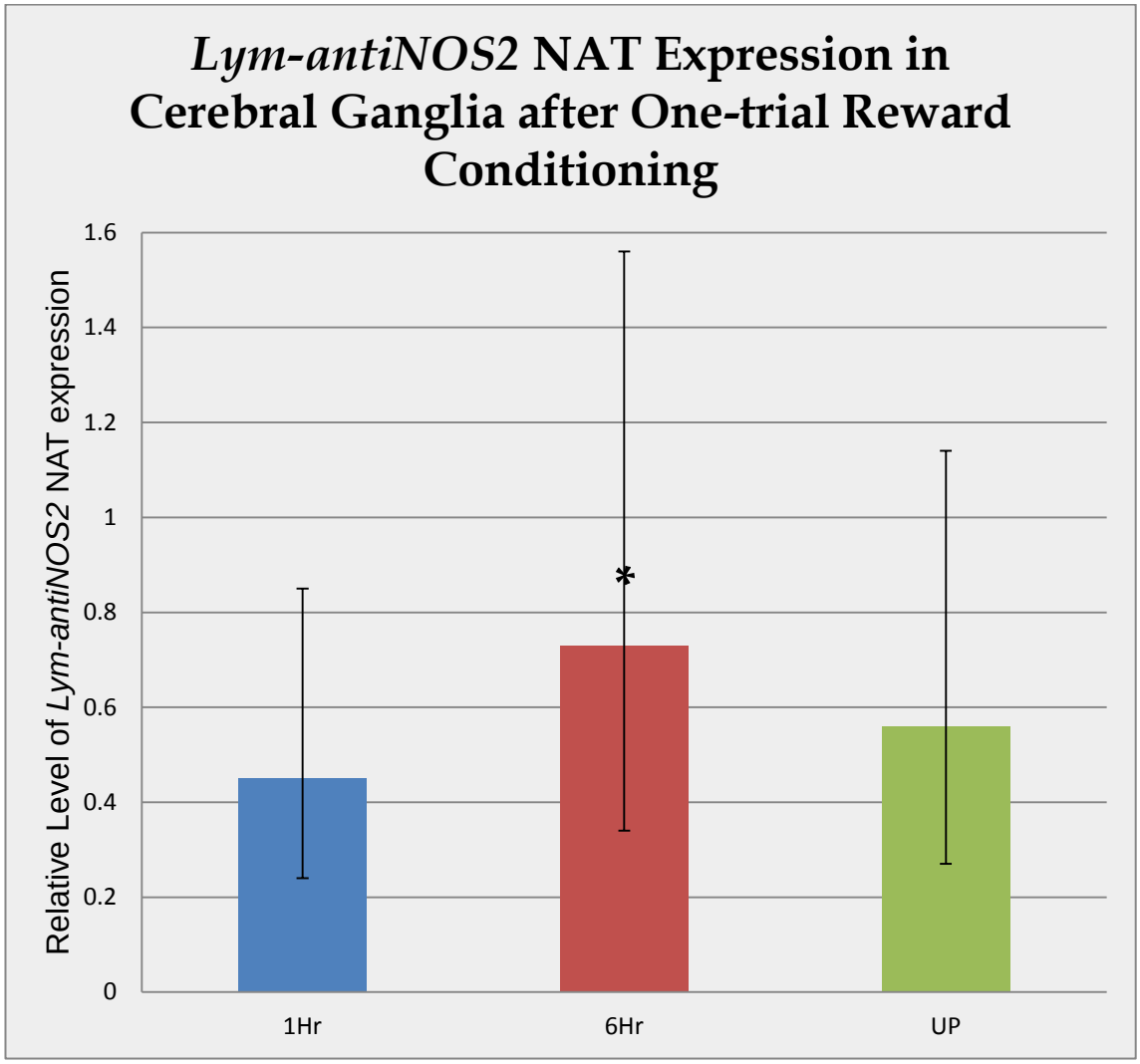

Figure 4.8 Training-induced regulation of *Lym-antiNOS2* NAT in *Lymnaea* cerebral ganglia. Real-time PCR analysis of the *Lym-antiNOS2* NAT expression in cerebral ganglia. Level of Lym-antiNOS2 in 1Hr (blue bar), 6Hr (red bar), unpaired control (UP) (green bar) normalised to an endogenous reference (β-tubulin) and relative to a calibrator (CAL) was calculated as $2^{-\Delta\Delta C_t}$=ΔC_t- $\Delta C_{t(cal)}$. ΔC_t and $\Delta C_{t(cal)}$ are the differences in threshold cycles for target (*Lym-antiNOS2*) and reference (β-tubulin) measured in the samples and in the calibrator, respectively. The bars show the mean value of eight samples ± standard deviation of the quotient. Note that there is a down-regulation of *Lym-antiNOS2* at 1 hour after training and up-regulated at 6 hours after training. The single asterisk at 6 hours group (red bar) indicates a significant difference from 1hr to 6hr $p<0.03$.

	1Hr	6Hr	UP
Lym-antiNOS2 Ct	26.53	27.00	26.66
(+/-)	0.69	0.83	0.76
βtub Ct	19.76	20.94	20.22
(+/-)	0.61	0.71	0.68
ΔCT *Lym-antiNOS2* - βtub	6.77	6.06	6.44
(+/-)	0.92	1.09	1.02
ΔΔCt	1.16	0.45	0.83
(+/-)	0.92	1.09	1.02
Relative	0.45	0.73	0.56
-	0.21	0.39	0.29
+	0.40	0.83	0.58

Table 4.5 Relative quantification of *Lym-antiNOS2* NAT using comparative ($\Delta\Delta C_t$) method in its products by real-time PCR.

4.6. Single Conditioning Trial Changes the Levels of Expression of *Lym-NOS1* mRNA in *Lymnaea* Brain

In order to form a better understanding of the requirements of the NO-cGMP signalling pathway during long-term memory formation following reward conditioning of feeding behaviour, and in light of the proposed role of *Lym-antiNOS2* gene in the regulation of NOS expression in the CNS, it was important therefore to investigate whether this NO-dependent memory formation is associated with specific changes in the expression of *Lym-NOS1* (*NOS1*).

A late up-regulation of the expression of *Lym-NOS1* at 6 hours after single trial feeding reward conditioning has been demonstrated (Korneev et al., 2005), but times earlier than 4 hours were not examined in this study. In order to compare the *Lym-NOS1* mRNA and *Lym-antiNOS2* RNA levels at this earlier period, Dr Natasha Pouchkina-Stantcheva performed real-time PCR at 10 minutes, 1 hour, 4 hours and 6 hours after single training reward conditioning on *Lymnaea* CNS samples.

I conducted an independent analysis of the raw data collected from that experiment. Results (Figure 4.9 and Table 4.6) show that the expression of *Lym-NOS1* fluctuates over time after single trial classical conditioning. Within-groups analysis demonstrated that responses to training on the paired group were statistically significant. T-test performed between paired groups versus unpaired and naïve groups show a significant increase in the expression of

Lym-NOS1 at 1 hour and 6 hours after training (1hour vs. UP: $p < 0.002$; 4 hours vs. UP: $p < 0.003$).

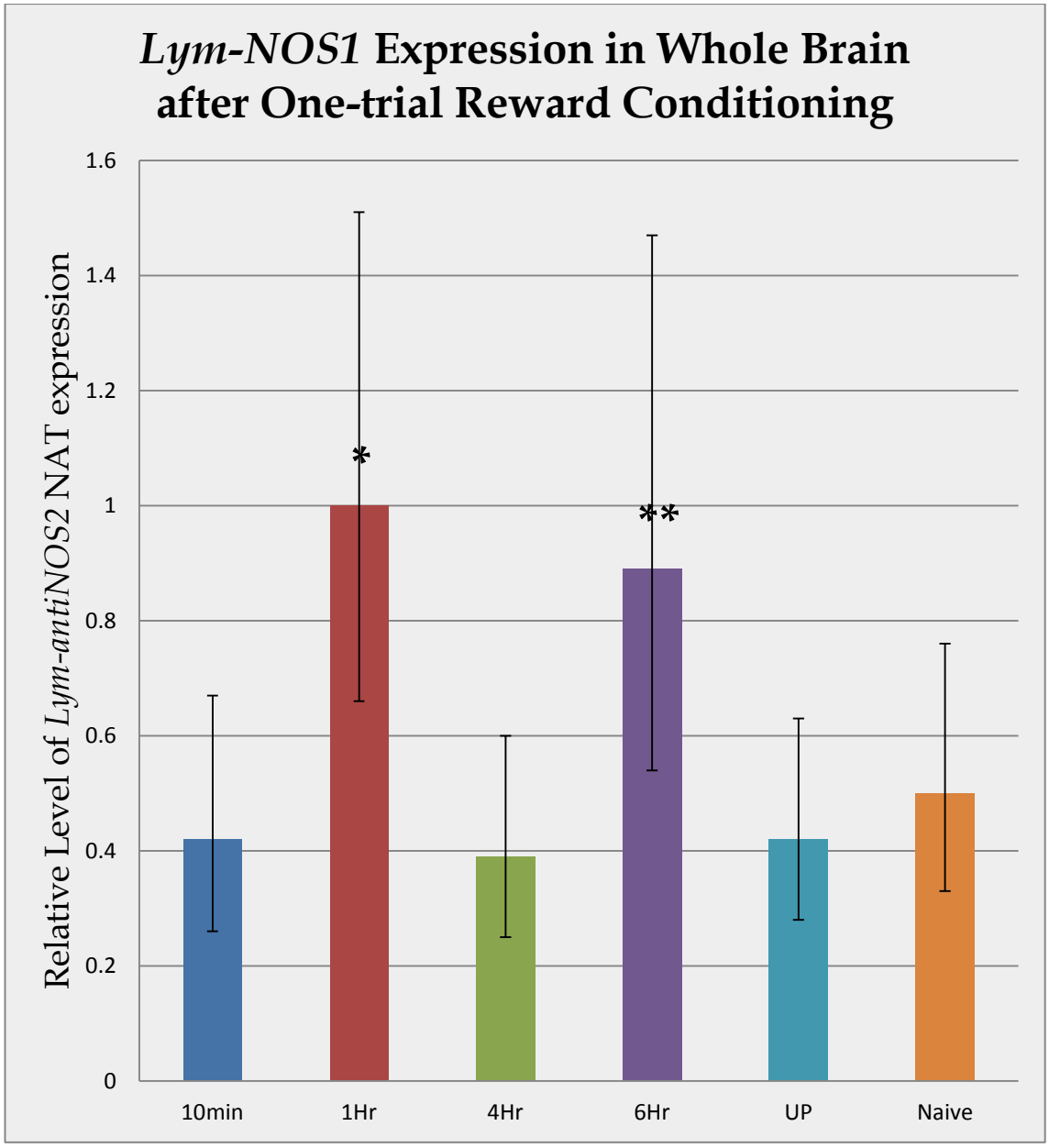

Figure 4.9 Training-induced regulation of *Lym-NOS1 mRNA* in *Lymnaea* CNS. Real-time PCR analysis of the *Lym-NOS1* mRNA expression in CNS. Levels of *Lym-NOS1* in 10min group (blue bar), 1Hr (red bar), 4Hr (green bar), 6Hr (purple bar), unpaired control (UP) (turquoise bar) and naïve group (orange bar) normalised to an endogenous reference (β-tubulin) and relative to a calibrator (CAL) were calculated as $2\text{-}\Delta\Delta C_t = \Delta C_t - \Delta C_{t(cal)}$. ΔC_t and $\Delta C_{t(cal)}$ are the differences in threshold cycles for target (*Lym-NOS1*) and reference (β-tubulin) measured in the samples and in the calibrator, respectively. The bars show the mean value of eight samples ± standard deviation of the quotient. Results show an up-regulation of *Lym-NOS1* at 1 hour and at 6 hours after training. The single asterisk at 1 hour group (red bar) indicates a significant difference from control UP p = 0.002. The double asterisk in the 6 hours conditioned group (purple bar) indicates a significant difference from the control p =0.003.

	10min	1Hr	4Hr	6Hr	UP	Naive
NOS1 ΔCt	25.76	24.43	25.48	25.83	26.17	25.40
(+/-)	0.40	0.42	0.41	0.53	0.38	0.51
βtub ΔCt	17.84	17.74	17.43	18.97	18.22	17.71
(+/-)	0.52	0.42	0.47	0.49	0.44	0.31
ΔCt NOS1-βtub	7.92	6.68	8.05	6.86	7.95	7.69
(+/-)	0.66	0.59	0.62	0.72	0.58	0.60
ΔΔCt	1.23	0.00	1.36	0.17	1.26	1.00
(+/-)	0.66	0.59	0.62	0.72	0.58	0.60
Relative	0.42	1.00	0.39	0.89	0.42	0.50
-	0.16	0.34	0.14	0.35	0.14	0.17
+	0.25	0.51	0.21	0.58	0.21	0.26

Table 4.6 Relative quantification of Lym-*NOS1* NAT using comparative ($\Delta\Delta C_t$) method in its products by real-time PCR

4.7. Discussion

Significant progress has been made in our understanding of the complex machinery involved in the regulation of LTM formation and the role of the molecular pathway of NO-cGMP signalling. Moreover it is clear that the regulation of NO signalling is very complex and it occurs at various levels. It can be mediated via unconventional mechanisms. In memory formation NATs represent a complex addition to the molecular mechanisms controlling gene expression.

This studies reveal that *Lym-antiNOS2* NAT is likely to play a role in the regulation of NO signalling. We have found that the *Lym-antiNOS2* gene is down-regulated at four hours and up-regulated at six hours after training. Moreover, these changes in expression occur in response to a very weak sensory cue (single pairing of US and CS), and their patterns –both spatial and temporal– vary across different ganglia.

During LTM formation the concentration of Ca^{2+} increases with transmitter release. 5-HT causes a big increase in cAMP levels, resulting in the translocation of PKA and MAPK into the nucleus. However, it is not clear that this process is sufficient for LTM to be formed. Many studies have increasingly shown the importance of NO during LTM formation (Harooni et al., 2009; Juch et al., 2009; Ribeiro et al., 2008). In this chapter I focus on the possible role that *Lym-NOS1*, *Lym-antiNOS1* and *Lym-antiNOS2* may have during the formation of LTM.

It is interesting to note that the temporal patterns of regulation of *Lym-NOS1*, *Lym-antiNOS1* and *Lym-antiNOS2* are all different: *Lym-NOS1* up-regulates at 1 and 6 hours, and is down-regulated at 4 hours (Figure 4.9); *Lym-antiNOS1* is down-regulated at 4 hours (Korneev et al., 2005); *Lym-antiNOS2* is down-regulated at 4 hours and up-regulated at 6 hours (Figure 4.6). This demonstrates that their expression is not associated with a common promoter, even if they belong to the same cluster.

It is also worth noting that the second peak of *Lym-NOS1* at six hours after training appears to be smaller than its peak at one hour. Our hypothesis is that this smaller six-hour peak is a manifestation of a higher *Lym-NOS1* peak before the five-hour mark, helped by the down-regulation of *Lym*-antiNOS1 (Figure 4.10) and *Lym*-antiNOS2 at four hours. This earlier *Lym-NOS1* peak would generate the NO necessary at five hours for long-term memory formation. An analysis of the level of expression of *Lym-NOS1* RNA and *Lym-antiNOS2* RNA after single conditioning trial at five hours would help confirm or disprove this hypothesis. The *Lym*-antiNOS2 peak at six hours would have the role of down-regulating *Lym-NOS1* after long term memory has been formed, and NO is therefore not needed anymore (Figure 4.11).

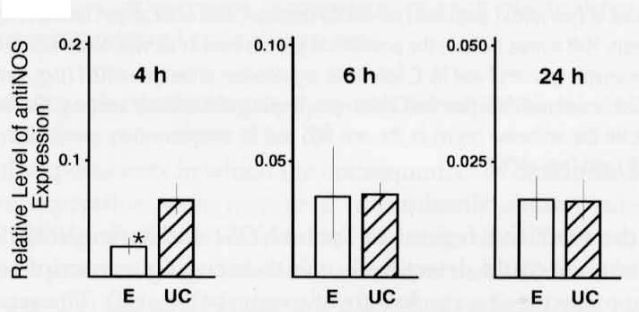

Figure 4.10 Training-induced regulation of *Lym-antiNOS1* RNA antiNOS down at 4h post training (Korneev et al., 2005)

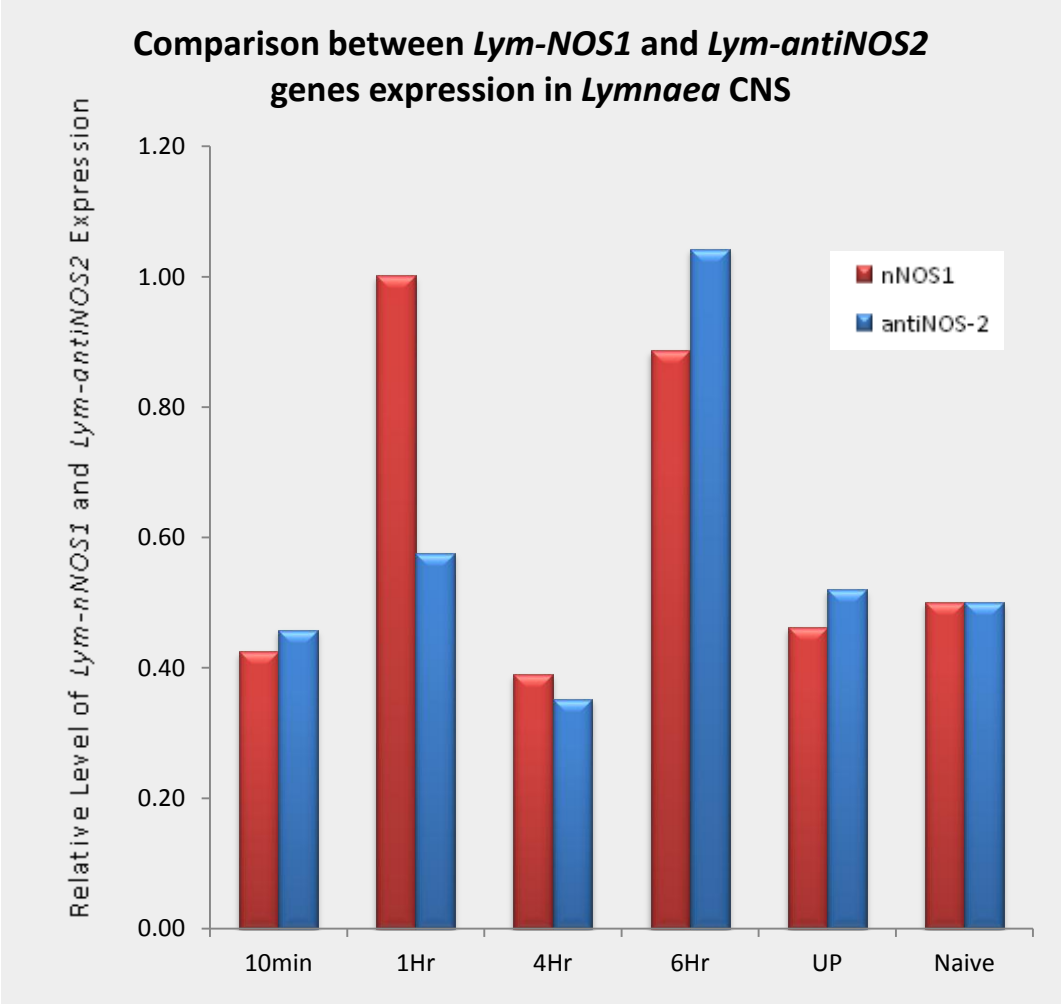

Figure 4.11 Training-induced regulation of *Lym-NOS1 mRNA* and *Lym-antiNOS2* in *Lymnaea* CNS. Real-time PCR analysis of the LymnNOS1 mRNA and *Lym-antiNOS2* expression in CNS. Level of Lym-nNOS1 (red bars) and *Lym-antiNOS2* (blue bars) in 10min group, 1Hr, 4Hr, 6Hr, unpaired control (UP) and naïve group.

Chapter 5: *Lym-antiNOS2* NAT is Subjected to Peripheral Trafficking

5.1. Introduction

It is now generally accepted that in neural cells, certain RNAs are targeted towards dendrites and axons by specific RNA trafficking pathways. Recent studies in mammals show that a disruption in the 3' untranslated region (UTR) of CaMKIIα reduces late-phase long-term potentiation and impairs memory(Mikl et al., 2010). The knock-out of CaMKII maked the onset for a new subfield in neuroscience, in which mouse mutants are used as a tool to gain insight into the molecular basis of cognition and brain plasticity. To investigate the physiological role of αCaMKII in vivo, several mutants have now been generated. With the help of gene targeting, hippocampal area (CA3)-restricted null mutants of αCaMKII were created, which demostrated that localization of CaMKIIα is indispensable for the establishment of long-term hippocampal-dependent memories (Elgersma et al., 2004).

In *Lymnaea* CNS, the cerebral ganglia and the buccal ganglia are connected by axons across the CBCs (cerebral-buccal connective). In the cerebral ganglion, the serotonergic giant cells are well known to project directly into the CBCs (Weiss and Kupfermann, 1976). This has been identified in *in vivo* recordings, and shown to be active mainly during the appetitive phase of feeding (Kupfermann and Weiss, 1982).

Some authors have focused on the role of the connections between the cerebral and buccal ganglia, both in the transmission descending from the cerebral to the buccal ganglia–command and control functions (Xin et al., 2000) and ascending in the opposite direction (Chiel et al., 1988; Kuslansky et al., 1978) showing that the transmission of information occurs in both directions.

It has been shown with *in vivo* electrode recording implanted around the cerebrobuccal connective that most of the activity travels in the cerebral-to-buccal direction. This reveals that the CBC impulse traffic (and therefore the dialogue between cerebral and buccal ganglia, see Figure 5.1) is activated bidirectionally even in the absence of full consummatory behaviour (which also involves activation of the neural circuits producing swallowing movements of the buccal mass) and food, provided that the cyclic motor pattern is produced (Fiore et al., 1992).

In Chapter 3 the discussion about *in situ* hybridisation experiments suggested the presence of *Lym-antiNOS2* RNA in the CBCs. Chapter 4 shows how the expression of *Lym-antiNOS2* RNA varies during LTM formation. Confirmation of trafficking of *Lym-antiNOS2* RNA in the CBCs, seen together with these results in mammals, would reinforce the hypothesis that *Lym-antiNOS2* plays an important role in LTM formation in *Lymnaea*.

5.2. *In Situ* Hybridisation Reveals the Presence of *Lym-antiNOS2* in the Cerebrobuccal Connectives

We inspected in more detail the slices obtained by *in situ* hybridisation staining against *Lym-antiNOS2* NAT, in the experiments described in Section 3.3 (Figure 5.2). As with Figure 3.8 and Figure 3.10, this inspection shows specific staining within the CBCs. The cerebrobuccal connectives show a particularly strong staining, and its staining resembles that of granules formed during peripheral trafficking of RNA. These suggest that trafficking of *Lym-antiNOS2* NAT occurs as a natural process in the brain of *Lymnaea*. These findings are important as they suggest that *Lym-antiNOS2* NAT is subject to peripheral trafficking. Moreover, many RNAs that have been found to undergo trafficking have been shown to play important roles in cellular processes, trafficking is an energy-intensive process involving moving components of the translation machinery (Carson and Barbarese, 2005).

It has been shown that a key regulatory event in translational regulation is the movement of the mRNA templates into the axonal compartment (Yoo et al., 2010). This result suggested to us that *Lym-antiNOS2* RNA could be travelling along the CBCs from CGCs to buccal ganglia, where it would play a part in the regulation of NO synthesis.

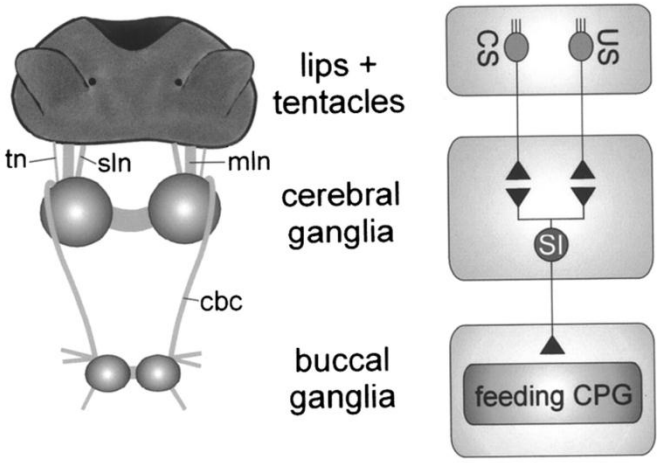

Figure 5.1 Schematic diagram of anatomical organization of lip and tentacle sensory pathways. The lips and tentacles are connected to the cerebral ganglia via the median lip nerve (mln), superior lip nerve (sln), and tentacle nerve (tn). The cerebral-buccal connective (cbc) forms the only connection between the cerebral and buccal ganglia that contain the feeding CPG. Primary chemosensory cells in the lips and tentacles extend direct projections in the lip and tentacle nerves that synapse onto sensory integrating neurons (SI) in the cerebral ganglia (for simplicity, interactions are shown as direct connections). These neurons affect the feeding CPG in the buccal ganglia via the cerebral-buccal connective (Straub et al., 2004)

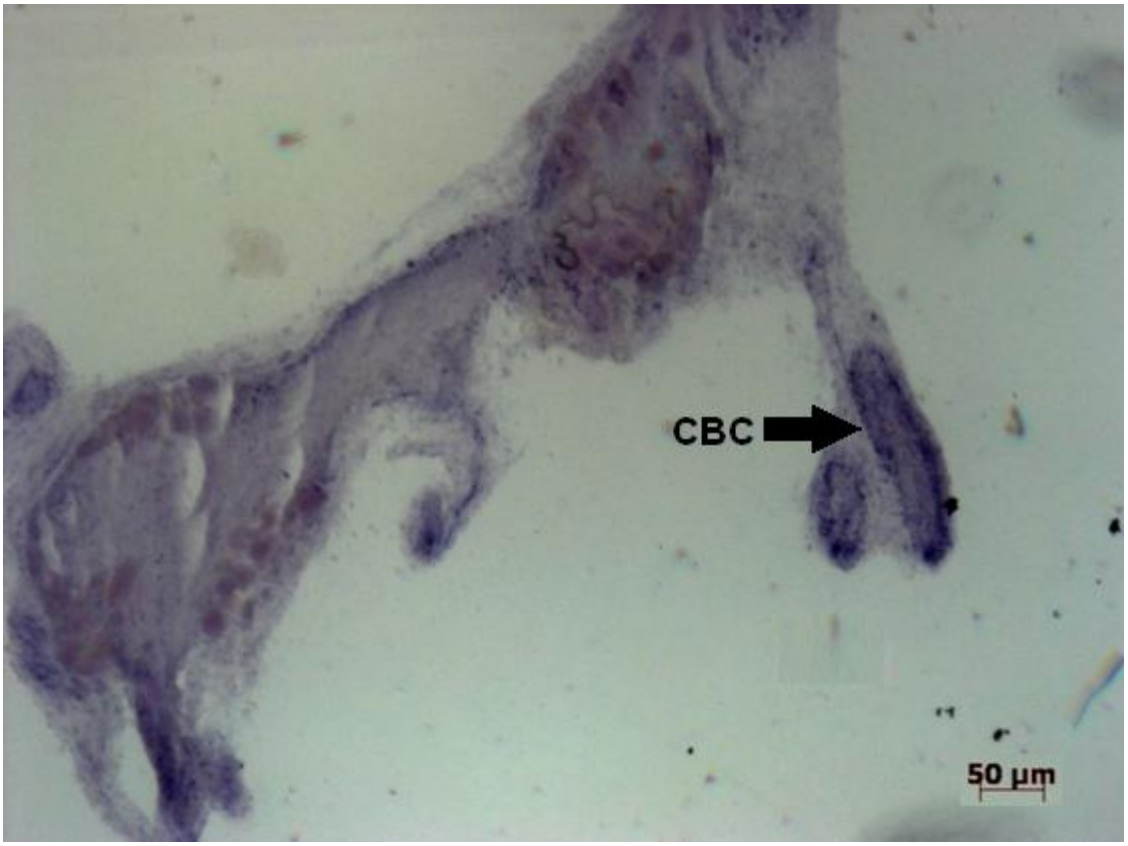

Figure 5.2 *In situ* hybridisation showing CBCs with granules containing *Lym-antiNOS2. In situ* hybridisation experiments on adjacent sections through the buccal ganglia showing the stained of *Lym-antiNOS2* NAT.

5.3. RT-PCR Confirms the Presence of *Lym-antiNOS2* RNA in the CBCs

Previous work in *Aplysia* has shown that many neurons that have axons in the CBC are part of the circuitry responsible for generating feeding. Moreover, it has been found that numerous neurons in the cerebral and buccal ganglia and many axons in the cerebrobuccal connective show neuropeptide immunoreactivity. This suggests that CBCs may be involved in the CPG for the feeding system of *Aplysia* (Fujisawa et al., 1999).

To confirm the existence of *Lym-antiNOS2* RNA in the cerebrobuccal connectives, quantitative real-time PCR was essential, since the RNA concentration in the axons of *Lymnaea* is unknown and potentially very low. Real-time PCR allows RNA concentrations that were previously undetectable using earlier techniques to be detected.

For this experiment CNS from *Lymnaea* was isolated. The brain commissure was cut and the brain pinned down to a Sylgard-coated dish containing snail saline. The brain was dissected and separated in three tubes containing: a) buccal ganglia, b) cerebral ganglia and c) CBCs.

RNA extraction was performed (Section 2.4) followed by synthesis of cDNA (Section 2.9) and quantitative real-time PCR (Section 2.15). Real-time PCR was performed using the primers Scorp1 and Scorp2 (Figure 2.2). The concentration of *Lym-antiNOS2* in each part of the brain was related to the concentration of the same RNA in *Lymnaea* whole CNS.

Results in Table 5.1 show in the 'Relative' column the value of the expression of *Lym-antiNOS2* in the different parts of the brain, divided by the value of the expression of *Lym-antiNOS2* in whole brain. These results indicate that the CBC samples contain 23.9 times as much *Lym-antiNOS2* RNA as the whole-brain sample (this is a relative value of the expression of *Lym-antiNOS2* to the concentration of β-tubulin RNA in the sample, assuming stably expressed in the CBCs). Expression levels in buccal ganglia and cerebral ganglia are close to those of *Lym-antiNOS2* RNA in whole brain. This demonstrates that in a naïve snail *Lym-antiNOS2* is not only travelling along the CBCs but it is accumulated in the CBCs (Figure 5.3 and Table 5.1).

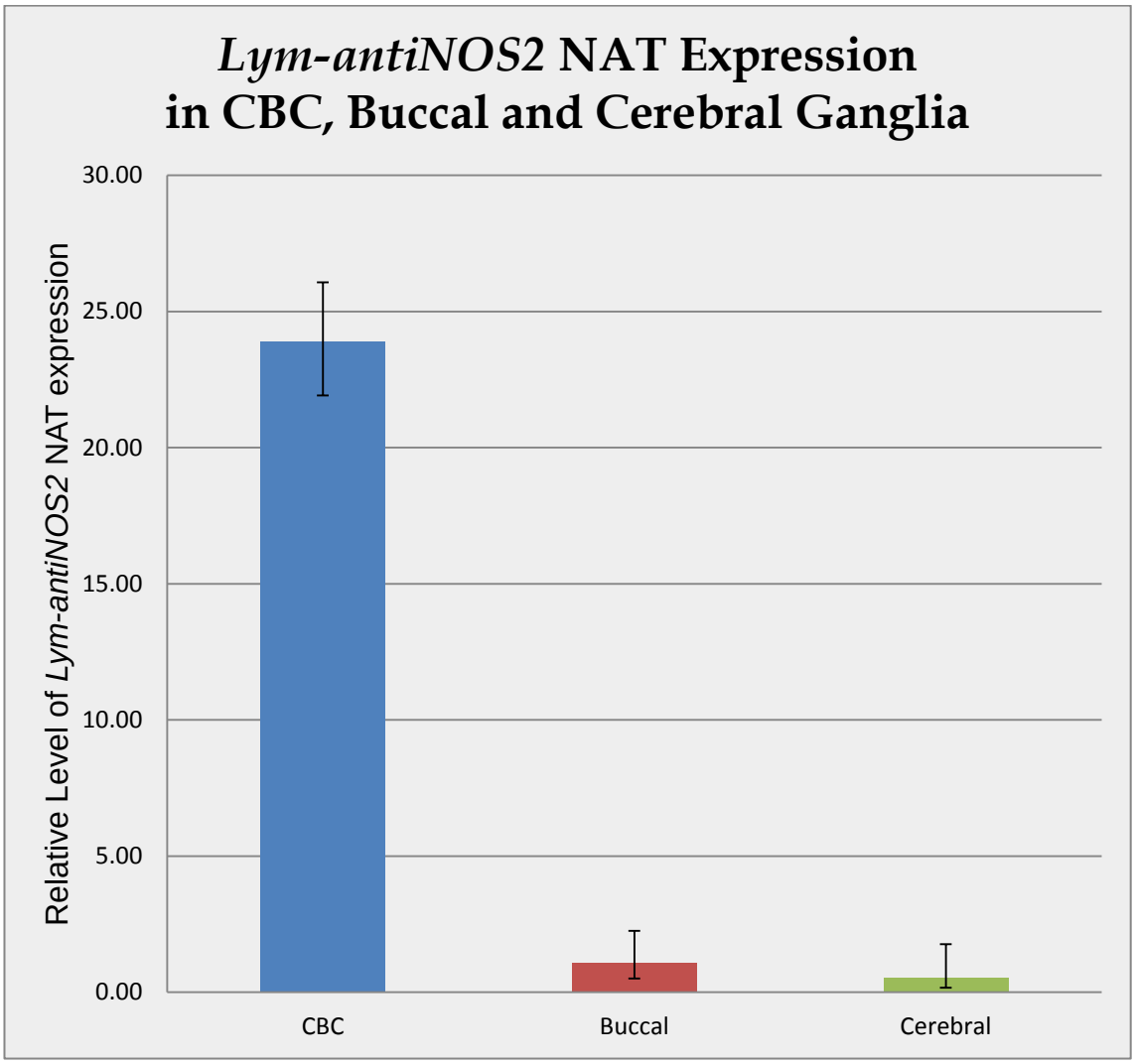

Figure 5.3 Peripheral trafficking of *Lym-antiNOS2* NAT in *Lymnaea* CBC. Real-time PCR analysis of the *Lym-antiNOS2* NAT expression in cerebral ganglia, buccal ganglia and CBCs. Level of *Lym-antiNOS2* in CBCs (blue bar), buccal ganglia (red bar), cerebra ganglia (green bar) normalised to an endogenous reference (β-tubulin) and relative to a calibrator (CAL) were calculated as $2^{-\Delta\Delta C_t}=\Delta C_t - \Delta C_{t(cal)}$. ΔC_t and $\Delta C_{t(cal)}$ are the differences in threshold cycles for target (*Lym-antiNOS2*) and reference (β-tubulin) measured in the samples and in the calibrator, respectively.

	CBC	Buccal	Cerebral
Lym-antiNOS2 Ct	25.18	30.42	26.66
(+/-)	0.11	0.69	0.76
βTub Ct	24.20	24.96	20.22
(+/-)	0.06	0.83	1.52
ΔCt	0.98	5.47	6.44
(+/-)	0.13	1.08	1.70
ΔΔCt= ΔCtc-ΔCt	-4.58	-0.09	0.88
(+/-)	0.13	1.08	1.70
Relative	23.90	1.07	0.54
-	1.99	0.56	0.38
+	2.17	1.18	1.22

Table 5.1 Relative quantification of *Lym-antiNOS2* NAT using comparative ($\Delta\Delta C_t$) method in its products by real-time PCR.

5.4. Analysis of the Sequence of *Lym-antiNOS2* Reveals a *cis*-acting Transport Element within the 3'UTR

Trafficking in neurons has been studied in recent years. Probably more than 20 different mammalian mRNAs have been identified including RNA encoding neuromodulin, MAP2, CaMKIIα, CREB, β-actin, fragile X mental retardation protein (FMRP), protein kinase C(γ) (Palacios and St Johnston, 2001). The nature of RNA localization pathways has emerged primarily from studies of *Drosophila* and *Xenopus* oocytes. The initial steps in the localization process are determined by the *cis*-acting elements within the RNA. This series of signals that are usually, but not exclusively, located within the 3' UTR direct the binding of *trans*-acting factors to the RNA (Kloc et al., 2002).

It has been demonstrated that not all the different RNAs use the same trafficking element, but several may use closely related elements. Recent studies suggest that the molecular mechanisms of RNA targeting in neurons are likely to be the same for a wide range of localized neuronal RNAs, and most neuronal RNAs are probably transported along microtubules in kinesin/dynein-containing granules (Hyun et al., 2011).

Cis-acting elements have been found by sequence comparisons in many localized RNAs. Several *trans*-acting transport elements have also been identified. Table 5.2 shows a list of some of the identified *cis*-acting elements and the correspondent *trans*-acting factor.

Subsequent experiments with oligodendrocytes and fibroblasts led to the current model (Figure 5.4) in which RNAs that are to be localized team up with their transacting factor during, or immediately following, maturation of the mRNA in the nucleus. The RNA with its cognate protein is exported to the cytoplasm, where they are incorporated into large transport granules. These granules, which have been observed in many cell types, contain multiple ribosomes and probably many of the molecules needed to translate the transported mRNA, including t-RNA synthetases and elongation factors (Smith, 2004).

Transported RNA	*Cis*-acting Element	Location	Size	*Trans*-acting Factor	Reference
CaMKIIα, neurogranin	CNDLE	3′UTR	28–30 nt[a]	hnRNP A2	Mori and others (2000); Blichenberg and others (2001)
BC1 (noncoding)	BTE	5′ proximal	62 nt $(GGN)_n$	TB-RBP (Translin), Purα and Purβ	Muslimov and others (1997); Ohashi and others (2002)
Ligatin, CaMKIIα	Y element	Various	~14 nt	TB-RBP	Severt and others (1999)
MAP2	DTE	3′UTR	640 nt	rMARTA1/ KSRP, rMARTA2	Rehbein and others (2000, 2002)
MAP2, CaMKIIα	CPE (AU-rich)	3′UTR	6 nt	CPEB	Huang and others (2003)
A2RE-containing[b]	A2RE11	Various	11 nt	hnRNP A2	Shan and others (2003)
β-actin	β-actin zipcode	3′UTR	54 nt	ZBP1, ZBP2/ KSRP	Eom and others (2003); Tiruchinapalli and others (2003)
Many, including BC1 RNA[c]	Purine quartet and unknown elements			FMRP	Miyashiro and others (2003); Antar and others (2004)
Vasopressin precursor protein	DLS	3′UTR	395 nt	PABP	Mohr and others (2001)

Table 5.2 *cis*-acting elements and *trans*-acting factors (Smith, 2004).

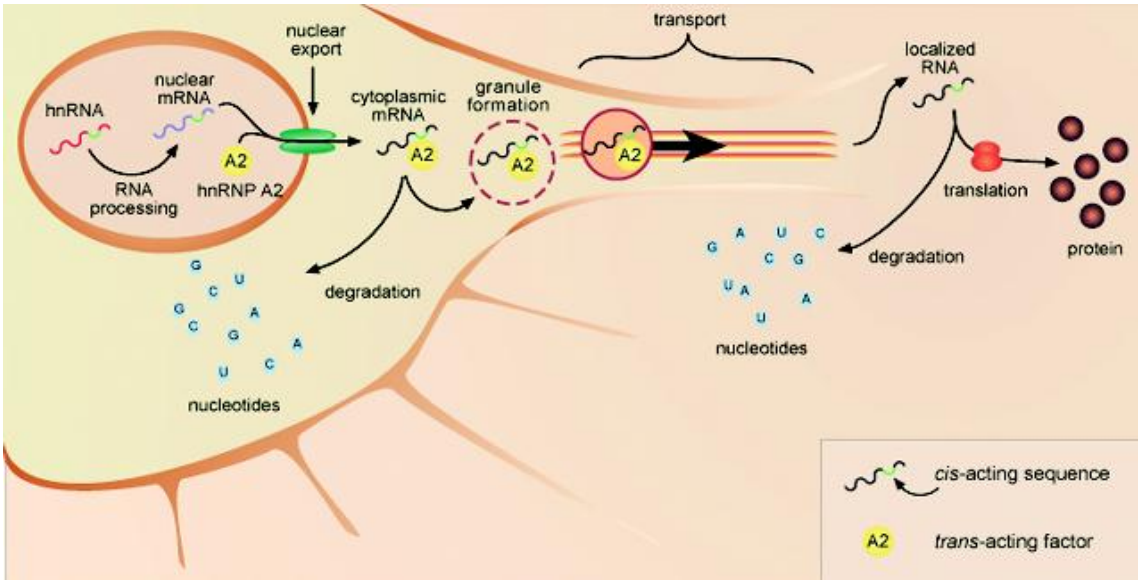

Figure 5.4 Model for trafficking of A2 response element (A2RE)-containing RNAs. The A2RE, which is represented in a different colour from the remainder of the mRNA, binds heterogeneous nuclear ribonucleoprotein (hnRNP) A2 or hnRNP A3 (yellow circle), and the complex is recruited to transport granules that move along the microtubules (orange unlabeled horizontal lines). The granules contain multiple copies of the RNA-protein complex. At its destination, the mRNA is anchored and translated. Each of the steps in this process, including RNA degradation, is a potential posttranscriptional control point for gene expression (Smith, 2004).

After the experiments described in Section 5.2-5.3 a further analysis of the *Lym-antiNOS2* sequence was necessary to determine which trafficking element *Lym-antiNOS2* could be using and where it is located in its sequence. This analysis reveals the presence of a sequence for a CPE-like element (UUUUAU) in the desired direction. Figure 5.4 shows the position of the CPE element (inside the nucleus, red circle) at the 3' UTR, which is the expected localization for this kind of element. As the CPE-like element is recognized by the CPE-binding protein (CPEB), the *Lym-antiNOS2* RNA to which it belongs may be recruited to be transported in granules.

The identification of a *cis*-acting element in the *Lym-antiNOS2* sequence completes the work started in Sections 5.2-5.3. Together, the experiments in

Sections 5.2 and Section 5.3 establish that *Lym-antiNOS2* is subjected to peripheral trafficking between cerebral ganglia and buccal ganglia, through the CBCs. Furthermore, within cerebral ganglia the expression of *Lym-antiNOS2* is restricted to a few neurons, and particularly the CGC pair. In view of this, it is possible to hypothesise that trafficking of *Lym-antiNOS2* actually occurs between the CGCs and the buccal ganglia, but more work has to be done to confirm this.

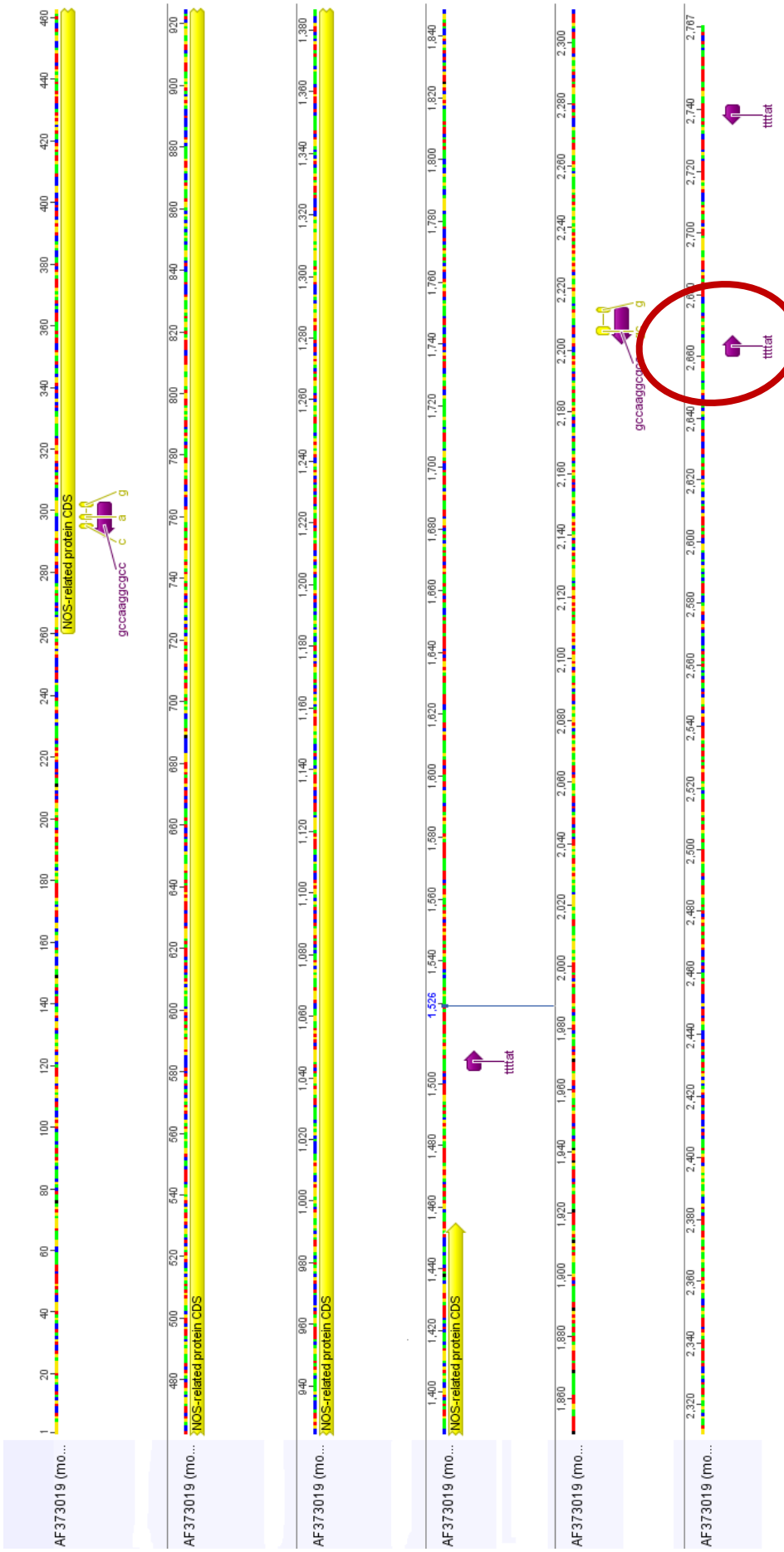

Figure 5.5 Sequence analysis of *Lym-antiNOS2* NAT showing *cis*-acting RNA Trafficking Signal. CPE-like element is marked with a red circle at the 3'UTR end of *Lym-antiNOS2* NAT.

5.5. Discussion

Early research suggested that protein synthesis may occur outside the neuronal cell body, since it was found that polyribosomes are localized to subsynaptic areas of the neuron. It is now clear that the trafficking process involves mRNA-binding proteins that are primarily bound to the 3'-UTR of responsive mRNAs. Our data indicates that trafficking of *Lym-antiNOS2* occurs in *Lymnaea.* We show that the CPE-like sequence (UUUUAU) is present in *Lym-antiNOS2*, and it is localized in the expected region corresponding to the 3'UTR. Moreover, the *in situ* hybridisation experiments in this chapter reveal the presence of *Lym-antiNOS2* RNA granules that are typical of trafficking processes in the CBCs. The presence of *Lym-antiNOS2* RNA in the CBCs was then confirmed using quantitative real-time PCR, showing that the concentration of *Lym-antiNOS2* RNA is nearly thirty times the concentration in the cerebral or buccal ganglia. Multiple lines of evidence indicate that targeted RNA trafficking coupled with local protein synthesis occur in neurites, such as the example of axonal transport and local translation of CREB mRNA in axons that is followed by its retrograde transport to the nucleus where it activates transcription of pro-survival genes in response to nerve growth factor (Andreassi and Riccio, 2009)

In the case of *Lym-antiNOS2* RNA, this thesis has studied the spatial regulation of its expression, how this regulation changes and exhibits temporal regulation after single conditioning trial, and now how *Lym-antiNOS2* RNA moves along the CBCs in a complex mechanism where the translation of *Lym-*

antiNOS2 RNA could be regulated by its localization in subsynaptic regions of the neuron, possibly between the buccal ganglia and the CGCs in the cerebral ganglia. Targeted RNA trafficking depends on the interaction between *cis*-acting elements and *trans*-acting factors. The *Lym*-antiNOS2 sequence has a CPE-like motif, which suggests that *Lym-antiNOS2* RNA undergoes an active peripheral trafficking, although little is known about *cis*-acting elements and *trans*-acting factors in molluscs.

The regulation of *Lym-antiNOS2* expression in neurons controls not only when but where they are going to be expressed, in a very complex way. RNAs which undergo such complex regulation are likely to play an important role in neuronal function. As an example, work in mammals suggests that most transported RNAs appear to be translationally dormant while en route (Kindler et al., 2005). mRNAs can be translated in response to an activation signal at their destination sites, as in the case of importin β and RanBP1 mRNAs, both of which undergo axonal trafficking. Local synthesis of RanBP1 and importin β contributes to the formation of a signalling complex that travels from the injured axon to the cell body (Yudin et al., 2008).

This thesis presents the first report suggesting trafficking of RNA in molluscs. Importantly, the trafficking process identified, involving CPEB, has also been reported previously in mammals. This would point to a highly-conserved process during evolution. Many molecular mechanisms are involved in the local control of translation. In eukaryotes, the entwined pathways of RNA transport and local translational regulation are key determinants in the

spatio-temporal articulation of gene expression. One of the main advantages of this mechanism over transcriptional control in the nucleus lies in the fact that it endows local sites with independent decision-making authority, a consideration that is of particular relevance in cells with complex cellular architecture such as neurons (Kindler et al., 2005). The complex mechanisms underlying such signalling are only now beginning to be addressed by scientists.

Chapter 6: Sequence Analysis of *Mm-antiNOS1* RNA and Characterization of the Expression during Brain Development

6.1. Introduction

NO regulates synapse formation and patterning, thus playing a role in embryonic and adult neurogenesis and development. Research shows that NO is a modulator of axon outgrowth and guidance, synaptic plasticity, neuronal precursor proliferation, and neuronal survival. NO-cGMP signalling contributes to neural precursors derived from human embryonic stem cells (hESC) and enhances the differentiation of precursors toward functional neurons (Tao Li et al., 2010).

Previous work on the molluscan model system *Lymnaea stagnalis* has shown that a *trans*NAT complementary to the NOS-encoding mRNA plays an important role in the regulation of the NO signalling pathway in the CNS (Korneev and O'Shea, 2002). The initial work on the same model (Chapter 3) shows a second *trans*-NAT that has an open reading frame encoding a truncated NOS-homologous protein of 397 amino acids.

This thesis hypothesised that the truncated homologue encoded by the *Lym-antiNOS2* gene has a strong suppression effect on *Lym-NOS1* enzymatic activity. The experiments carried out in Chapter 3 and Chapter 4 give strong

support to this hypothesis. Moreover, a similar organization of a locus in the human genome has been discovered, which also evolved by gene duplication followed by an internal DNA inversion and is reminiscent of our findings in *Lymnaea*. This human locus is transcribed into a noncoding RNA containing a region of significant complementary to *NOS2A* mRNA. These two RNAs exhibit concurrent reciprocal changes in undifferentiated human embryonic stem cells and in hESCs induced to differentiate into neurogenic precursors. The results suggest that *anti-NOS2A* is involved in the regulation of neuronal differentiation through the modulation of the *NOS2A* gene (Korneev et al., 2008). Other cases of regulation of NOS via natural antisense transcript have been reported in mammals, where eNOS expression can be regulated by an overlapping *cis*-antisense transcript by a hypoxia stimulus (Robb et al., 2004).

These results point to the regulation of NO via the regulation of the expression of NOS through a NOS-related NAT as a highly-conserved process. To explore further this hypothesis where NOS expression can be regulated by an overlapping NAT, Dr Korneev explored using computational analysis a database of all known mice cDNA sequences. A NOS-related pseudogene was found whose full-insert sequence exhibits significant sequence similarity to NOS-encoding mRNAs (GenBank accession number AK146140). This NOS-related pseudogene was identified in the database as a previously-unclassified RNA. We named this RNA *Mm-antiNOS1* RNA, as its sequence was shown to be related to that of *NOS1*.

In this chapter the *Mm-antiNOS1* sequence is first analysed. Then, the possibility of *Mm-antiNOS1* expressing in the brain on *Mus musculus* embryos and adults is studied, along with its regulation during neuronal differentiation in embryonic brain.

Results discussed in Section 1.6 show that NOS1 is expressed in rat between E13 and E20 of the gestation period. This would suggest that NO production in rodents is of particular importance during late stages of gestation. If *Mm-antiNOS1* were to have a role in the regulation of NO production, it is likely that its expression would be confined to this late gestation period.

The transcriptional status of *Mm-antiNOS1* was investigated using RT-PCR analysis of RNA extracted from embryonic brains at different stages of development (10 days, 14 days and 18.5 days), using primers against *Mm-antiNOS1 cis*-NAT. Once confirmed that *Mm-antiNOS1* is expressed in mice CNS, quantitative RT-PCR experiments were conducted to evaluate the level of expression of *Mm-antiNOS1* at different stages of embryonic development, and in newborn and adult mice.

6.2. Sequence Analysis of *Mm-antiNOS1* RNA

Alignment between *NOS1* mRNA and *Mm-antiNOS1* RNA The homologies to NOS were thoroughly examined using Geneious software (Geneious Pro™ 5.4, http://www.geneious.com/).

Figure 6.1 shows the sequence comparison between *NOS1* mRNA and *Mm-antiNOS1* RNA. Two important observations can be made from these

results. First, the *Mm-antiNOS1* RNA is 1308bp long, which is significantly shorter than *NOS1* mRNA (4388bp). Second, the region of complementarity to the NOS-encoding transcript is restricted to exons 20 and 21. The sequence was found to have a polyadenylation signal and polyA tail.

Mm-antiNOS1 is a novel NOS-related transcript containing a large region (~300bp) which is identical to a region within *NOS1* mRNA (more than 96%of antisense identity). NOS-encoding *cis*-transcripts that affect the regulation of NO production have also been found in other mammals. Such is the case of eNOS in human, where the regions of homology between eNOS (NOS3) and its *cis*-NAT are oriented in a tail-to-tail configuration, and the mRNAs encoding antisense transcript and eNOS are complementary for 662bp (Robb et al., 2004). The *trans*-NAT *antiNOS2A* affects the regulation of *NOS2A* in humans(Korneev et al., 2008). In *Lymnaea*, *Lym-antiNOS1* and *Lym-antiNOS2* affect the regulation of *nNOS*. In both cases (*NOS2A* and *nNOS* and their transcripts), the regions of homology are shorter (~100bp) and with a lower homology (~70%).

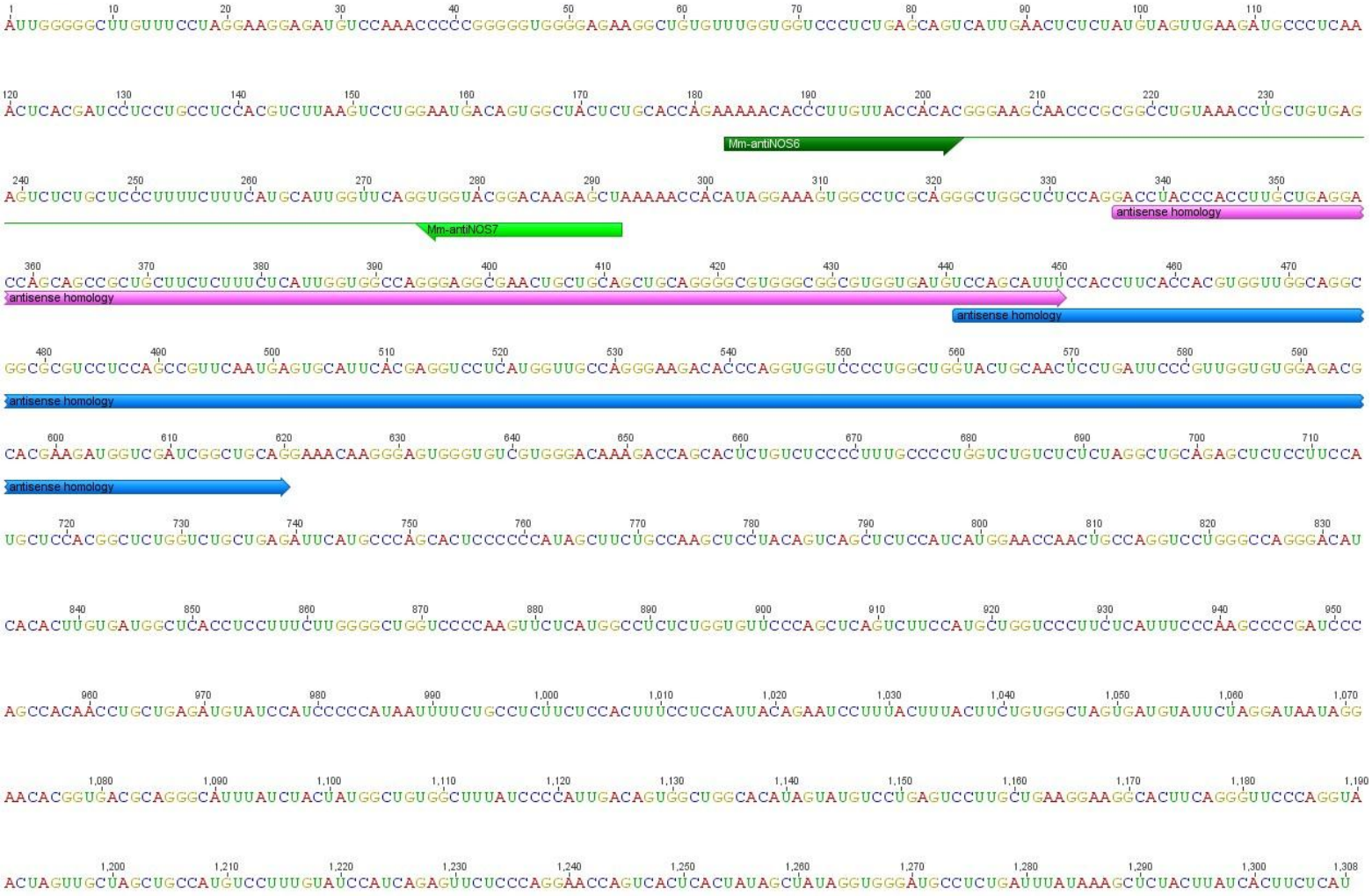

Figure 6.1 Sequence analysis of *Mm-antiNOS1* RNA. PCR amplicon is shown underlined in green, and the primers are shown in green arrows. The antisense identity sequence between *Mm-antiNOS1* RNA and *nNOS1* mRNA is shown in a blue and pink arrow.

Sequence alignment between *Mm-antiNOS1* RNA and *NOS1* mRNA (Figure 6.2) reveals 97% of antisense identity between nucleotides 345-442 of *Mm-antiNOS1* RNA and exon 21 of *NOS1* mRNA, and 95% antisense identity between nucleotides 443-630 of *Mm-antiNOS1* RNA and exon 20 of *nNOS1* mRNA. The antisense identity is located at the centre of the *Mm-antiNOS1* RNA sequence (full-overlap, Figure 1.10). The transcription of the opposite DNA strand from *NOS1* gene introduced new instructions for the termination and initiation of transcription, and changes in the splicing of the RNA. As a result, *Mm-antiNOS1* does not contain an open reading frame.

It has been shown that as much as 20% of human transcription clusters might form sense-antisense pairs (Chen et al., 2004). However, when the length of the overlapping region is <600bp, 24.5% of *cis*-NATs in a full-overlap manner show high expression (Osato et al., 2007). *Mm-antiNOS1* as a fully-overlapping *cis*-NAT with <<600bp overlap with *NOS1* mRNA, and is therefore likely to be highly expressed. Moreover, sense-antisense transcripts pairs have a significantly higher probability of involvement in the regulation of translational activity. In the case of *Mm-antiNOS1 cis*-NAT, the hypothesis is that this antisense homology could trigger the degradation of functional *nNOS1* RNA via the formation of an RNA–RNA duplex, resulting in a negative regulation of nNOS expression that would effectively be controlling the production of NO.

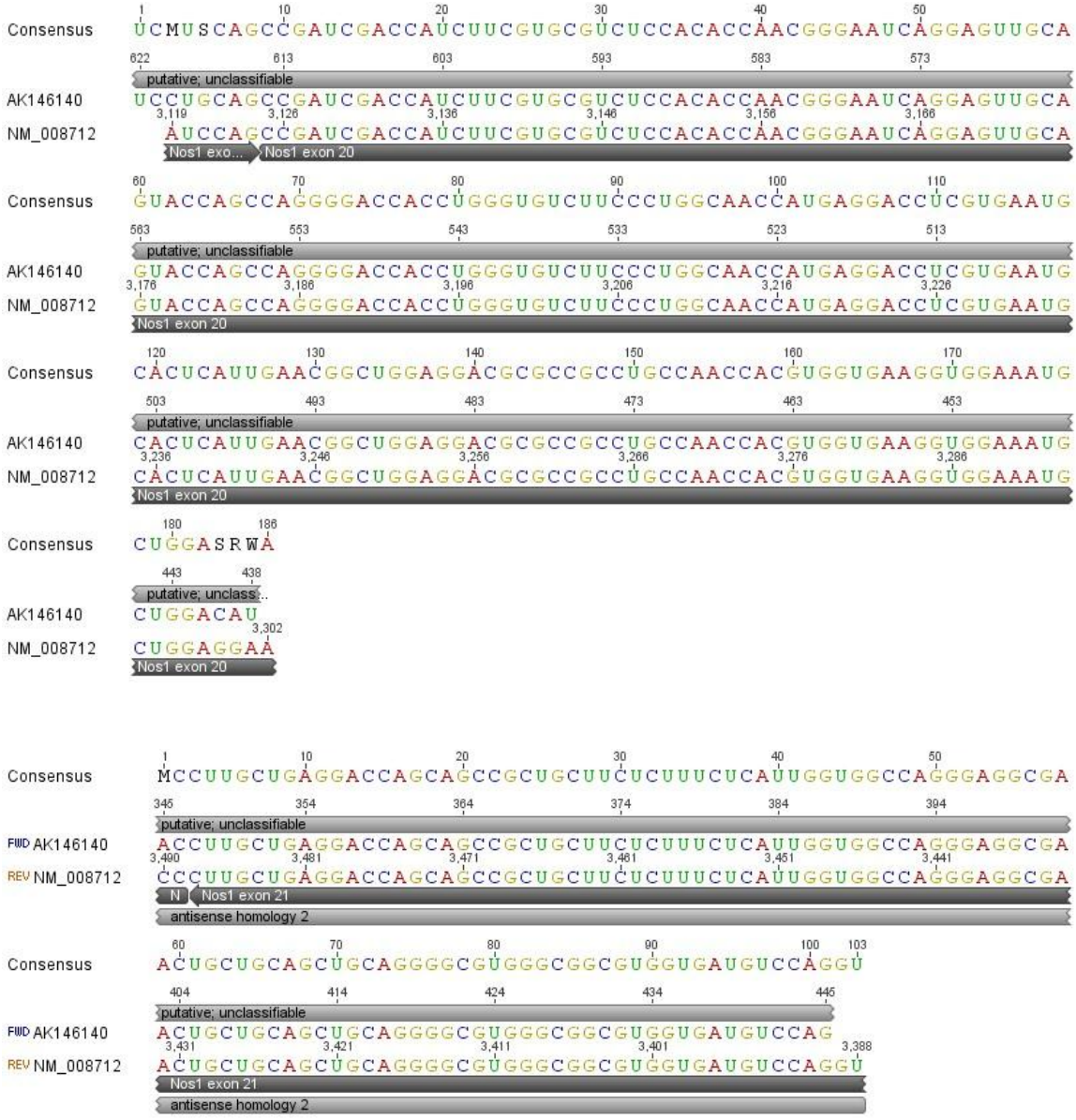

Figure 6.2 Sequence alignment between *NOS1* mRNA and *Mm-antiNOS1* RNA. An identical sequence in opposite direction is shown between bases 345 and 622 for *Mm-antiNOS1* (AK146140) on the second line and bases 3,119 and 3,388 of *NOS1 (*NM_008712) in the third line. A 97% of identity in approximately 300bp is shown between sequences.

Alignment between *NOS1* gene and *Mm-antiNOS1* RNA Figure 6.3 and Figure 6.4 show how the organization of exon/intron is affected by the fact that they are transcribed in opposite directions. A clear example of this is the presence of the *NOS1* intron 19 in the *Mm-antiNOS1* RNA sequence. It is important to have in mind that this is a comparison between an RNA sequence and its related gene sequence. A detailed description of the alignment between *Mm-antiNOS1* RNA and *NOS1* gene is shown in Table 6.1, indicating that *Mm-antiNOS1* RNA has an identical sequence to that of the *NOS1* gene over the fragments detailed in Figure 6.5.

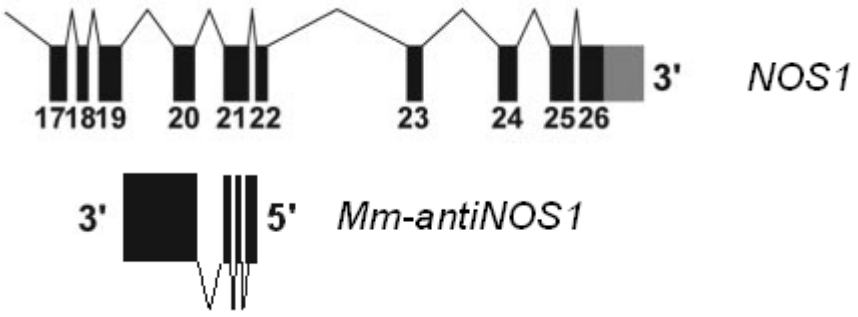

Figure 6.3 Schematic representation of *Mm-antiNOS1* illustrating the deduced intron/exon structure.

Figure 6.4 provides an alignment comparison between the sequences of *Mm-antiNOS1* RNA and *NOS1* gene. This analysis reveals that both sequences are fully homologous, as opposed to the cases of *trans*-NATs whose NATs are transcribed from areas originated from inversions within gene duplication. The average sequence homology between the *Mm-antiNOS1* RNA and the corresponding region of the *NOS1* gene is almost identical, at about 96%.

Mm-antiNOS1 RNA	*NOS1* gene		Identity
1bp - 55bp	72,391bp - 72,323bp	intron 21	96%
55bp - 160bp	71,778bp - 71,873bp		95%
160bp - 305bp	71,391bp - 71,546bp	intron 21	98%
305bp - 430bp	71,078bp - 71,219bp	exon 21	97%
430bp - 1301bp	68,601bp - 69,473bp	intron 19/exon 20	96%

Table 6.1 Areas of antisense homology between *Mm-antiNOS1* RNA and *NOS1* gene.

Figure 6.4 and Figure 6.5 show the comparison between the *NOS1* gene and *Mm-antiNOS1* RNA. It is possible to observe that *Mm-antiNOS1* has a full match with the *NOS1* gene with full identity. Because they are almost identical, we can assert that *Mm-antiNOS1* is produced from the opposite direction of the very same *NOS1* genomic locus, leaving no doubt that *Mm-antiNOS1* belongs to the family of *cis*-NATs. This change of the strand from which the genomic sequence transcribes the RNA affects the exon/intron organization significantly (Figure 6.3). Figure 6.6 shows that *NOS1* is located in mouse chromosome 5 in the region between 118,304,123 and 118,416,825 base pairs.

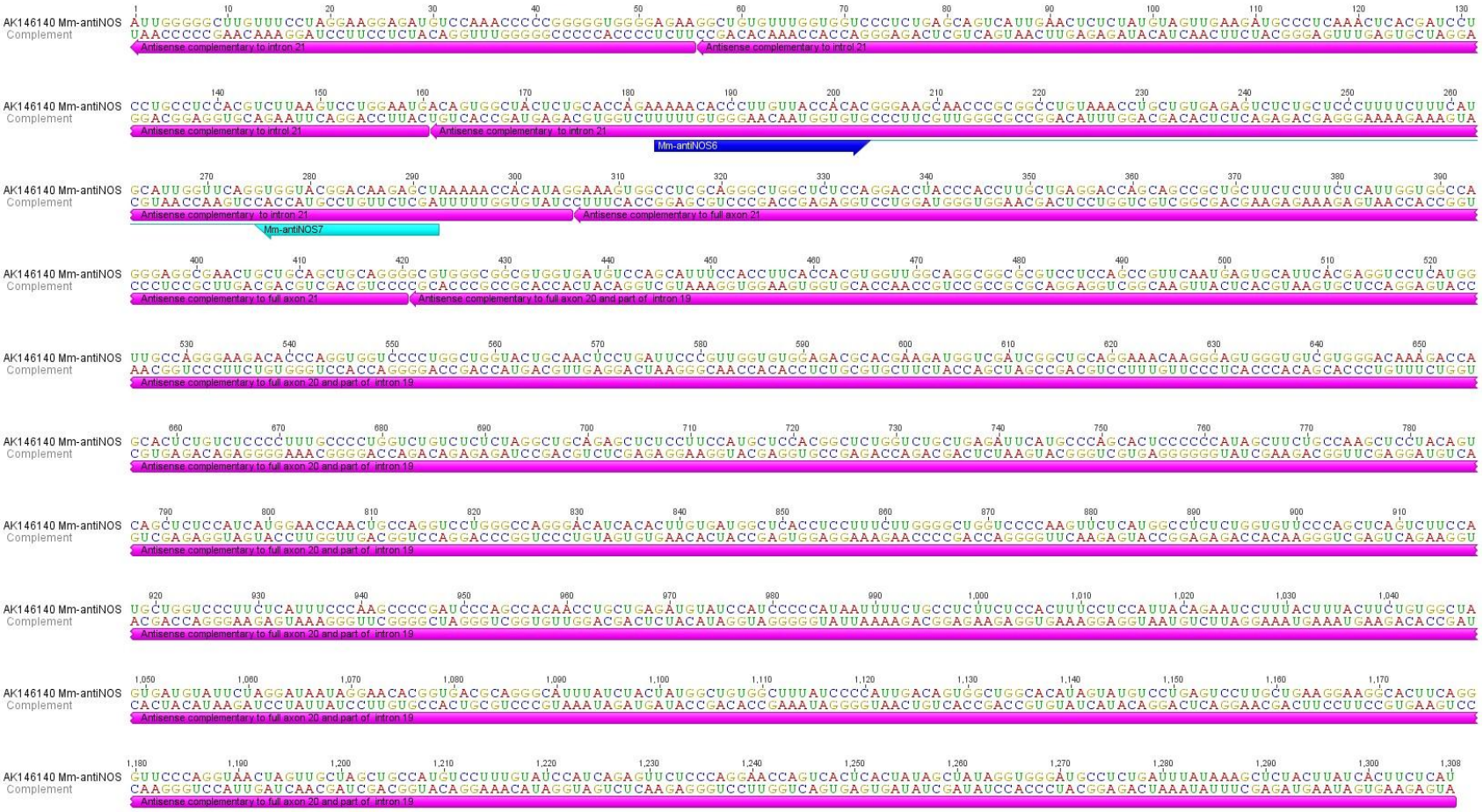

Figure 6.4 cDNA sequence of *Mm-antiNOS1* transcript. Sequence of a full-length cDNA clone isolated from a mouse cDNA library. The full length of the sequence is identical in opposite direction to the DNA sequence for *NOS1*. The region of high homology (more than 97%) to the nNOS-encoding DNA is shown in pink. In blue and light blue arrows, the position of the primers used for RT-PCR and quantitative PCR. Underlined in light blue, the amplicon product of PCR and qPCR amplification.

Figure 6.5 Sequence analysis of the alignment between *Mm-antiNOS1* and *NOS1* gene. An identical sequence in opposite direction is shown between bases over the full *Mm-antiNOS1* sequence (AK146140) on the first line and *NOS1* gene (NM_008712) in the second line. Due to the amplification of the sequence in opposite direction the intron/exon arrangement has been affected. *Identities* counts the number of positions over the length of the alignment where all of the residues or bases at that position are identical. *Positives* counts the number of positions where >= 51% of the residues or bases at that position are similar. *Gaps* count the number of positions over the length of the alignment where there are one or more sequences with a gap. 97% of the sequence was identical to *NOS1* gene.

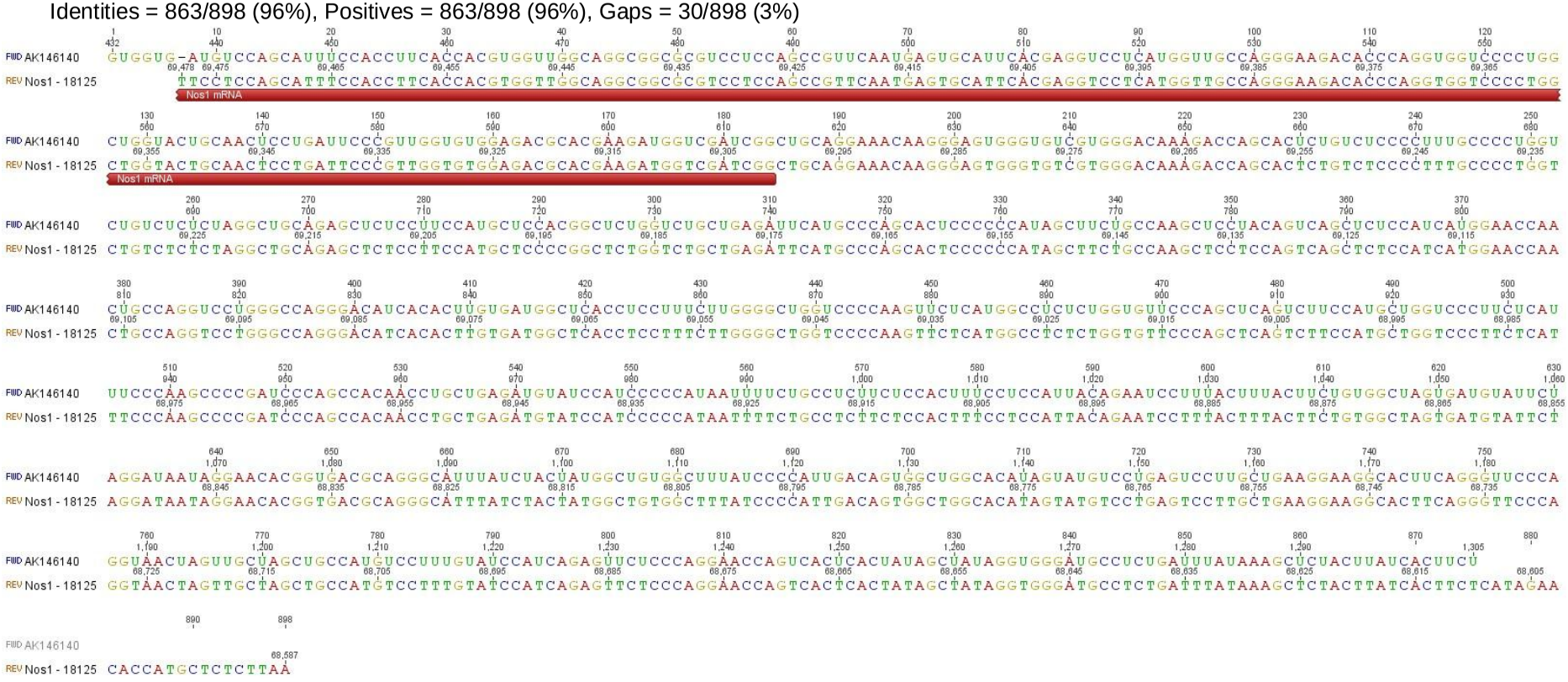

Figure 6.5 (cont.)

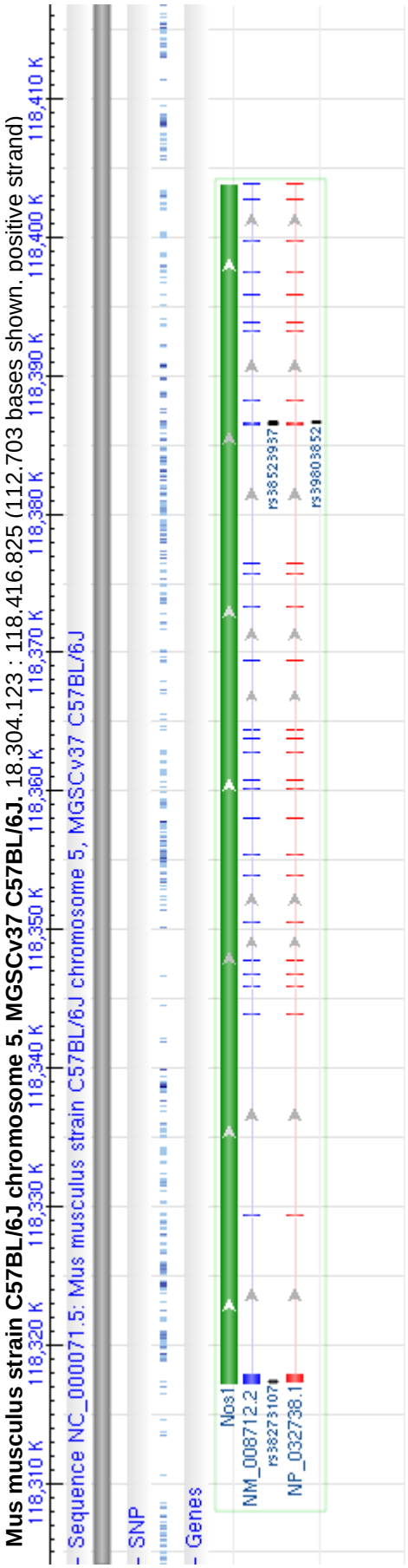

Figure 6.6 Genomic localization of the locus *NOS1*/*Mm-antiNOS1*. *NOS1* locus at chromosome 5 of mice C57 at position 18,304,123 : 118,416,825.

6.3. *Mm-antiNOS1* NAT is Detected in Embryonic and Adult Brain of Mice

Gene-specific primers for RT-PCR were designed by Dr Sergei Korneev using the *Mm-antiNOS1* sequences described in Figure 6.1. The primers are superimposed over the *Mm-antiNOS1* sequence in the figure. The sequences for these primers are:

Forward Mm-antiN6: 5′-AAAACACCCTTGTTACCACAC-3′

Reverse Mm-antiN7: 5′-AGCTCTTGTCCGTACCAC-3′

The expression of *Mm-antiNOS1* was analysed during the development of the mouse brain on embryonic days E10, E14 and E18.5. Results from the RT-PCR experiments are shown in Figure 6.7. An amplicon of 110bp was of the expected size from the amplification of pair primers Mm-antiN6/7. Expression of *Mm-antiNOS1* was first seen on E14, demonstrated by a band near the 100bp range at lane 3. The same band is visualised at a higher intensity at E18.5 (lane 5), suggesting that at E18.5 the expression of *Mm-antiNOS1* is up-regulated. The absence of bands in the RT- controls (lanes 4 and 6) validate our hypothesis that *Mm-antiNOS1* is indeed transcribed at those stages of mice embryonic brain development. No bands were detected at E10 embryonic development, and the integrity of the RNA sample was confirmed by the ability of the RNA sample to amplify a reference gene in later RT-PCR reactions. A control step of cloning and sequencing of the PCR product contained the expected *Mm-antiNOS1* sequence, confirming these results.

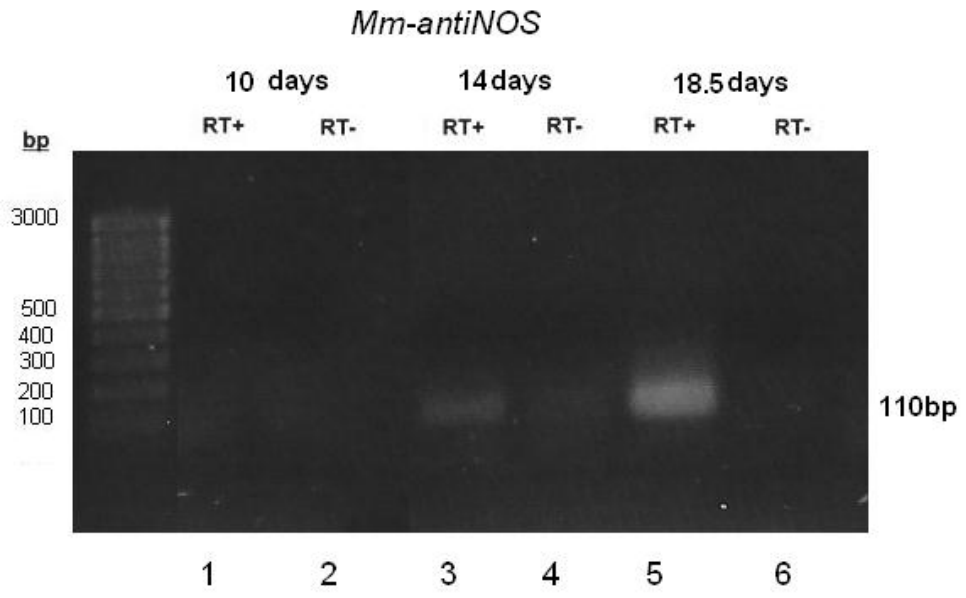

Figure 6.7 Results of the RT-PCR experiments performed on total RNA extracted from murine embryonic brains: 10-day embryo brain (lanes 1, 2), 14-day embryo brain (lanes 3, 4), and 18.5-day embryo brain (lanes 5, 6). Staining with ethyl bromide reveals bands at around 100bp in lanes 3 and 5, and no bands at the respective controls (lanes 4 and 2).

As discussed in the previous paragraph, Figure 6.7 reveals that the intensity of the bands around 100bp in the experiment varies across the different stages of embryonic development. If, as in some other NATs, *Mm-antiNOS1* were to suppress the production of NO, a differential expression of *Mm-antiNOS1* over the different stages of embryonic development would fit with the hypothesis that *Mm-antiNOS1* is involved in the process of embryonic brain development.

6.4. Quantitative Analysis of *Mm-antiNOS1* NAT Expression in Embryonic CNS

Real-time RT-PCR was conducted on RNA extracted from 10-day, 14-day and 18.5-day embryonic brain, and also on newborn and adult mice. cDNA from 14-day embryonic mouse brain was used as a calibrator.

Primer Optimization Glyceraldehyde 3-phosphate dehydrogenase (GAPDH) was chosen to be used as a reference gene, because GAPDH is an enzyme that is often stably and constitutively expressed at high levels in most tissues and cells. During real-time RT-PCR we amplified GAPDH using the following primers:

Forward MmGAPDH2: 5′-TGTCTCCTGCGACTTCAAC-3′

Reverse MmGAPDH3: 5′-AGCCGTATTCATTGTCATACC-3′

As in Section 4.3, real-time RT-PCR assays were optimised to ensure an efficient and accurate quantification of the target template. Assays were first optimised by evaluating primer concentrations. To do that, four concentrations with equimolar amounts of each primer pair were tested: 100nM, 200nM, 400nM and 600nM. The amount of template added was the same in all the samples in the optimization exercise. All the samples were run in duplicate. The ideal primer pair should yield the lowest average Ct value, as well as presenting a dissociation curve that shows a single product.

First-strand synthesis of cDNA (Section 2.9) was performed using total RNA (provided by Dr Korneev) from all the developmental stages described above. Real-time RT-PCR was conducted on these cDNA samples. Each sample was run in triplicate along with RT- control and a calibrator.

Standard-Curve Analysis of Assay Performance Standard-curve analysis was performed using a serial dilution of a calibrator sample in order to test the efficiency, precision and sensitivity of the real-time RT-PCR reaction. Two-fold

dilution series starting with 1:50 diluted cDNA and consisting of four points were generated in duplicate.

To obtain the standard curves, the Ct values of the serial dilution of the calibrator sample were plotted for each gene (Figure 6.8). After amplification, the Ct's for each standard dilution were determined and plotted. The amplification of cDNA serial dilution with Mm-antiNOS1 primers generated a standard curve with an efficiency of amplification of 99.7%, RSq = 0.985. For the cDNA amplification serial dilution with GAPDHs primers the efficiency was close to that of the Mm-antiNOS1 primers, at 97.8%, with RSq = 0.987. The lowest average Ct values were achieved for 600nM GAPDH and 400nM *Mm-antiNOS1* concentrations.

The amplification of the reference gene generated a single product with a melting temperature of 81°C (Figure 6.8A). Calibrator cDNA amplified with the Mm-antiNOS1 primer pair yielded a single product (Figure 6.8B) at a melting temperature of 81°C. The no-template control for both genes did not record any amplification.

The reactions in the real-time RT-PCR amplification generated products that agree with those expected. After cloning and sequencing, the sequences obtained confirmed the identity of the fragments as *Mm-antiNOS1*.

A

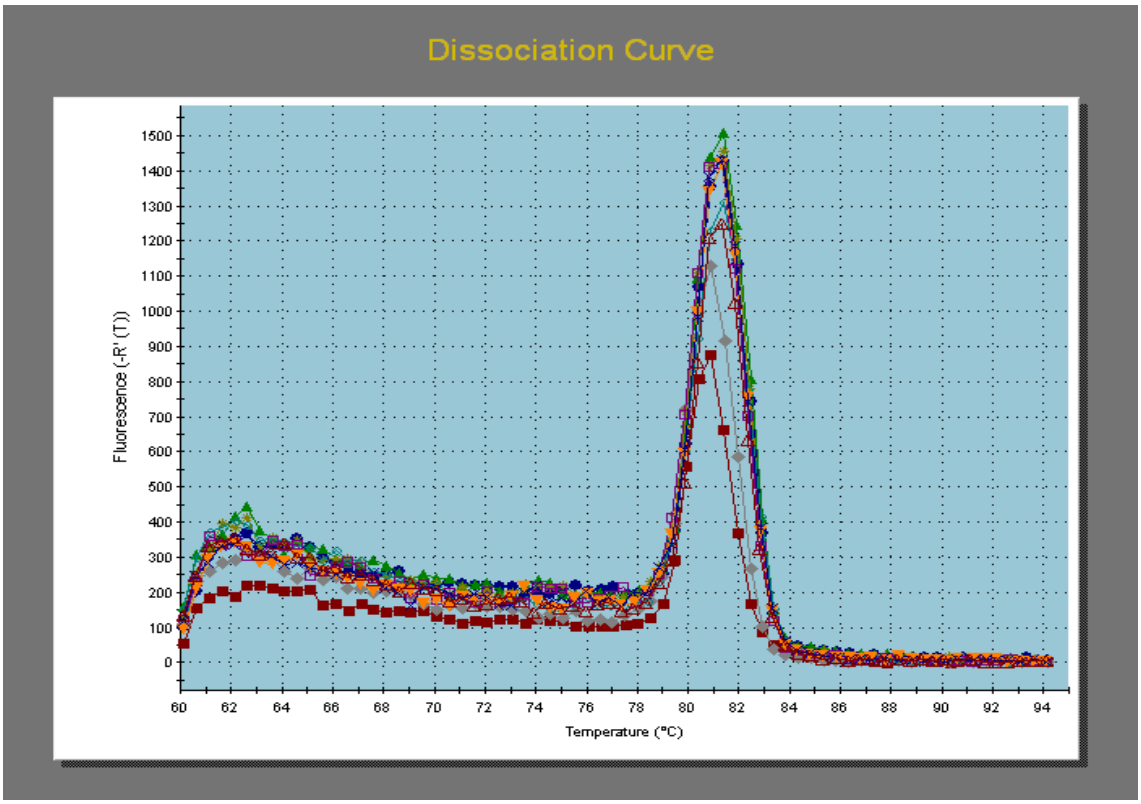

B

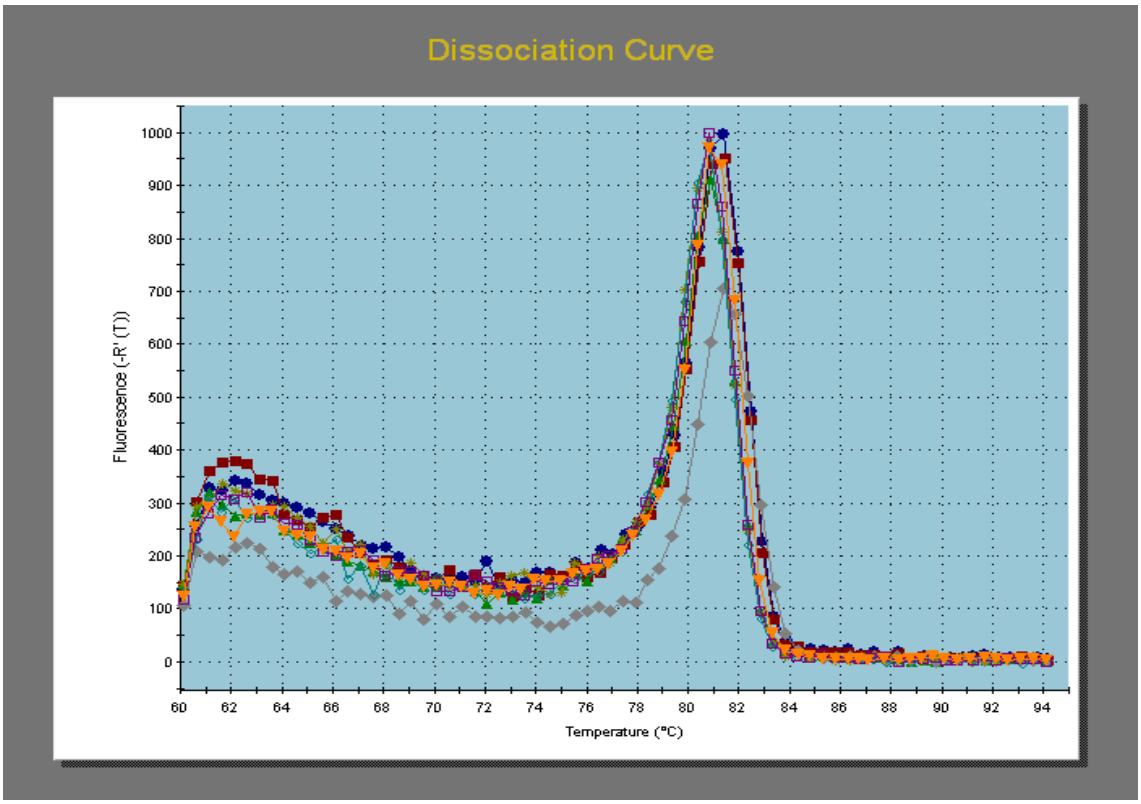

Figure 6.8 Dissociation curves of the real-time amplification of *Mm-antiNOS1* (a) and GAPDH (b). In the next page, standard curves generated from *Mm-antiNOS1* amplification data (c) and *GAPDH* amplification data (d).

C

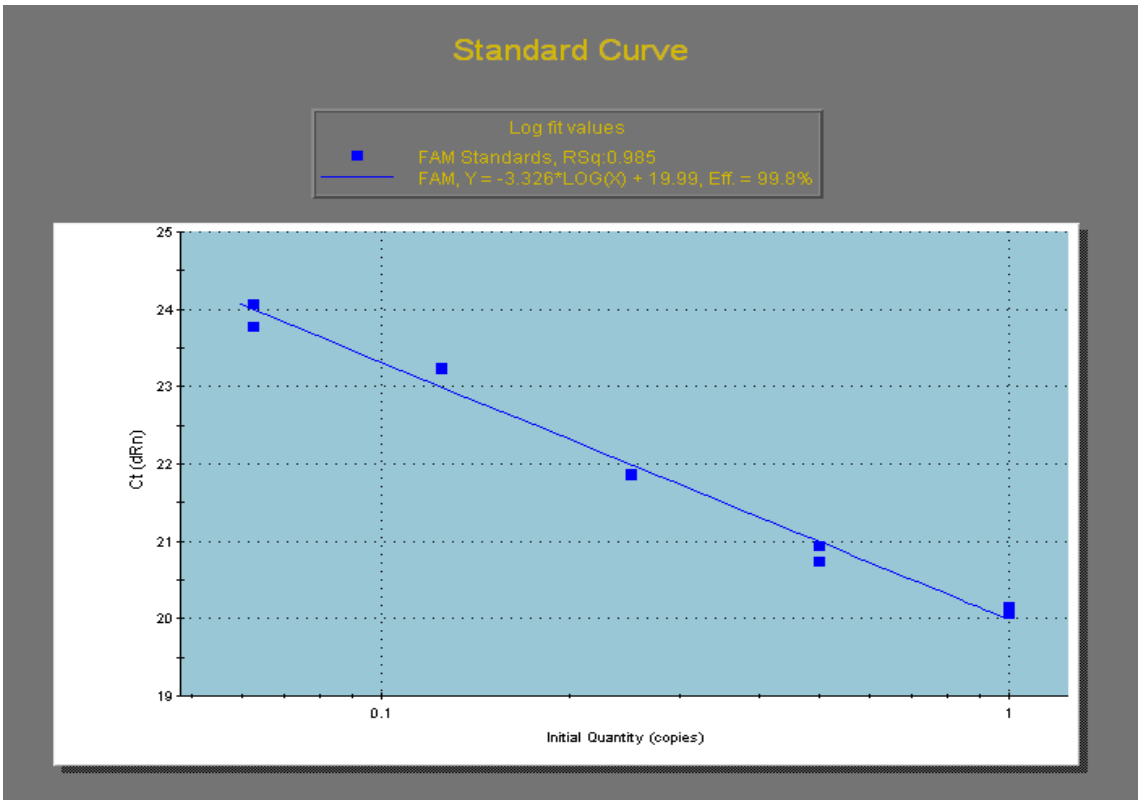

D

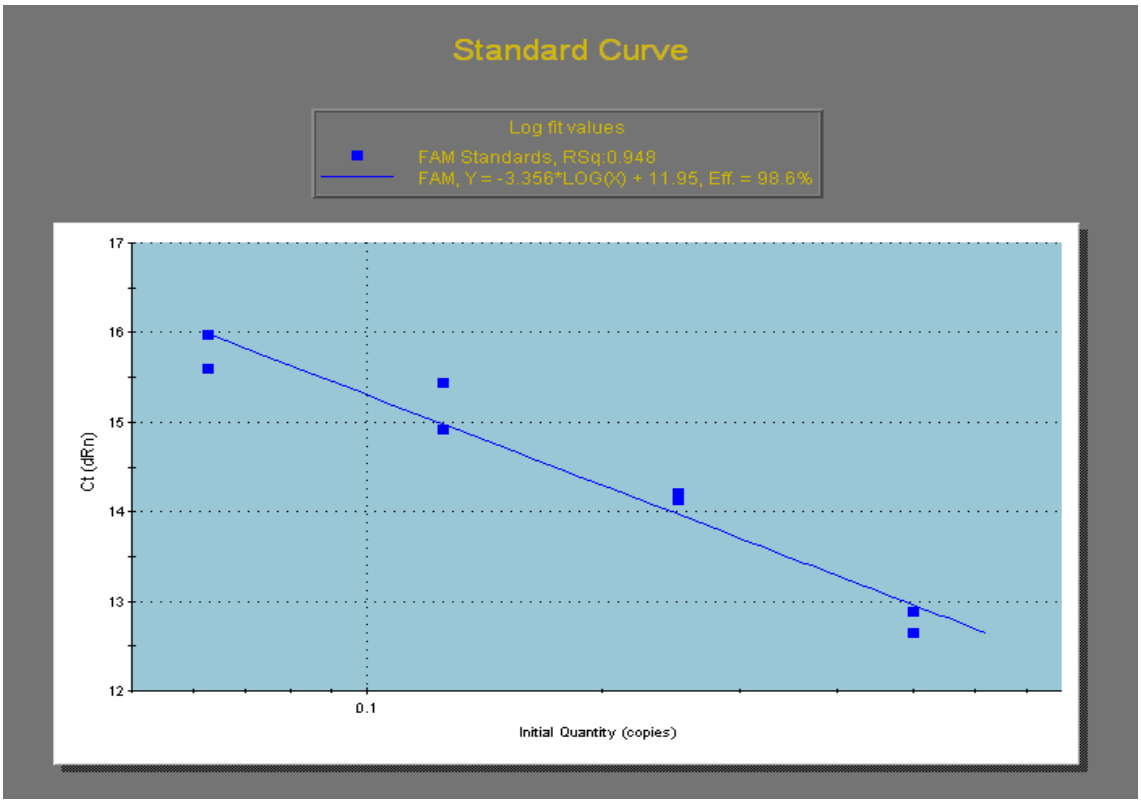

Figure 6.8 (cont.)

Differential Regulation of *Mm-antiNOS1* During Embryonic Brain Development It has been proven that *NOS1* is expressed during embryonic brain development (see Section 1.6), and its expression decreases at the end of the gestation period. In the previous section the expression of *Mm-antiNOS1* was identified in embryonic brain at different stages of development. This lead to the hypothesis that *Mm-antiNOS1* RNA expression may contribute to neuron maturation in each period, by regulating the production of NO through the regulation of *NOS1* gene expression –a crucial function in the basic development of brain function in mammals.

To validate this hypothesis, we investigated quantitative changes in the expression levels of *Mm-antiNOS1* RNA by means of real-time RT-PCR in embryonic brain taken at different stages of development (10 days, 14 days, 18.5 days), newborn and adult brains.

These quantitative experiments led to the following important results. First, it was found that the expression level of the *Mm-antiNOS1* RNA in 10-day old embryonic brain is extremely low, but by day 14 it increases by more that twelve times, and continues to increase until day 18.5 (just before birth). It is interesting to note that the level of expression has its peak at 18.5 days of gestation (full gestation of 18-20 days), at thirteen times higher than the level of expression at fourteen days. However, in brains from newborn mice the level of expression of *Mm-antiNOS1* was found to be three times lower than the one measured just before birth, and even lower in adults where its level of expression decreases to half of the level of a newborn (Table 6.2 and Figure 6.9).

From these results we can conclude that brain development in mouse embryos is associated with up-regulation of *Mm-antiNOS1* cis-NAT. An involvement of *Mm-antiNOS1* RNA in neuronal differentiation is suggested. Because *Mm-antiNOS1* is up-regulates at the time when *NOS1* is down-regulated. Also it has been suggested that NAT with homology superior to 80% have a high probability to form dsRNA. In this case *Mm-antiNOS1* is practically identical to *NOS1* sequence in the opposite direction. Therefore, it can be predicted that *Mm-antiNOS1* will form dsRNA. This information suggests that *Mm-antiNOS1* may be involved in the down-regulation of the expression of *NOS1*. This in turn leads to the hypothesis that *Mm-antiNOS1* RNA expression may contribute to neuron maturation during brain development via the regulation of *NOS1* gene expression in mammals. Further research needs to be conducted to confirm this. An important future step would be to quantify the expression of *NOS1* in mouse at the same developmental stages than those used on *Mm-antiNOS1* RNA, in order to better understand the interplay in their levels of expression.

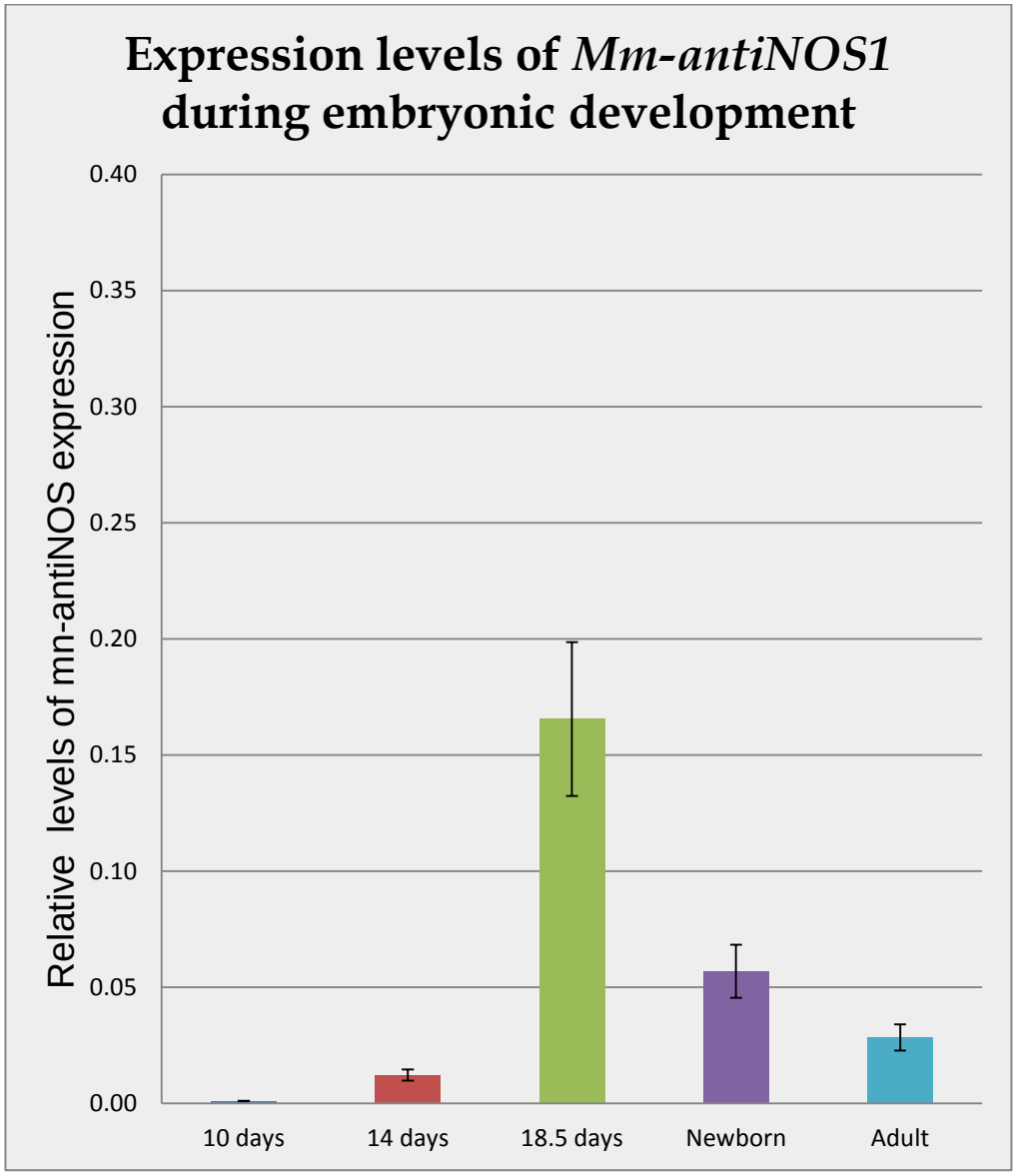

Figure 6.9 Development-induced regulation of *Mm-antiNOS1 RNA* in *mice* CNS. Real-time PCR analysis of the *Mm-antiNOS1* RNA expression in CNS of mice embryo. Level of *Mm-antiNOS1* in 10 days (blue bar), 14 days (red bar), 18.5 days (green bar), newborn (purple bar) and adult (turquoise bar) normalised to an endogenous reference (GAPDH) and relative to a calibrator (CAL) was calculated as $2^{-\Delta\Delta C_t} = \Delta C_t - \Delta C_{t(cal)}$. ΔC_t and $\Delta C_{t(cal)}$ are the differences in threshold cycles for target (*Mm-antiNOS1*) and reference (GAPDH) measured in the samples and in the calibrator, respectively. The bars show the mean value of eight samples ± standard deviation of the quotient. Note that there is an up-regulation of *Mm-antiNOS1* at 18.5 days and the expression decrease after born.

	10 days	14 days	18.5 days	Newborn	Adult
Mm-antiNOS1 C_t	32.34	29.24	24.56	25.53	28.51
(+/-)	0.65	0.94	1.17	0.56	0.19
GAPDH C_t	13.62	14.12	13.20	12.63	14.60
(+/-)	0.43	0.30	0.34	0.43	0.29
ΔC_t	18.72	15.12	11.36	12.90	13.90
(+/-)	0.77	0.98	1.21	0.70	0.34
$\Delta\Delta Ct = \Delta C_{t(cal)} - \Delta C_t$	9.96	6.35	2.60	4.14	5.14
(+/-)	0.77	0.98	1.21	0.70	0.34
Relative	0.0010	0.0122	0.1655	0.0569	0.0284
-	0.0004	0.0061	0.0944	0.0220	0.0061
+	0.0007	0.0120	0.2200	0.0359	0.0077

Table 6.2 Relative quantification of *Mm-antiNOS1* NAT using comparative ($\Delta\Delta C_t$) method in its products by real-time PCR.

6.5. Discussion

This chapter reports the discovery of a novel *cis*-NAT *Mm-antiNOS1* transcribed from the murine genome. It is demonstrated that *Mm-antiNOS1* transcript is produced from the same locus as their sense counterpart *NOS1*, and is transcribed into a non-coding NOS-related *cis*-NAT which has the potential ability to act as a negative regulator of *NOS* gene expression. Importantly, *Mm-antiNOS1* RNA exhibits high sequence identity to *NOS1* mRNA exons 20 and 21 (full identity; no isoforms containing splicing of exons 20/21 have been found in the literature).

Other non-coding NOS-related NATs have been shown to be involved in the regulation of NO through the regulation of NOS expression, such as the case of eNOS-related NAT regulated by hypoxia. In *NOS3* regulation it has been

shown that the expression of *NOS3* can be regulated by an overlapping cis-antisense transcript in a stimulus-dependent fashion. This provides evidence of sense/antisense interactions.

It has also been demonstrated in *Lymnaea* that during LTM formation, the expression of *anti-NOS1* and *Lym-antiNOS2* trans-NAT is regulated by single-trial appetite conditioning. Another case has been found in humans, where *antiNOS2A* trans-NAT expression is regulated during neurogenesis(Korneev et al., 2008)

A higher identity of 80% should result in a higher probability of *Mm-antiNOS1* and *nNOS1* forming an RNA-RNA duplex. We show that *Mm-antiNOS1* and *nNOS1* are identical (more than 97%), which would give a high probability of this event to occur. Also the length of homology region would bring extra stability to the RNA-RNA duplex formed, which should help avoid unwanted translation of the RNA-RNA duplex in those cases where this duplex is recruited by the translation machinery before it's degraded.

Neurogenesis in the mammalian brain has been associated with the upregulation of NOS2 gene expression (Corsani et al., 2008; Zhu et al., 2003). It has also been shown that NO levels derived from NOS1 and NOS2 at an early age constitute a major factor of risk for sleep and/or memory impairments in mice (Colas et al., 2006). Importantly, it has been shown that *NOS1* is expressed during embryonic brain development, and its expression decreases at the end of the gestation period (see Section 1.6). These findings are in line with the

discoveries in this thesis through real-time RT-PCR on murine embryonic brains, where an increase in the levels of expression of *Mm-antiNOS1* RNA closely before birth is demonstrated.

A very exciting outcome of these quantitative studies is how the level of expression of *Mm-antiNOS1* is upregulated during development. Of particular interest is the extremely large and sudden change in the expression levels of *Mm-antiNOS1* in the embryo from day 18.5 (just hours before birth) and the newborn (hours after being born), where the expression of *Mm-antiNOS1* drops to about a third of its previous value. Such a change may be related to the mechanisms of neuronal plasticity. When seen together, the results of *NOS1* and *Mm-antiNOS1* expression would imply that brain development in embryos is associated with up-regulation of *Mm-antiNOS1 cis*-NAT and the down-regulation of *NOS1* just before birth. The results suggest that the down-regulation of *NOS1* could be directly related with up-regulation of *Mm-antiNOS1*.

Chapter 7: General Discussion and Future Work

7.1. Introduction

It has been described that more than 20% of the genes on the human transcription clusters might form sense-antisense pairs. This figure is higher than previously thought. It has also been predicted that 15% of mouse genes form sense-antisense transcript pairs (Chen et al., 2004). NOS is regulated in different processes by natural antisense transcripts. Such is the case in mammals, where hypoxia induces the expression of a *cis*-transcript of an NOS3-encoding antisense gene in human (Robb et al., 2004). Also, *Lym-antiNOS1* has proven to be involved in long term memory formation in *Lymnaea* (Korneev et al., 2008; Korneev et al., 2005). *AntiNOS2A* is differentially regulated during neuronal differentiation of embryonic stem cells (Korneev, Korneeva et al. 2008). All of this supports the hypothesis that antisense regulation may be more widespread than previously estimated, and that the production of NO seems to be regulated via the regulation of the expression of NOS through NATs.

7.2. The Role of NOS-Related NATs in Memory Formation

This thesis is based on the hypothesis that *Lym-antiNOS2* NAT could be a putative bi-functional RNA because it can function as a protein-encoding mRNA that also contains a potential regulatory antisense region localised in the 3′ UTR (Korneev and O'Shea, 2007). Together with the knowledge that

endogenous NO produced by the enzyme NOS has an important role in the formation of long term memory, this could mean that *Lym-antiNOS2* NAT is involved in the regulation of long term memory formation.

My first target was to identify where *Lym-antiNOS2* was expressed in the CNS of *Lymnaea.* In the thesis I show by *in situ* hybridization that *Lym-antiNOS2* expression is restricted to neurons in buccal ganglia and some neurons in the cerebral ganglia. The most noticeable of those neurons is the modulatory interneuron CGC connected to the central pattern generator interneuron of the feeding system (Figure 4.1 and Figure 5.1). This neuron gates the conditioned feeding response and is an essential part of the neural network involved in LTM formation. The presence of *Lym-antiNOS2 trans*-NAT in the CGCs was confirmed by identified CGC RT-PCR, co-expressed with *Lym-NOS1* mRNA. The *in situ* hybridisation staining with probes specific against *Lym-antiNOS2* showed localisation to be mainly cytoplasmatic. An unexpected result was that the CBCs presented staining that is typical of RNA granules involved in peripheral trafficking. The presence of *Lym-antiNOS2* in the CBCs was confirmed by quantitative RT-PCR, showing that the concentration of *Lym-antiNOS2* RNA in the CBCs is much higher than the concentration in the cerebral or buccal ganglia. A further analysis of *Lym-antiNOS2* sequence shows a CPE-like sequence localized in the 3′ UTR, which agrees with its localisation in the axon. Further experiments using *Lym-antiNOS2* CPE-less mutants, showing no migration to the axons, would help to support the theory of *Lym-antiNOS2* RNA peripheral trafficking to the axon.

It is interesting to note that the NO-cGMP signalling pathway has been implicated in LTM formation. In one-trial appetitive associative conditioning it was shown that there is an obligatory requirement for this pathway during the first five hours of LTM formation (Kemenes et al., 2002). Moreover, *Lym-NOS1* gene is transiently upregulated in cerebral ganglia after conditioning. The activation of the gene is precisely timed and occurs at the end of a critical period during which NO is required for memory consolidation. It has also been demonstrated that the expression of *Lym-antiNOS1* is down-regulated by training at four hours after conditioning (Korneev et al., 2005).

Unlike most other endogenous messengers that are deposited in vesicles, processed on demand and/or secreted in a regulated fashion, NO is a highly active molecule that readily diffuses through cell membranes and thus cannot be stored inside the producing cell. Rather, its signalling capacity must be controlled at the levels of biosynthesis and local availability. The importance of temporal and spatial control of NO production is highlighted by the finding that differential localization of NOS translates into distinct effects of NO. Thus NOSs belong to the most tightly controlled enzymes at all levels (transcriptional, translational, co- and post-translational modifications, substrate availability and specific sorting to subcellular compartments), its close proximity to their target proteins being essential (Oess et al., 2006).

The work on this thesis reveals a spatial regulation of *Lym-antiNOS2* expression. *Lym-antiNOS2* RNA undergoes peripheral trafficking through the CBCs via a complex mechanism that regulates the localization to subsynaptic

regions of the neuron, increasing the likelihood of *Lym-antiNOS2* RNA being involved in NO production and hence in NO's role in LTM formation.

In this study it was found that the *Lym-antiNOS2* gene is down-regulated at four hours, as *Lym-antiNOS1* has been reported to be down-regulated (Korneev et al., 2005) in response to a very weak sensory cue stimulus (single conditioning food trial). The down-regulation at four hours coincides with the time at which the NO-cGMP pathway is required for the formation of LTM. I also show that *Lym-NOS1* is up-regulated at one hour after training, which confirms and extends previous work (Kemenes et al., 2002) where the requirement for NO for the memory trace was shown to be obligatory from the first point tested at one hour. I also demonstrate that *Lym-antiNOS2* is up-regulated at six hours.

Interestingly, this study found that the second peak of *Lym-NOS1* mRNA at six hours after training appears to be smaller than its one-hour peak (Figure 4.9). One possibility is that this smaller six-hour peak is a manifestation of a higher *Lym-NOS1* peak before the six-hour mark. This *Lym-NOS1* peak before the six-hour mark would generate NO necessary before six hours for LTM formation. The down-regulation of *Lym-antiNOS1* and *Lym-antiNOS2* RNA at four hours may be helping increase Lym-*NOS1* RNA levels, attaining a peak at between four and six hours. The *Lym-antiNOS2* RNA peak at six hours could be down-regulating the production of NO after LTM has been formed and NO is therefore not required anymore.

It was also demonstrated that the regulation of the expression of *Lym-antiNOS2* NAT is not affecting the whole brain. In particular it is remarkable how *Lym-antiNOS2* is transiently down-regulated in the buccal ganglia after training, while in cerebral ganglia it seems to follow the regulation pattern observed for whole CNS.

In this thesis it is demonstrated that the regulation of *Lym-antiNOS2* RNA expression in neurons is controlled not only temporally but also where it is going to be expressed, in a very complex way. This regulation can be triggered by single-conditioning trial. We demonstrate that *Lym-antiNOS2* changes its localization to subsynaptic regions via peripheral trafficking. To our knowledge, this is the first report of trafficking of RNA in molluscs, setting this as a unique discovery for understanding how expression of certain RNAs is regulated at multiple levels. Importantly, the potential trafficking process we have identified, which may involve CPEB, has also been reported previously in mammals, pointing to a highly-conserved process during evolution.

The dynamic sensitivity to a sensory cue of *Lym-antiNOS2* is shared also with *Lym-antiNOS1* and *Lym-NOS1*, providing a clear illustration of a pseudogene whose expression is regulated by a behavioural stimulus.

The results discussed in this section allow us to suggest that *Lym-antiNOS2* is clearly regulating the production of NO during LTM formation through the regulation of expression of *Lym-NOS1* mRNA.

7.3. The Role of NOS-Related NAT during Embryonic Brain Development

This thesis also reports the discovery of a novel NOS1-related *cis*-NAT in mouse, *Mm-antiNOS1*, which is produced from the same sequence as *NOS1* from the opposite strand of DNA. We also demonstrate that *Mm-antiNOS1* is transcribed in embryonic CNS from the fourteenth day of gestation.

Because of its identical sequence with *NOS1* mRNA over 300bp, but in opposite direction, *Mm-antiNOS1 cis*-NAT is very likely to act as a negative regulator of *NOS1* mRNA expression. Other NOS-related *cis*-NATs have been proven to act as regulators of NO production, as in the case of eNOS expression regulation via hypoxia stimulus in humans (Fish et al., 2007).

Levels of *NOS1* mRNA in the cortex and the hippocampus decrease with age in mice (Colas et al., 2006). The expression *NOS1* mRNA is first detected in the CNS at fourteen days of embryonic gestation, and its expression decreases at the end of the gestation period (Santacana et al., 1998). A very exciting outcome of this work, derived from the quantitative RT-PCR experiments examining expression levels of *Mm-antiNOS1*, is that the *Mm-antiNOS1* gene is up-regulated during the embryonic gestation until it peaks at eighteen and a half days, the end of the gestation period. After birth, expression of *Mm-antiNOS1* RNA drops to about a third of its previous value.

It is important to note that the values for the levels of expression of *NOS1* RNA previously reported (Nobakht et al., 2007; Santacana et al., 1998) and the

values of the expression of *Mm-antiNOS1* seem to follow inverted patterns of up- and down-regulation during brain development. Together, our results suggest that the down-regulation of the *NOS1* gene during embryonic development could be driven by a reciprocal up-regulation of *Mm-antiNOS1*. Results currently available do not allow the establishment of a conclusive correlation, given that the results on *NOS1* RNA are made on rats and are semi-quantitative, while the studies on *Mm-antiNOS1* conducted in this thesis were performed on mouse, using quantitative techniques. Further work is required to show the expression levels of *NOS1* RNA in mouse embryos at 10 weeks, 14 weeks and 18.5 weeks, newborn and adult mouse.

7.4. Future Work

This thesis addresses two different models of unconventional mechanisms in the regulation of NO production. Each of these are attractive areas for further research.

***Lymnaea* model of LTM formation** There are a number of different directions in which this work could be continued to further characterise the unconventional molecular mechanisms involved in the regulation of NO production through the *Lym-antiNOS2* gene, which is involved in the appetitive conditioning of *Lymnaea* feeding behaviour.

The thesis works on the hypothesis that if a dimer were formed between a full-length NOS protein and the truncated version encoded by *Lym*-antiNOS2 gene, the resulting dimer would not possess NO-synthesising activity.

Therefore, it is possible that *Lym*-antiNOS2 protein functions as a natural dominant negative regulator of NOS activity through the formation of a non-functional heterodimer with a normal NOS monomer. *In vitro* translation of *Lym*-antiNOS2 RNA shows that *Lym*-antiNOS2 RNA is translated into protein (Korneev and O'Shea, 2002). However future work has to be done on the *in vivo* translation of *Lym*-antiNOS2 RNA, and its dimerisation with a normal NOS monomer still needs to be proven, both *in vitro* and *in vivo*.

There are currently no known specific antibodies against *Lym-NOS1*, making the visualization of these protein enzymes in tissue very difficult. A novel technique called *morpholino oligomers* (an antisense technology used to block access of other molecules to specific sequences within nucleic acid) is sometimes used in cases where no antibodies are available. The homology between *Lym-NOS1* sequences and *Lym-antiNOS2* sequences, starting at the beginning of the *Lym-antiNOS2* RNA sequence and much earlier than the open reading frame, makes this technique impractical in this case, but there may still be a case for experimenting with this technique because morpholino oligomers have to be directed to the beginning of the ORF.

It would also be interesting to construct a fuller picture of the expression patterns triggered by single-conditioning trials. In particular, it would be important to analyze the level of expression of *Lym-NOS1* and *Lym-antiNOS2* *trans*-NAT in more detail a) through the CGC and CBCs; b) at the five-hour time point and c) after six hours. Studying the expression at the five-hour point would help to validate our hypothesis in relation to a possible *Lym-NOS1* peak

before six hours. Looking at expression after six hours would address our hypothesis of the six-hour *Lym-antiNOS2* RNA peak triggering down-regulation of NO production.

When investigating the expression and co-expression of *Lym-antiNOS2* RNA and *Lym-NOS1* RNA in CGC and CBCs, a further analysis of the *Lym-NOS1* RNA sequence is necessary to reveal peripheral trafficking motifs. To prove that RNA peripheral trafficking is active in snails it would be necessary to show that the proteins attach to the RNA in the axons. A first possible step is to experiment using CPEB antibodies commercially available for others species. Morpholino oligomers could be injected in the snail against the area in *Lym-antiNOS2* RNA containing CPE motif. Combined with *in situ* hybridization, showing if *Lym-antiNOS2* RNA is still present on the CBCs or not, this would further our understanding of the peripheral trafficking processes discovered in this thesis.

***Murine* model in embryonic development** Previous research has studied the pattern of expression of *nNOS* in CNS during embryonic development in rats. This thesis reports the discovery of the NOS1-related *cis*-NAT *Mm-antiNOS1*. However it is still unknown whether *Mm-antiNOS1 cis*-NAT has a role in the regulation of NO production. A natural first step towards answering this question is to understand the temporal and spatial levels of expression of *Mm-antiNOS1 cis*-NAT in the brain of mice embryos at 18 days of gestation, where we have observed its highest expression peak. Specific probes against

Mm-antiNOS1 cis-NAT have already been generated in this thesis for *in situ* hybridization.

At the same time, the initial studies on the expression levels of *nNOS* RNA relied on semi-quantitative methods (immunostaining, histochemistry) which work at the protein level. A highly recommended next step is the identification of the levels of *NOS1* mRNA expression through quantitative RT-PCR, which would help confirm the reciprocal regulation of *NOS1* mRNA and *Mm-antiNOS1 cis*-NAT during the embryonic development, and determine whether the regulation of NOS1 protein synthesis is influenced by *Mm-antiNOS1*.

Further directions Together, the results from the studies in *Lymnaea* model of LTM formation and those in *Murine* model in embryonic development could enhance our understanding of the differences in molecular mechanisms between invertebrate and mammalians species. This in turn would allow us to gain insight into the extent to which it is possible to extrapolate between species**.**

Bibliography

Abu-Soud, H. M., Yoho, L. L., and Stuehr, D. J. (1994). Calmodulin controls neuronal nitric-oxide synthase by a dual mechanism. Activation of intra- and interdomain electron transfer. J Biol Chem *269*, 32047-32050.

Alderton, W. K., Cooper, C. E., and Knowles, R. G. (2001). Nitric oxide synthases: structure, function and inhibition. Biochem J *357*, 593-615.

Alexander, J., Jr., Audesirk, T. E., and Audesirk, G. J. (1984). One-trial reward learning in the snail Lymnaea stagnalis. J Neurobiol *15*, 67-72.

Ambros, V. (2004). The functions of animal microRNAs. Nature *431*, 350-355.

Andrew, P. J., and Mayer, B. (1999). Enzymatic function of nitric oxide synthases. Cardiovasc Res *43*, 521-531.

Arnold, W. P., Mittal, C. K., Katsuki, S., and Murad, F. (1977). Nitric oxide activates guanylate cyclase and increases guanosine 3':5'-cyclic monophosphate levels in various tissue preparations. Proc Natl Acad Sci U S A *74*, 3203-3207.

Bender, A. T., Silverstein, A. M., Demady, D. R., Kanelakis, K. C., Noguchi, S., Pratt, W. B., and Osawa, Y. (1999). Neuronal nitric-oxide synthase is regulated by the Hsp90-based chaperone system in vivo. J Biol Chem *274*, 1472-1478.

Benjamin, P. R., Kemenes, G., and Staras, K. (2005). Encyclopaedia of Life Science. In Molluscan Nervous Systems (John Wiley & Sons).

Benjamin, P. R., Staras, K., and Kemenes, G. (2000). A systems approach to the cellular analysis of associative learning in the pond snail Lymnaea. Learn Mem *7*, 124-131.

Benjamin, P. R. a. K., György (2010). Lymnaea learning and memory. Scholarpedia *5*, 4247.

Borsani, O., Zhu, J., Verslues, P. E., Sunkar, R., and Zhu, J. K. (2005). Endogenous siRNAs derived from a pair of natural cis-antisense transcripts regulate salt tolerance in Arabidopsis. Cell *123*, 1279-1291.

Boumil, R. M., and Lee, J. T. (2001). Forty years of decoding the silence in X-chromosome inactivation. Hum Mol Genet *10*, 2225-2232.

Bredt, D. S. (2003). Nitric oxide signaling specificity--the heart of the problem. J Cell Sci *116*, 9-15.

Bredt, D. S., and Snyder, S. H. (1990). Isolation of nitric oxide synthetase, a calmodulin-requiring enzyme. Proc Natl Acad Sci U S A *87*, 682-685.

Calabrese, V., Mancuso, C., Calvani, M., Rizzarelli, E., Butterfield, D. A., and Stella, A. M. (2007). Nitric oxide in the central nervous system: neuroprotection versus neurotoxicity. Nat Rev Neurosci *8*, 766-775.

Cao, X., Yeo, G., Muotri, A. R., Kuwabara, T., and Gage, F. H. (2006). Noncoding RNAs in the mammalian central nervous system. Annu Rev Neurosci *29*, 77-103.

Carmichael, G. G. (2003). Antisense starts making more sense. Nat Biotechnol *21*, 371-372.

Carson, J. H., and Barbarese, E. (2005). Systems analysis of RNA trafficking in neural cells. Biol Cell *97*, 51-62.

Chase, R. (2002). The Central Nervous System. In Behavior and Its Neural Control in Gastropod Molluscs (Oxford University Press).

Chen, J., Sun, M., Kent, W. J., Huang, X., Xie, H., Wang, W., Zhou, G., Shi, R. Z., and Rowley, J. D. (2004). Over 20% of human transcripts might form sense-antisense pairs. Nucleic Acids Res *32*, 4812-4820.

Chiel, H. J., Kupfermann, I., and Weiss, K. R. (1988). An identified histaminergic neuron can modulate the outputs of buccal-cerebral interneurons in Aplysia via presynaptic inhibition. J Neurosci *8*, 49-63.

Chitwood, D. H., and Timmermans, M. C. (2011). Small RNAs are on the move. Nature *467*, 415-419.

Choate, J. K., Danson, E. J., Morris, J. F., and Paterson, D. J. (2001). Peripheral vagal control of heart rate is impaired in neuronal NOS knockout mice. Am J Physiol Heart Circ Physiol *281*, H2310-2317.

Colas, D., Gharib, A., Bezin, L., Morales, A., Guidon, G., Cespuglio, R., and Sarda, N. (2006). Regional age-related changes in neuronal nitric oxide synthase (nNOS), messenger RNA levels and activity in SAMP8 brain. BMC Neurosci *7*, 81.

Corsani, L., Bizzoco, E., Pedata, F., Gianfriddo, M., Faussone-Pellegrini, M. S., and Vannucchi, M. G. (2008). Inducible nitric oxide synthase appears and is co-expressed with the neuronal isoform in interneurons of the rat hippocampus after transient ischemia induced by middle cerebral artery occlusion. Exp Neurol *211*, 433-440.

Corson, M. A., James, N. L., Latta, S. E., Nerem, R. M., Berk, B. C., and Harrison, D. G. (1996). Phosphorylation of endothelial nitric oxide synthase in response to fluid shear stress. Circ Res *79*, 984-991.

Daff, S., Sagami, I., and Shimizu, T. (1999). The 42-amino acid insert in the FMN domain of neuronal nitric-oxide synthase exerts control over Ca(2+)/calmodulin-dependent electron transfer. J Biol Chem *274*, 30589-30595.

Denninger, J. W., and Marletta, M. A. (1999). Guanylate cyclase and the .NO/cGMP signaling pathway. Biochim Biophys Acta *1411*, 334-350.

Dirix, C. E., Nijhuis, J. G., Jongsma, H. W., and Hornstra, G. (2009). Aspects of fetal learning and memory. Child Dev *80*, 1251-1258.

Dudai, Y. (1989). The Neurobiology of Memory: Concepts, Findings, Trends, Oxford University Press).

Eissa, N. T., Yuan, J. W., Haggerty, C. M., Choo, E. K., Palmer, C. D., and Moss, J. (1998). Cloning and characterization of human inducible nitric oxide synthase splice variants: a domain, encoded by exons 8 and 9, is critical for dimerization. Proc Natl Acad Sci U S A *95*, 7625-7630.

Elgersma, Y., Sweatt, J. D., and Giese, K. P. (2004). Mouse genetic approaches to investigating calcium/calmodulin-dependent protein kinase II function in plasticity and cognition. J Neurosci *24*, 8410-8415.

Elphick, M. R., Kemenes, G., Staras, K., and O'Shea, M. (1995). Behavioral role for nitric oxide in chemosensory activation of feeding in a mollusc. J Neurosci *15*, 7653-7664.

Feng, Z. P., Zhang, Z., van Kesteren, R. E., Straub, V. A., van Nierop, P., Jin, K., Nejatbakhsh, N., Goldberg, J. I., Spencer, G. E., Yeoman, M. S., *et al.* (2009). Transcriptome analysis of the central nervous system of the mollusc Lymnaea stagnalis. BMC Genomics *10*, 451.

Fiore, L., Geppetti, L., De Santis, A., Pieneman, A. W., and Ferguson, G. P. (1992). Bidirectional transmission in the cerebrobuccal connective of Aplysia during feeding. Acta Biol Hung *43*, 343-350.

Fish, J. E., Matouk, C. C., Yeboah, E., Bevan, S. C., Khan, M., Patil, K., Ohh, M., and Marsden, P. A. (2007). Hypoxia-inducible expression of a natural cis-antisense transcript inhibits endothelial nitric-oxide synthase. J Biol Chem *282*, 15652-15666.

Fujisawa, Y., Furukawa, Y., Ohta, S., Ellis, T. A., Dembrow, N. C., Li, L., Floyd, P. D., Sweedler, J. V., Minakata, H., Nakamaru, K., *et al.* (1999). The Aplysia mytilus inhibitory peptide-related peptides: identification, cloning, processing, distribution, and action. J Neurosci *19*, 9618-9634.

Fukoto J.M., C. J. Y. a. S. C. H. (2000). The chemical properties of nitric oxide. In Nitric Oxide Biology and Pathobiology, I. L.J., ed.

Furchgott, R. F., and Zawadzki, J. V. (1980). The obligatory role of endothelial cells in the relaxation of arterial smooth muscle by acetylcholine. Nature *288*, 373-376.

Gachhui, R., Abu-Soud, H. M., Ghosha, D. K., Presta, A., Blazing, M. A., Mayer, B., George, S. E., and Stuehr, D. J. (1998). Neuronal nitric-oxide synthase interaction with calmodulin-troponin C chimeras. J Biol Chem *273*, 5451-5454.

Gachhui, R., Presta, A., Bentley, D. F., Abu-Soud, H. M., McArthur, R., Brudvig, G., Ghosh, D. K., and Stuehr, D. J. (1996). Characterization of the reductase domain of rat neuronal nitric oxide synthase generated in the methylotrophic yeast Pichia pastoris. Calmodulin response is complete within the reductase domain itself. J Biol Chem *271*, 20594-20602.

Garthwaite, J., and Boulton, C. L. (1995). Nitric oxide signaling in the central nervous system. Annu Rev Physiol *57*, 683-706.

Glanzman, D. L. (2009). Habituation in Aplysia: the Cheshire cat of neurobiology. Neurobiol Learn Mem *92*, 147-154.

Gruetter, C. A., Barry, B. K., McNamara, D. B., Gruetter, D. Y., Kadowitz, P. J., and Ignarro, L. (1979). Relaxation of bovine coronary artery and activation of coronary arterial guanylate cyclase by nitric oxide, nitroprusside and a carcinogenic nitrosoamine. J Cyclic Nucleotide Res *5*, 211-224.

Hallberg, B., Lund, F., and et al. (1948). The treatment of hypertension with nitroglycerin preparations. Acta Med Scand *131*, 76-80.

Halvey, E. J., Vernon, J., Roy, B., and Garthwaite, J. (2009). Mechanisms of activity-dependent plasticity in cellular nitric oxide-cGMP signaling. J Biol Chem *284*, 25630-25641.

Harooni, H. E., Naghdi, N., Sepehri, H., and Rohani, A. H. (2009). The role of hippocampal nitric oxide (NO) on learning and immediate, short- and long-term memory retrieval in inhibitory avoidance task in male adult rats. Behav Brain Res *201*, 166-172.

Hawkins, R. D., Kandel, E. R., and Bailey, C. H. (2006). Molecular mechanisms of memory storage in Aplysia. Biol Bull *210*, 174-191.

Hayashi, Y., Nishio, M., Naito, Y., Yokokura, H., Nimura, Y., Hidaka, H., and Watanabe, Y. (1999). Regulation of neuronal nitric-oxide synthase by calmodulin kinases. J Biol Chem *274*, 20597-20602.

Hemmens, B., Woschitz, S., Pitters, E., Klosch, B., Volker, C., Schmidt, K., and Mayer, B. (1998). The protein inhibitor of neuronal nitric oxide synthase (PIN): characterization of its action on pure nitric oxide synthases. FEBS Lett *430*, 397-400.

Hepper, P. G. (1996). Fetal memory: does it exist? What does it do? Acta Paediatr Suppl *416*, 16-20.

Holmqvist, B., Ellingsen, B., Alm, P., Forsell, J., Oyan, A. M., Goksoyr, A., Fjose, A., and Seo, H. C. (2000). Identification and distribution of nitric oxide synthase in the brain of adult zebrafish. Neurosci Lett *292*, 119-122.

Hyun, T. K., Uddin, M. N., Rim, Y., and Kim, J. Y. (2011). Cell-to-cell trafficking of RNA and RNA silencing through plasmodesmata. Protoplasma *248*, 101-116.

Ignarro (2000). Introduction and Overview. In Nitric Oxide Biology and Pathobiology, I. LJ, ed. (Academic Press).

Ignarro, L. J., Buga, G. M., Wood, K. S., Byrns, R. E., and Chaudhuri, G. (1987). Endothelium-derived relaxing factor produced and released from artery and vein is nitric oxide. Proc Natl Acad Sci U S A *84*, 9265-9269.

Ignarro, L. J., Lippton, H., Edwards, J. C., Baricos, W. H., Hyman, A. L., Kadowitz, P. J., and Gruetter, C. A. (1981). Mechanism of vascular smooth muscle relaxation by organic nitrates, nitrites, nitroprusside and nitric oxide: evidence for the involvement of S-nitrosothiols as active intermediates. J Pharmacol Exp Ther *218*, 739-749.

Ignarro, L. J., Ross, G., and Tillisch, J. (1991). Pharmacology of endothelium-derived nitric oxide and nitrovasodilators. West J Med *154*, 51-62.

Jacq, C., Miller, J. R., and Brownlee, G. G. (1977). A pseudogene structure in 5S DNA of Xenopus laevis. Cell *12*, 109-120.

Jaffrey, S. R., and Snyder, S. H. (1996). PIN: an associated protein inhibitor of neuronal nitric oxide synthase. Science *274*, 774-777.

Juch, M., Smalla, K. H., Kahne, T., Lubec, G., Tischmeyer, W., Gundelfinger, E. D., and Engelmann, M. (2009). Congenital lack of nNOS impairs long-term social recognition memory and alters the olfactory bulb proteome. Neurobiol Learn Mem *92*, 469-484.

Kalb, R. G., and Agostini, J. (1993). Molecular evidence for nitric oxide-mediated motor neuron development. Neuroscience *57*, 1-8.

Kandel, E. R., Schwartz, J.H., Jessell, T.M. (2000). Principles of neural science, McGraw-Hill).

Katsuki, S., Arnold, W., Mittal, C., and Murad, F. (1977). Stimulation of guanylate cyclase by sodium nitroprusside, nitroglycerin and nitric oxide in various tissue preparations and comparison to the effects of sodium azide and hydroxylamine. J Cyclic Nucleotide Res *3*, 23-35.

Kemenes, G. (2008). Molecular Mechanisms of Associative Learning: Lymnaea. In Learning and Memory: A Comprehensive Reference., E. D. Sweatt, ed. (Oxford: Elsevier).

Kemenes, G., Kemenes, I., Michel, M., Papp, A., and Muller, U. (2006a). Phase-dependent molecular requirements for memory reconsolidation: differential roles for protein synthesis and protein kinase A activity. J Neurosci *26*, 6298-6302.

Kemenes, G., Staras, K., and Benjamin, P. R. (2001). Multiple types of control by identified interneurons in a sensory-activated rhythmic motor pattern. J Neurosci *21*, 2903-2911.

Kemenes, I., Kemenes, G., Andrew, R. J., Benjamin, P. R., and O'Shea, M. (2002). Critical time-window for NO-cGMP-dependent long-term memory formation after one-trial appetitive conditioning. J Neurosci *22*, 1414-1425.

Kemenes, I., O'Shea, M., and Benjamin, P. R. (2011). Different circuit and monoamine mechanisms consolidate long-term memory in aversive and reward classical conditioning. Eur J Neurosci *33*, 143-152.

Kemenes, I., Straub, V. A., Nikitin, E. S., Staras, K., O'Shea, M., Kemenes, G., and Benjamin, P. R. (2006b). Role of delayed nonsynaptic neuronal plasticity in long-term associative memory. Curr Biol *16*, 1269-1279.

Kim, V. N., and Nam, J. W. (2006). Genomics of microRNA. Trends Genet *22*, 165-173.

Kindler, S., Wang, H., Richter, D., and Tiedge, H. (2005). RNA transport and local control of translation. Annu Rev Cell Dev Biol *21*, 223-245.

Kloc, M., Zearfoss, N. R., and Etkin, L. D. (2002). Mechanisms of subcellular mRNA localization. Cell *108*, 533-544.

Knowles, R. G., and Moncada, S. (1994). Nitric oxide synthases in mammals. Biochem J *298 (Pt 2)*, 249-258.

Komeima, K., Hayashi, Y., Naito, Y., and Watanabe, Y. (2000). Inhibition of neuronal nitric-oxide synthase by calcium/ calmodulin-dependent protein

kinase IIalpha through Ser847 phosphorylation in NG108-15 neuronal cells. J Biol Chem *275*, 28139-28143.

Korneev, S., and O'Shea, M. (2002). Evolution of nitric oxide synthase regulatory genes by DNA inversion. Mol Biol Evol *19*, 1228-1233.

Korneev, S., and O'Shea, M. (2005). Natural antisense RNAs in the nervous system. Rev Neurosci *16*, 213-222.

Korneev, S., and O'Shea, M. (2007). Regulatory role and evolution of unconventional NOS-related RNAs. In Nitric Oxide, B. Tota, and B. Trimmer, eds. (Elsevier).

Korneev, S. A., Korneeva, E. I., Lagarkova, M. A., Kiselev, S. L., Critchley, G., and O'Shea, M. (2008). Novel noncoding antisense RNA transcribed from human anti-NOS2A locus is differentially regulated during neuronal differentiation of embryonic stem cells. Rna *14*, 2030-2037.

Korneev, S. A., Park, J. H., and O'Shea, M. (1999). Neuronal expression of neural nitric oxide synthase (nNOS) protein is suppressed by an antisense RNA transcribed from an NOS pseudogene. J Neurosci *19*, 7711-7720.

Korneev, S. A., Piper, M. R., Picot, J., Phillips, R., Korneeva, E. I., and O'Shea, M. (1998). Molecular characterization of NOS in a mollusc: expression in a giant modulatory neuron. J Neurobiol *35*, 65-76.

Korneev, S. A., Straub, V., Kemenes, I., Korneeva, E. I., Ott, S. R., Benjamin, P. R., and O'Shea, M. (2005). Timed and targeted differential regulation of nitric oxide synthase (NOS) and anti-NOS genes by reward conditioning leading to long-term memory formation. J Neurosci *25*, 1188-1192.

Koshland, D. E., Jr. (1992). The molecule of the year. Science *258*, 1861.

Krasno, L. R., and Ivy, A. C. (1950). The response of the flicker fusion threshold to nitroglycerin and its potential value in the diagnosis, prognosis, and therapy of subclinical and clinical cardiovascular disease. Circulation *1*, 1267-1276.

Kupfermann, I., and Weiss, K. R. (1982). Activity of an identified serotonergic neuron in free moving Aplysia correlates with behavioral arousal. Brain Res *241*, 334-337.

Kuslansky, B., Weiss, K. R., and Kupfermann, I. (1978). A neural pathway mediating satiation of feeding behavior in Aplysia. Behav Biol *23*, 230-237.

Lasek, R. J., and Dower, W. J. (1971). Aplysia californica: analysis of nuclear DNA in individual nuclei of giant neurons. Science *172*, 278-280.

Lehner, B., Williams, G., Campbell, R. D., and Sanderson, C. M. (2002). Antisense transcripts in the human genome. Trends Genet *18*, 63-65.

Li, H., and Poulos, T. L. (2005). Structure-function studies on nitric oxide synthases. J Inorg Biochem *99*, 293-305.

Liu, Q., and Gross, S. S. (1996). Binding sites of nitric oxide synthases. Methods Enzymol *268*, 311-324.

Love, S. (1999). Oxidative stress in brain ischemia. Brain Pathol *9*, 119-131.

Luo, C. X., and Zhu, D. Y. (2011). Research progress on neurobiology of neuronal nitric oxide synthase. Neurosci Bull *27*, 23-35.

Martinez-Fernandez, M., Bernatchez, L., Rolan-Alvarez, E., and Quesada, H. (2011). Insights into the role of differential gene expression on the ecological adaptation of the snail Littorina saxatilis. BMC Evol Biol *10*, 356.

Masters, B. S. (2000). Structural Variations to Accommodate Functional Themes in the Isoforms of NO Synthases. In Nitric Oxide: Biology and Pathobiology, L. J. Ignarro, ed. (Academic Press).

Matera, A. G., Terns, R. M., and Terns, M. P. (2007). Non-coding RNAs: lessons from the small nuclear and small nucleolar RNAs. Nat Rev Mol Cell Biol *8*, 209-220.

Mikl, M., Vendra, G., Doyle, M., and Kiebler, M. A. (2010). RNA localization in neurite morphogenesis and synaptic regulation: current evidence and novel approaches. J Comp Physiol A Neuroethol Sens Neural Behav Physiol *196*, 321-334.

Milner, B., Squire, L. R., and Kandel, E. R. (1998). Cognitive neuroscience and the study of memory. Neuron *20*, 445-468.

Moroz, L. L., and Kohn, A. (2007). On the comparative biology of Nitric Oxide (NO) synthetic pathways: Parallel evolution of NO-mediated signaling. In Nitric Oxide, B. Tota, and B. Trimmer, eds. (Elsevier).

Murad, F., Mittal, C. K., Arnold, W. P., Katsuki, S., and Kimura, H. (1978). Guanylate cyclase: activation by azide, nitro compounds, nitric oxide, and hydroxyl radical and inhibition by hemoglobin and myoglobin. Adv Cyclic Nucleotide Res *9*, 145-158.

Murashima, Y. L., Suzuki, J., and Yoshii, M. (2005). Developmental program of epileptogenesis in the brain of EL mice. Epilepsia *46 Suppl 5*, 10-16.

Muro, E. M., and Andrade-Navarro, M. A. (2010). Pseudogenes as an alternative source of natural antisense transcripts. BMC Evol Biol *10*, 338.

Nakane, M., Mitchell, J., Forstermann, U., and Murad, F. (1991). Phosphorylation by calcium calmodulin-dependent protein kinase II and protein kinase C modulates the activity of nitric oxide synthase. Biochem Biophys Res Commun *180*, 1396-1402.

Nobakht, M., Majidzadeh, S., Fattahi, M., Samadi, M., and Tabatabaeei, P. (2007). Expression of neuronal nitric oxide synthase during embryonic development of the rat optic vesicle. Pak J Biol Sci *10*, 1078-1082.

Nobelprize.org (1998). The Nobel Prize in Physiology or Medicine.

Oess, S., Icking, A., Fulton, D., Govers, R., and Muller-Esterl, W. (2006). Subcellular targeting and trafficking of nitric oxide synthases. Biochem J *396*, 401-409.

Ohyu, J., and Takashima, S. (1998). Developmental characteristics of neuronal nitric oxide synthase (nNOS) immunoreactive neurons in fetal to adolescent human brains. Brain Res Dev Brain Res *110*, 193-202.

Osato, N., Suzuki, Y., Ikeo, K., and Gojobori, T. (2007). Transcriptional interferences in cis natural antisense transcripts of humans and mice. Genetics *176*, 1299-1306.

Palacios, I. M., and St Johnston, D. (2001). Getting the message across: the intracellular localization of mRNAs in higher eukaryotes. Annu Rev Cell Dev Biol *17*, 569-614.

Paton, J. F., Deuchars, J., Ahmad, Z., Wong, L. F., Murphy, D., and Kasparov, S. (2001). Adenoviral vector demonstrates that angiotensin II-induced depression of the cardiac baroreflex is mediated by endothelial nitric oxide synthase in the nucleus tractus solitarii of the rat. J Physiol *531*, 445-458.

Pavlov, I. P. (1927). Conditioned Reflexes: An Investigation of the Physiological Activity of the Cerebral Cortex. Oxford University Press *Classics in the History of Psychology*.

Pavlov, I. P. (1951). [Conditioned reflex]. Feldsher Akush *10*, 3-10; contd.

Peunova, N., Scheinker, V., Ravi, K., and Enikolopov, G. (2007). Nitric oxide coordinates cell proliferation and cell movements during early development of Xenopus. Cell Cycle *6*, 3132-3144.

Ponting, C. P., Oliver, P. L., and Reik, W. (2009). Evolution and functions of long noncoding RNAs. Cell *136*, 629-641.

Ribeiro, M., Schofield, M., Kemenes, I., Benjamin, P. R., O'Shea, M., and Korneev, S. A. (2010). Atypical guanylyl cyclase from the pond snail Lymnaea stagnalis: cloning, sequence analysis and characterization of expression. Neuroscience *165*, 794-800.

Ribeiro, M., Straub, V. A., Schofield, M., Picot, J., Benjamin, P. R., O'Shea, M., and Korneev, S. A. (2008). Characterization of NO-sensitive guanylyl cyclase: expression in an identified interneuron involved in NO-cGMP-dependent memory formation. Eur J Neurosci *28*, 1157-1165.

Ribeiro, M. J., Serfozo, Z., Papp, A., Kemenes, I., O'Shea, M., Yin, J. C., Benjamin, P. R., and Kemenes, G. (2003). Cyclic AMP response element-binding (CREB)-like proteins in a molluscan brain: cellular localization and learning-induced phosphorylation. Eur J Neurosci *18*, 1223-1234.

Robb, G. B., Carson, A. R., Tai, S. C., Fish, J. E., Singh, S., Yamada, T., Scherer, S. W., Nakabayashi, K., and Marsden, P. A. (2004). Post-transcriptional regulation of endothelial nitric-oxide synthase by an overlapping antisense mRNA transcript. J Biol Chem *279*, 37982-37996.

Rodriguez-Crespo, I., Straub, W., Gavilanes, F., and Ortiz de Montellano, P. R. (1998). Binding of dynein light chain (PIN) to neuronal nitric oxide synthase in the absence of inhibition. Arch Biochem Biophys *359*, 297-304.

Rosok, O., and Sioud, M. (2005). Systematic search for natural antisense transcripts in eukaryotes (review). Int J Mol Med *15*, 197-203.

Roy, B., and Garthwaite, J. (2006). Nitric oxide activation of guanylyl cyclase in cells revisited. Proc Natl Acad Sci U S A *103*, 12185-12190.

Santacana, M., Uttenthal, L. O., Bentura, M. L., Fernandez, A. P., Serrano, J., Martinez de Velasco, J., Alonso, D., Martinez-Murillo, R., and Rodrigo, J. (1998). Expression of neuronal nitric oxide synthase during embryonic development of the rat cerebral cortex. Brain Res Dev Brain Res *111*, 205-222.

Schmidt, H. H., and Murad, F. (1991). Purification and characterization of a human NO synthase. Biochem Biophys Res Commun *181*, 1372-1377.

Schmidt, H. H., Wilke, P., Evers, B., and Bohme, E. (1989). Enzymatic formation of nitrogen oxides from L-arginine in bovine brain cytosol. Biochem Biophys Res Commun *165*, 284-291.

Schuman, E. M., and Madison, D. V. (1991). A requirement for the intercellular messenger nitric oxide in long-term potentiation. Science *254*, 1503-1506.

Smith, R. (2004). Moving molecules: mRNA trafficking in Mammalian oligodendrocytes and neurons. Neuroscientist *10*, 495-500.

Straub, V. A., Styles, B. J., Ireland, J. S., O'Shea, M., and Benjamin, P. R. (2004). Central localization of plasticity involved in appetitive conditioning in Lymnaea. Learn Mem *11*, 787-793.

Stuehr, D. J., Cho, H. J., Kwon, N. S., Weise, M. F., and Nathan, C. F. (1991). Purification and characterization of the cytokine-induced macrophage nitric oxide synthase: an FAD- and FMN-containing flavoprotein. Proc Natl Acad Sci U S A *88*, 7773-7777.

Szabo, C., Ischiropoulos, H., and Radi, R. (2007). Peroxynitrite: biochemistry, pathophysiology and development of therapeutics. Nat Rev Drug Discov *6*, 662-680.

Taft, R. J., Glazov, E. A., Lassmann, T., Hayashizaki, Y., Carninci, P., and Mattick, J. S. (2009). Small RNAs derived from snoRNAs. RNA *15*, 1233-1240.

Tao Li, J., Somasundaram, C., Bian, K., Xiong, W., Mahmooduddin, F., Nath, R. K., and Murad, F. (2010). Nitric oxide signaling and neural stem cell differentiation in peripheral nerve regeneration. Eplasty *10*, e42.

Tranguch, S., Steuerwald, N., and Huet-Hudson, Y. M. (2003). Nitric oxide synthase production and nitric oxide regulation of preimplantation embryo development. Biol Reprod *68*, 1538-1544.

Tufarelli, C. (2006). The silence RNA keeps: cis mechanisms of RNA mediated epigenetic silencing in mammals. Philos Trans R Soc Lond B Biol Sci *361*, 67-79.

Tufarelli, C., Stanley, J. A., Garrick, D., Sharpe, J. A., Ayyub, H., Wood, W. G., and Higgs, D. R. (2003). Transcription of antisense RNA leading to gene silencing and methylation as a novel cause of human genetic disease. Nat Genet *34*, 157-165.

Vanhee-Brossollet, C., and Vaquero, C. (1998). Do natural antisense transcripts make sense in eukaryotes? Gene *211*, 1-9.

Vanin, E. F. (1985). Processed pseudogenes: characteristics and evolution. Annu Rev Genet *19*, 253-272.

Venema, V. J., Ju, H., Zou, R., and Venema, R. C. (1997). Interaction of neuronal nitric-oxide synthase with caveolin-3 in skeletal muscle. Identification of a novel caveolin scaffolding/inhibitory domain. J Biol Chem *272*, 28187-28190.

Verona, R. I., Mann, M. R., and Bartolomei, M. S. (2003). Genomic imprinting: intricacies of epigenetic regulation in clusters. Annu Rev Cell Dev Biol *19*, 237-259.

Wan, H., Mackay, B., Iqbal, H., Naskar, S., and Kemenes, G. (2010). Delayed intrinsic activation of an NMDA-independent CaM-kinase II in a critical time window is necessary for late consolidation of an associative memory. J Neurosci *30*, 56-63.

Wang, L., Li, D., Plested, C. P., Dawson, T., Teschemacher, A. G., and Paterson, D. J. (2006). Noradrenergic neuron-specific overexpression of nNOS in cardiac sympathetic nerves decreases neurotransmission. J Mol Cell Cardiol *41*, 364-370.

Weiss, K. R., and Kupfermann, I. (1976). Homology of the giant serotonergic neurons (metacerebral cells) in Aplysia and pulmonate molluscs. Brain Res *117*, 33-49.

Xia, Y., Berlowitz, C. O., and Zweier, J. L. (2006). PIN inhibits nitric oxide and superoxide production from purified neuronal nitric oxide synthase. Biochim Biophys Acta *1760*, 1445-1449.

Xin, Y., Weiss, K. R., and Kupfermann, I. (2000). Multifunctional neuron CC6 in Aplysia exerts actions opposite to those of multifunctional neuron CC5. J Neurophysiol *83*, 2473-2481.

Yoo, S., van Niekerk, E. A., Merianda, T. T., and Twiss, J. L. (2010). Dynamics of axonal mRNA transport and implications for peripheral nerve regeneration. Exp Neurol *223*, 19-27.

Yudin, D., Hanz, S., Yoo, S., Iavnilovitch, E., Willis, D., Gradus, T., Vuppalanchi, D., Segal-Ruder, Y., Ben-Yaakov, K., Hieda, M., *et al.* (2008). Localized regulation of axonal RanGTPase controls retrograde injury signaling in peripheral nerve. Neuron *59*, 241-252.

Zancanaro, C., Merigo, F., Mucignat-Caretta, C., and Cavaggioni, A. (2002). Neuronal nitric oxide synthase expression in the mouse vomeronasal organ during prenatal development. Eur J Neurosci *16*, 659-664.

Zhou, L., and Zhu, D. Y. (2009). Neuronal nitric oxide synthase: structure, subcellular localization, regulation, and clinical implications. Nitric Oxide *20*, 223-230.

Zhou, Q. G., Hu, Y., Hua, Y., Hu, M., Luo, C. X., Han, X., Zhu, X. J., Wang, B., Xu, J. S., and Zhu, D. Y. (2007). Neuronal nitric oxide synthase contributes to chronic stress-induced depression by suppressing hippocampal neurogenesis. J Neurochem *103*, 1843-1854.

Zhu, D. Y., Liu, S. H., Sun, H. S., and Lu, Y. M. (2003). Expression of inducible nitric oxide synthase after focal cerebral ischemia stimulates neurogenesis in the adult rodent dentate gyrus. J Neurosci *23*, 223-229.